

## **Preface**

---

The following report concludes the writers', Tomas Stafström and Joakim Palmberg, Masters thesis in mechanical engineering. The thesis was carried out at Tetra Pak, Lamination Technology and at the Division of Machine Design at the Department of Design Science at LTH from August 2009 to February 2010.

We would especially like to thank our supervisors at Tetra Pak, Christine Billstein and Malin Lager, for the guidance and insight they have given us throughout this thesis. We would also like to thank Michael Olsson at Tetra Pak's Flow Group for the valuable advice he has given us.

Furthermore, we would like to thank our supervisor at the division of machine design, Giorgos Nikoleris for his support during this work.

Lund, February 2010

Tomas Stafström and Joakim Palmberg



## Abstract

---

**Title:** Computer Based Simulations of Polymer Pellets Flow in Pneumatic Conveying Systems and Hoppers

**Division:** Division of Machine Design, Department of Design Science at LTH

**Authors:** Tomas Stafström and Joakim Palmberg

**Supervisors:** Christine Billstein and Malin Lager at Tetra Pak, Lamination Technologies and Giorgos Nikoleris, associate professor, Department of Design Science at LTH.

**Objective:** To investigate the possibility of conducting computer-based simulations of the flow of polymer pellets in hoppers and pneumatic conveying systems and to evaluate the simulation software. Tetra Pak wants to determine if computer based simulations can be used to acquire knowledge of important material properties and process parameters for this flow.

**Method:** By performing practical tests and equivalent computer-based simulations the software is evaluated by comparing the results of these. To ensure the validity of the simulation models two different polymer types are tested in two diverse hopper geometries. The flow pattern is observed and the time to empty a full hopper is determined.

**Conclusion:** The study shows that EDEM, the software used in this study, is able to simulate a flow in hoppers very similar to reality. However, the simulations are very time consuming and factors like temperature and moisture have been neglected in this study. The simulations have been compared to practical tests performed in ambient temperature.

**Keywords:** Hopper, Pneumatic Conveying, Computer based simulations, EDEM, FLUENT



## Sammanfattning

---

I lamineringsprocessen är polymer pellets en viktig komponent för den färdiga produkten. Innan polymer pelletsen smälts och formas till slutlig produkt i en extruder, måste de transporteras från sin lagerhållningsplats in till processen genom rörsystem. Under denna transport uppstår slitage av pelletsen i form av damm och avlagringar som har en negativ effekt på processen.

Innan pelletsen når processen fylls de i en hopper, placerad direkt ovanför extrudern. Hopporn i sin tur matar extrudern med pellets, men fungerar också som en lokal lagringsenhet för att försäkra att extrudern konstant förses med erforderliga pellets. Att ha ett väl fungerande flöde i hopporn är därför viktigt för att undvika avbrott i produktionen.

Tetra Pak vill utöka sin förståelse inom detta området för att kunna minimera problem i processen och säkerställa kvalitén i slutprodukten. Man vill därför förutom att göra en teoretisk studie, även undersöka möjligheterna att utföra datorsimuleringar av flödet av polymer pellets i rörsystem och i hopprar.

Avsikten med detta examensarbete har varit att först genomföra en teoretisk studie för att identifiera vilka materialegenskaper och processparametrar som påverkar dessa flöden, men också att finna lämpliga programvaror för dessa simuleringar samt att utvärdera programvaran för hoppersimuleringar.

I den teoretiska studien identifierades vilka materialegenskaper för polymerpelletsen som var nödvändiga för att kunna utföra datorsimuleringar. Metoder för att mäta dessa materialegenskaper utvecklades och utvärderades sedan statistiskt med Gage R&R.

Programvaran, EDEM, utvärderades genom att utföra praktiska tester som sedan jämfördes med simuleringarna. Första simuleringensmodellen sattes upp med de uppmätta materialeparametrar, men också med en del uppskattade som inte kunde mätas. Resultatet från denna simuleringen visade sig inte stämma överens med det praktiska testet. En känslighetsanalys utfördes i simuleringsprogrammet för att undersöka vilka materialparametrar som påverkade resultatet. Ett antal vidare simuleringar utfördes där dessa parametrar justerades tills resultatet från simuleringen stämde överens med det praktiska testet.

För att verifiera att dessa materialparametrar var representabla, utfördes ytterligare ett praktiskt test och en simulering på en annorlunda hoppergeometri. Om

materialparametrarna från den första simuleringen är representabla, skulle de ge en överensstämmande simulering även för den andra hoppergeometrin. Samma undersökning gjordes sedan med en annan polymertyp med andra materialegenskaper för att ytterligare validera simuleringsmodellen.

Studien visar att simuleringsresultat som ligger väldigt nära verkligheten kan uppnås. De fyra slutgiltiga simuleringarna i studien visar alla goda resultat med avvikelser inom 3,9 % vad gäller tömningstid av hopprarna. Vidare så stämmer flödesmönsterna väl överens med observationer gjorda under de praktiska testerna. Man ska dock ha i åtanke att simuleringarna är väldigt tidskrävande och kräver hög datorprestanda. En simulering av flödet i en fylld hopper av den typ som Tetra Pak använder sig av kan ta flera månader att slutföra. För att spara tid har istället små hoppermodeller använts i detta arbetet.

I kombination med dessa mindre hoppermodeller kan EDEM fungera som ett bra verktyg att utföra känslighetsanalyser med för att undersöka hur materialegenskaper och hoppergeometrier påverkar flödet av pellets.

# Content

---

<b>1. Introduction .....</b>	<b>1</b>
1.1 Background .....	1
1.2 Problem Formulation .....	1
1.3 Objective .....	2
1.4 Limitations .....	2
1.5 Method .....	2
1.6 Disposition.....	3
<b>2. Theory of Pneumatic Conveying Systems.....</b>	<b>5</b>
2.1 Hydraulic Conveying System.....	5
2.2 Pneumatic Conveying System.....	5
2.2.1 Dilute Phase.....	6
2.2.2 Strand Phase .....	6
2.2.3 Dense Phase.....	7
2.3 Degradation Types .....	8
2.3.1 Attrition and Wear.....	8
2.4 Equipment/Design .....	8
2.4.1 Bends.....	9
2.4.2 Common-radius Bends.....	9
2.4.3 Specialized Bends.....	10
2.4.4 Placing .....	11
2.4.5 Material .....	12
2.5 Process Parameters.....	13
2.5.1 Temperature.....	13
2.5.2 Velocity .....	13
2.6 Conveying Material.....	13
2.6.1 Particle Hardness .....	13
2.6.2 Particle Size and Shape .....	14
2.7 Summary.....	14

<b>3. Theory of Computer Based Simulations of Conveying Systems</b>	<b>15</b>
3.1 Introduction	15
3.1.1 Two Fluid Model (TFM)	15
3.1.2 Combined Continuum and Discret Model	16
3.2 Comments – Conveying Simulations	23
<b>4. Theory of Hopper Design</b>	<b>25</b>
4.1 Background	25
4.2 Hopper Flow Patterns	25
4.3 Designing a Hopper	26
4.3.1 Flow Function	26
4.3.2 Flow Factor	30
4.3.3 Deciding the Hopper Wall Angle	31
4.3.4 Outlet Size Determination	33
4.3.5 Flow Rate Considerations	36
4.4 Segregation Problems	37
4.4.1 Segregation Mechanisms	37
4.5 Comments – Theory of Hopper Design	39
<b>5. Theory of Computer Based Hopper Simulations</b>	<b>41</b>
5.1 Computer Software	41
5.2 Contact Models	41
5.3 Frictions	45
5.4 DEM Computational Cycle	45
<b>6. Material Properties Tests</b>	<b>47</b>
6.1 Laboratory Analysis	47
6.1.1 Coefficient of Restitution	47
6.1.2 Coefficient of Static Friction	52
6.1.3 Pellet Size and Shape Distribution – PSSD	55
6.2 Results Laboratory Analysis	57
6.2.1 Coefficient of Restitution	57
6.2.2 Coefficient of Static Friction	58
6.2.3 Pellet Size and Shape Distribution – PSSD	59



<b>7. Practical Tests</b> .....	<b>61</b>
7.1 Setup.....	62
7.2 Method.....	62
7.2.1 Time to Empty.....	62
7.2.2 Flow Pattern – Top View.....	63
7.2.3 Flow Pattern – Side View.....	64
7.3 Test Listing.....	64
<b>8. Computer Based Simulations</b> .....	<b>65</b>
8.1 EDEM User Interface.....	65
8.1.1 EDEM Creator.....	65
8.1.2 EDEM Simulator.....	66
8.1.3 Analyzing the Simulation.....	67
8.2 Simulation Setup.....	68
8.2.1 Contact Model.....	68
8.2.2 Material Properties and Particle Size.....	68
8.2.3 Simulation Settings.....	69
8.3 Simulation 1 – Hopper 1, mPE.....	70
8.4 Sensitivity Analysis – Design of Experiments.....	72
8.4.1 Theory.....	72
8.4.2 Sensitivity Analysis.....	72
8.4.3 Simulation Setup - DoE.....	74
8.4.4 Simulations.....	74
8.5 Sensitivity Analysis – Simulation Time.....	75
8.6 Simulation 2 – Hopper 1, mPE.....	76
8.7 Simulation 3 – Hopper 2, mPE.....	78
8.8 Simulation 4 – Hopper 1, PP.....	79
8.9 Simulation 5 – Hopper 2, PP.....	81
<b>9. Results</b> .....	<b>83</b>
9.1 Practical Test 1 and Simulation 1.....	83
9.1.1 Time to Empty.....	83
9.1.2 Flow Pattern – Center Plane.....	84

9.2	Sensitivity Analysis – Design of Experiments .....	86
9.2.1	Reviewing the DoE Simulations Results .....	86
9.2.2	Analyzing the DoE Model .....	87
9.3	Sensitivity Analysis – Simulation Time.....	90
9.4	Practical Test 1 and Simulation 2 .....	92
9.4.1	Time to Empty .....	92
9.4.2	Flow Pattern – Top View .....	93
9.4.3	Flow Pattern – Side View .....	95
9.4.4	Flow Pattern – Center Plane.....	96
9.5	Practical Test 2 and Simulation 3 .....	99
9.5.1	Time to Empty .....	99
9.5.2	Flow Pattern – Top View .....	100
9.5.3	Flow Pattern – Center Plane.....	102
9.6	Practical Test 3 and Simulation 4 .....	103
9.6.1	Time to Empty .....	103
9.6.2	Flow Pattern – Center Plane.....	104
9.7	Practical Test 4 and Simulation 5 .....	105
9.7.1	Time to Empty .....	105
9.7.2	Flow Pattern – Center Plane.....	105
9.8	Comments – Results .....	107
<b>10.</b>	<b>Conclusions.....</b>	<b>109</b>
<b>11.</b>	<b>Discussion and Further Work.....</b>	<b>111</b>
	<b>Notation.....</b>	<b>113</b>
	<b>References .....</b>	<b>115</b>
	<b>Appendix A – Gage R&amp;R .....</b>	<b>119</b>
	<b>Appendix B – DoE .....</b>	<b>129</b>
	<b>Appendix C – Bin velocities.....</b>	<b>133</b>
	<b>Appendix D – EDEM Considerations.....</b>	<b>142</b>
	<b>Appendix E – Hopper Drawings .....</b>	<b>143</b>

# 1. Introduction

---

*In this chapter the thesis is introduced and described.*

## 1.1 Background

In a lamination process polymer pellets, also known as polymer granules, are an important component of the product produced. Before the polymer pellets are processed into a specific and desired shape, it needs to be transported from point A to point B. The distance and routing can vary a lot between plants, but the main issue is the same. When conveying pellets through the system, particle attrition and pipe wear arise. The residues varies a lot in shape and amount for different systems, but all of them has an negative effect on the overall process, e.g. unplanned maintenance, waste, system breakdown and in worst case claims, if the barrier preventing semi material with poor quality fails.

During the lamination process polymer pellets are fed into an extruder where the pellets are melted and transformed into the desired shape e.g. plastic film or bottles through a nozzle. Before entering the extruder the pellets are loaded into a hopper, located directly above, that feeds the extruder. The hopper functions both as a feeder to the extruder and as a local storage device for pellets to ensure that the process is fed the amount of pellets needed to prevent starvation in the extruder.

After being loaded into the hopper the pellets begins to flow down through it due to gravitational forces only. During this flow Tetra Pak has experienced problems for some hopper configurations in some plants.

With a better understanding of what factors and parameters that has an impact on the flow through bends and hoppers, potential flow problems can be predicted and minimized in the future.

## 1.2 Problem Formulation

Earlier, Tetra Pak had a limited theoretical understanding of the flow in conveying systems and hoppers. The hopper configurations presently used are setup relying on empirical knowledge only. In this thesis, polymer conveying systems will be researched theoretically and the flow in hoppers will be researched both theoretically and by computer based simulations.

Both particle attrition and pipe wear is undesirable in a conveying system, but it is hard to fully eliminate. Tetra Pak wants to expand their knowledge in this area in order to limit this occurrence.

When flow problems occur in hoppers the true cause is difficult to identify. Tetra Pak is interested in acquiring the knowledge to understand what material properties and process parameters that have an impact on the flow in hoppers.

They also want to investigate if computer based simulations can be used to gain this knowledge.

### **1.3 Objective**

The objective with this thesis was to investigate the possibility of conducting computer based simulations of the flow of polymer pellets in hoppers and pneumatic conveying systems. The aim was to find the appropriate software, evaluate it by setting up simulation models and validate them through practical tests. For these simulations certain material properties were needed. To test these properties, testing methods had to be established and evaluated.

### **1.4 Limitations**

Because the software was new to us as well as to Tetra Pak, it has been necessary to first gain an understanding of the software before new problems could be applied. The simulations are very time consuming and due to the limited license period of the software the simulation models have been kept small.

Another limitation is the difficulties to verify the results. It is hard to measure physical quantities in the practical tests.

The project is limited to evaluate the software and the simulation models, measure necessary material properties and perform sensitivity analysis.

### **1.5 Method**

The approach for this study is defined in six steps.

1. Establish and evaluate methods to measure the material properties needed for the simulations.
2. Perform practical tests on two diverse hopper geometries with two different polymer types.
3. Conduct a computer based simulation representing one of the practical tests and validate the result.
4. Conduct a sensitivity analysis using Design of Experiments (DoE).
5. Based on the results from the first simulation and the sensitivity analysis, adjust the material properties until the simulation corresponds with the practical test.

6. Conduct additional simulations representing the rest of the practical tests to further verify the simulation model.

## **1.6 Disposition**

This report starts with a theoretical review of pneumatic conveying and flow in hoppers combined with theory of computer based simulations in chapter 2-5. Thereafter the laboratory analysis to determine the material properties is described in chapter 6. In chapter 7 the practical tests are handled and in chapter 8 the computer based simulations are described. Finally the results are evaluated in chapter 9 and conclusions and further work is discussed in chapter 10 and 11.



## 2. Theory of Pneumatic Conveying Systems

---

*This chapter explains the theory behind conveying systems and some key points to consider when designing a pneumatic conveying system.*

Different types of mechanisms can be used when transporting solids from point A to point B in pipeline systems. In industries the most common ones are pneumatic conveying and hydraulic conveying systems.

### 2.1 Hydraulic Conveying System [8]

Hydraulic conveying is basically when solids are conveyed through the system with a liquid carrier where the material is flushed from slug area, ground up and then pumped to discharge area. Hydraulic conveyors are widely used in industrial and commercial areas, where the conveying material doesn't get damaged by the liquid carrier.

### 2.2 Pneumatic Conveying System [9]

Pneumatic conveying is widely used in process industries to transport granular materials of different types, because of its cleanness and flexibility. It carries a mixture of materials in a stream of air through pipes. Pneumatic conveyors are either using a push, pull or a combination push/pull system. The characteristics for these are:

- The push system - Simply push material from one entry point to one exit point in which a positive pressure is used
- The pull system - Using a suction or vacuum to draw the material with the surrounding air
- The combined push/pull system - Using both push/pull methods to guide materials through various entry and/or exit points. In general Tetra Pak uses the push/pull system

Different types of phases can occur when conveying particles in a pneumatic conveying system. The mechanism by which such materials can be conveyed through a pipeline depends on the physical characteristics of the product, but typically the phase is in the form of dilute, strand or dense.

### 2.2.1 Dilute Phase [1]

Dilute phase is a form of pneumatic conveying, where the product are completely dispersed in gas flow at relative high velocities through the pipe. This is also known as “suspension conveying”.

The characteristics for dilute phase according to a presentation by Pelletron Corporation<sup>1</sup> are:

- High gas velocities,  $v = 25-40$  m/s
- Low product to air mass ratio, 1-10 to 1
- Low to medium pressure drop,  $p = 0.1-1$  bar



**Figure 2.1** – Dilute phase<sup>2</sup>

### 2.2.2 Strand Phase [1]

Strand phase, also called “moving bed”, is conveyed with a high concentration of air. The product is partially dispersed in gas flow and partially moving at higher concentration at the bottom of horizontal runs. This phase conveys in lower velocities and only those materials that have either good air retention or good permeability can handle it.

The majority of the particles are mutually self-supported at low velocities by pushing and rolling on each other, thereby preventing contact with the pipe walls. A well-designed system that can operate on this basis will result in a major reduction in particle attrition and pipeline wear, compared with a dilute phase system operating at the same function.

The characteristics for strand phase according to a presentation by Pelletron Corporation are:

- Gas velocities, typical in the range  $v = 15-25$  m/s
- Medium product to air mass ratio, 5-20 to 1
- Medium to high pressure drop,  $p = 0.5-2$  bar

---

<sup>1</sup> Pelletron Corporation, Lancaster, PA, USA

<sup>2</sup> <http://www.efluid.com.cn/images/upfile/20080313145045143.gif>



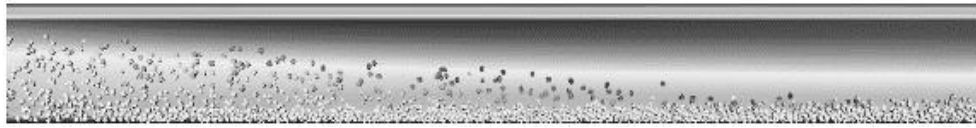


**Figure 2.2** – Strand phase

### 2.2.3 Dense Phase [1]

Conveying material in dense phase can be very hard to handle, many materials will simply block the pipe if the air velocity isn't sufficient for suspension flow. Another phenomenon that can occur in dense phase is a significant pressure drop along the conveying length. This gives a high expansion effect towards the end of the system. Due to the gas expansion the air velocity accelerates to very high velocities, this cycle is also known as “blowdown” and can lead to very high wear and particle attrition, unless prevention is taken.

To eliminate this problem stepped bore (diameter) pipelines can be used. Stepped bore pipelines is incremental raising the bore of the pipe, and makes the pressure and velocity drop. Another common way to eliminate the problem is to use vented pipes

The characteristics for dense phase according to a presentation by Pelletron Corporation are:

- Low gas velocities,  $v = 2-10$  m/s
- High product to air mass ratio, 15-50 to 1
- High pressure drop,  $p = 0.5-3.5$  bar

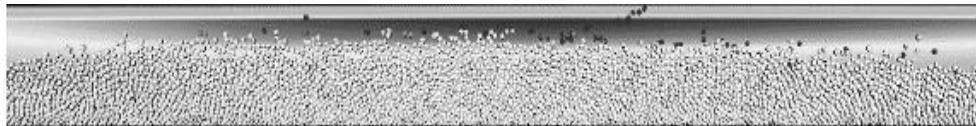


**Figure 2.3** – Dense phase

When conveying material in a pneumatic conveying system different factors and parameters can affect the flow the system. Such as:

- Equipment/Design – Bends, placing and material
- Process Parameters – Temperature and velocity
- Conveying material – Particle hardness, Particle size and shape

These factors and parameters can give rise to different degradation types.

## 2.3 Degradation Types

The main cause of particle attrition and pipeline wear is the same, collisions between particles and pipe wall, especially in bends. When a particle is approaching a bend, with almost the same velocity as the air it is conveyed in, it tends to go in a straight line and collides with the pipe wall. This is due to the inertia of the particle that prevents the particle from following the airflow.

### 2.3.1 Attrition and Wear [1,2]

Particle attrition can result in:

- Increased dust content in the product, in turn leading to
  - Problems with dust emission in further handling
  - Poorer “handle ability” of the material, e.g. hang-ups in hoppers and pipeline blockages
- Increased width of particle size distribution, making segregation more severe
- Problems with customer perception of the product, due to quality defects

Wear in pipelines gives rise to:

- Downtime on process
- Spillage leaking out from punctures in pipe
- Contamination of transported product with wear particles
- Planned/Unplanned maintenance cost in replacing components

## 2.4 Equipment/Design

Pneumatic conveying transfer lines are often routed over pipe racks and around large process equipment. Such design flexibility is made possible by the use of bends. The importance of choosing the right bend and place them right for a system should not be underestimated. If the bend type is not properly selected and designed they can contribute significantly to overall pressure drop, particle attrition, pipe wear and system maintenance according to [1-3,11]

### 2.4.1 Bends [1,3]

Bends are a very common part in a pneumatic conveying system. The majority of collisions occurs in bends, and is between particle-particle and particle-wall, as mentioned earlier this is known to be responsible for various problems such as high pressure loss, particle attrition and pipe wear. In order to minimize those problems, there are different bend designs and geometries. Two common designs groups are common-radius bends and specialized bends.

### 2.4.2 Common-radius Bends [3]

Common-radius bends are simply made by bending standard tubes or pipes. The radius of curvature  $R_B$  may range from 1 to 24D where D is the diameter of the tube or pipe. The conveyed material may suffer multiple impacts with the pipe wall or just slide along the outer pipe wall. This is depending on pipe design, material properties, pellets/air ratio and gas velocity (Figure 2.4).

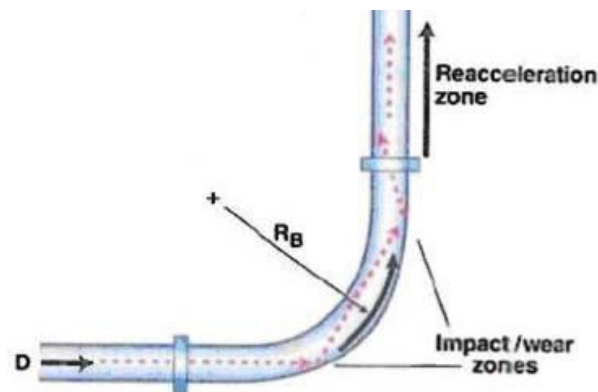


Figure 2.4 – Common-radius bend

- Short radius ( $R_B/D = 3$  to  $7$ )
  - Low pressure drop comparable to that of long radius bend
  - Available in many materials of construction
  - No accumulation in the bend, so less chance of cross-contamination when changing product
  - High particle attrition, due to impact
  - Low wear resistance

- Long radius ( $R_B/D = 8$  to  $14$ )
  - Low pressure drop comparable to that of short radius bend
  - Available in many materials of construction
  - No accumulation in the bend, so less chance of cross-contamination
  - Large space requirements
  - Extended pellets-wall contact results in “snake skin”
  - Erosive wear (friction) on ductile materials due to low impact angle

### 2.4.3 Specialized Bends [3]

Specialized designed bends are available to control the flow within the bend, in order to minimize attrition and wear. A replenishing pocket or a layer of material achieves this. Redirecting the pellets/air suspension away from typical wear points minimizes wear inside the piping. One example of a specialized bend available on the market is the Pellbow<sup>®</sup> shown in figure 2.5.

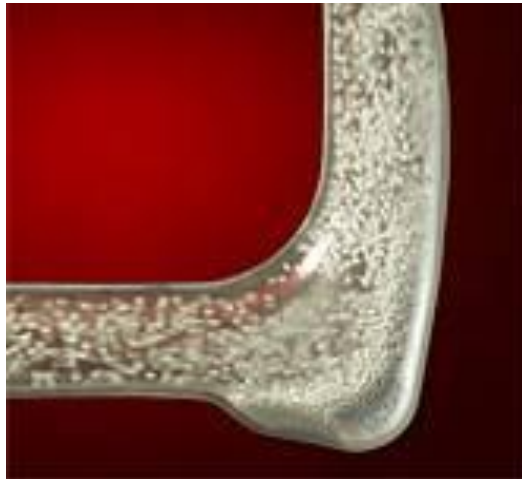


**Figure 2.5** – Pellbow<sup>®</sup> special transparent design, normally in cast iron, stainless or aluminum<sup>3</sup>

---

<sup>3</sup> [http://www.pelletroncorp.com/uploads/assets/components/pellbow\\_cut.jpg](http://www.pelletroncorp.com/uploads/assets/components/pellbow_cut.jpg)

- Pellbow<sup>®</sup>
  - Higher pressure drop compared to short and long radius bends (20-30%)
  - Low particle attrition
  - Self cleaning
  - Wear resistant if a stable material layer can be formed
  - Low noise
  - Higher cost
  - Needs a low pellets/air ratio for a proper operation

The Pellbow<sup>®</sup> bend from Pelletron Corp. is shown in Figure 2.5. It is similar to a short radius bend but with an expanded pocket which will accumulate a small amount of solids. The solids are accumulated at the primary impact location so that most of the impacts are between particles themselves. The incoming particles will either fill the chamber or circulate within the chamber before exiting. In either case, it results in significant reduction in wear and attrition of the pipe and pellets that is conveyed. The Pellbow<sup>®</sup> has a significant lower pressure drop compared to other specialized bends such as “Hammertek” and “Smart Elbow” who has similar reduction in wear and attrition of material.

#### 2.4.4 Placing

When designing a pneumatic conveying system, the conveying distance is important. Schneider and Wilms have investigated the influence of different polymer grades on wear behavior, especially on the total fines generation with conveying distance. Their investigation shows the increase of fines when increasing the conveying distance. [2]

According to Dhodapkar et al. [3] the bend location is also important, regardless of the type of conveying system, or the phase. The pressure always decreases from pickup location to destination. When the pressure decrease the gas velocity will proportionally increase from pickup location to the destination (Figure 2.6).

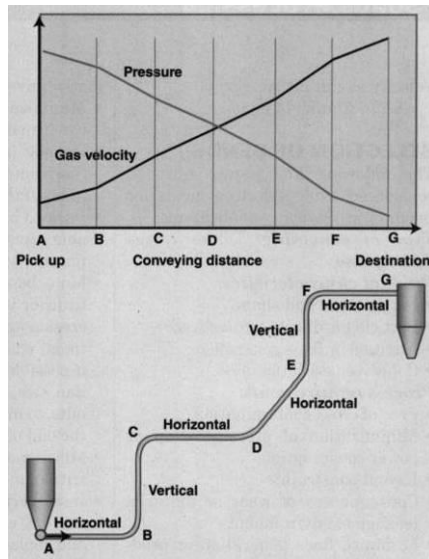


**Figure 2.6** – Pressure vs. gas velocity

Therefore, any bends located toward the end of the conveying system will experience velocities that are higher than those closer to the pickup location. Since pressure drop, attrition and wear are all strongly affected by gas and particle velocities, bends towards the end of the system experience greater attrition and wear.

#### 2.4.5 Material [10]

According to Tian et al. the material of the conveying system will affect the particle flow properties, especially the wall roughness. In their investigation they revealed that increased wall roughness significantly reduced the “particle free zone” and smoothing the particle number density profiles, by altering the particle rebounding behaviors (Figure 2.7).

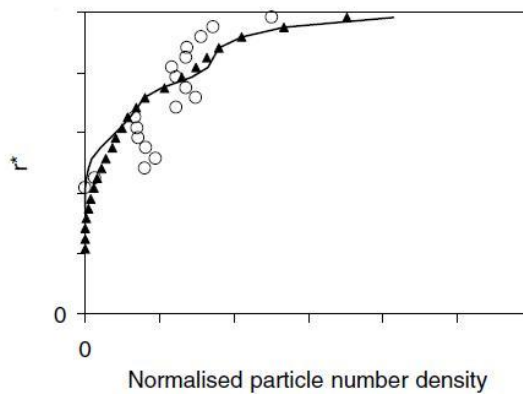


**Figure 2.7** – Particle number concentration with different wall roughness angles, roughness rising after symbols in order: Circles, line and solid triangle

Where  $r^* = \frac{r - r_i}{r_o - r_i}$ , is a non-dimensional wall distance,  $r_i$ ,  $r_o$  are respectively inner and outer pipe radius and  $r$  is the general pipe radius.

It was also found that increased wall roughness reduced the particle mean velocities. Also the varying particle velocities were increased when wall roughness was taken into consideration, since the wall roughness produced greater randomness in the particle velocities and trajectories after the first impact (Figure 2.8).

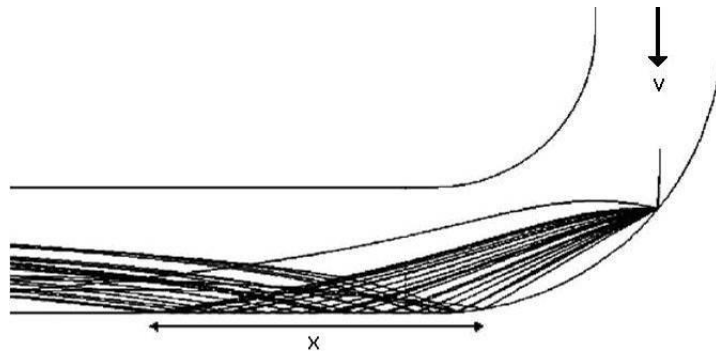


**Figure 2.8** – Trajectories for particles, x represents the length of the second impact region

## 2.5 Process Parameters

Process parameters are the parameters that can vary and affect the process, e.g. temperature and gas velocity.

### 2.5.1 Temperature [2]

According to Schneider and Wilms the temperature plays an important role in fines generation in pneumatic conveying systems. Their investigation shows that the polymers with low glass transition temperature<sup>4</sup> generate more fines than the polymers with high glass transition temperature.

### 2.5.2 Velocity [3]

As mentioned earlier, since pressure drop, attrition and wear are all strongly affected by gas and particle velocities, higher velocities give rise to greater attrition and wear in the conveying system.

## 2.6 Conveying Material

### 2.6.1 Particle Hardness [3,2]

Erosion rate is proportional to particle hardness, which means that a very hard particle more likely causes pipe wear, than a less hard particle. And the opposite for fines and streamers generated in pneumatic conveying system.

<sup>4</sup> Glass transition is a glass transformation range, which refers to the dynamic phenomenon occurring between two distinct states of matter, each with different physical properties.

## 2.6.2 Particle Size and Shape [2]

- Specific erosion rate increases with particle size until a critical particle size, and then the rate does not change
- Bend failure due to penetration occurs faster with smaller particles
- Angular particles will increase erosion rate

## 2.7 Summary [1]

Both attrition and wear is undesirable in a conveying system, but it's hard to fully eliminate. According to Dr MSA Bradley there are some key points that should be considered, and always have to be kept in mind when designing a conveying system.

Key points for minimizing particle attrition and pipe wear are according to Dr MSA Bradley:

- Reduce air velocity – Use the lowest possible air velocity for reliable flow
- Minimize the conveying length – Plan the routing well, don't make the routing longer than it needs to be
- Convey in dense phase if possible – To do this you can increase the pellets/air ratio. But for many materials and propellant (vacuum for example) it's not possible to have a dense phase, due to the pressure drop. In that case it's no point trying to "force" it convey in dense phase
- Minimize the pressure drop – If you have a pressure drop  $> 0.4$  bar, you can use stepped bore pipelines or vented pipes to minimize the pressure drop
- Minimize the number of bends and place them right – Only use bends when you really need to, ensure correct pipe alignment to estimate edges against the flow
- Choose appropriate bend geometries, shape and material – These factors can vary a lot depending on what type of material you want to convey in your system
- Prevent a blow tank from venting its charge of air along the pipeline as it empties



## 3. Theory of Computer Based Simulations of Conveying Systems

---

*This chapter concludes the theory behind computer based simulations of conveying systems. Also how the coupling between CFD-DEM works.*

### 3.1 Introduction [4,5]

In the past there have been limited understanding of the internal flow in a conveying system. Many experimental and numerical studies have been completed to try to increase the understanding. In recent years numerical methods have been widely used to study particle-fluid flow. The mathematical models used can be grouped into two categories:

- Continuum – Approach at a microscopic level represented by the so called two fluid model (TFM)
- Continuum-discrete – Approach at a microscopic level mainly represented by the so called combined continuum and discrete model (CCDM) which is sometime referred to as computational fluid dynamics and discrete element method (CFD-DEM)

#### 3.1.1 Two Fluid Model (TFM) [4]

In TFM, both gas and solid phases are treated as mutually penetrated continuum media in a computational cell that is much larger than individual particles but still small compared to the size of process equipment. This model is preferred in process modeling and applied research because of its computational simplicity. Its effective use depends heavily on the activity and interactions between solids within each cell. In cases with high particle concentrations, important interactions between solids may not be considered.

### 3.1.2 Combined Continuum and Discreet Model [4,5]

CCDM has been recognized as an effective method to study the fundamentals of particle-fluid two-phase flow. In CCDM, the motion of individual particles is obtained by solving Newton's equation of motion.

$$\sum \mathbf{F} = m_i \frac{d\mathbf{v}_{p,i}}{dt} \quad (3.1)$$

$$\sum \mathbf{M} = I_i \frac{d\mathbf{w}_{p,i}}{dt} \quad (3.2)$$

Where  $\mathbf{F}$ ,  $\mathbf{M}$ ,  $m_i$ ,  $t$ ,  $I_i$ ,  $\mathbf{v}_i$ ,  $\mathbf{w}_i$  are, respectively, the force and momentum applied, mass, time, moment of inertia and translational and rotational velocities of particle  $i$ .

While the flow of continuum gas is determined by computational fluid dynamics (CFD) calculated from the continuity and the Navier-Stokes equations based on the local mean variables over a computational cell scale.

$$\frac{\delta \varepsilon}{\delta t} + \nabla \cdot (\varepsilon \mathbf{u}) = 0 \quad (3.3)$$

$$\frac{\delta(\rho_f \varepsilon \mathbf{u})}{\delta t} + \nabla \cdot (\rho_f \varepsilon \mathbf{u} \mathbf{u}) = 0 \quad (3.4)$$

Where  $\varepsilon$ ,  $\mathbf{u}$ ,  $t$ ,  $\rho_f$  are, gas porosity, fluid velocity, time and fluid density respectively.

By applying these mathematical models on this basis the interactions between gas-particles, particles-particles and between particles-wall can be accounted for:

- Effect of particles on fluid flow
  - Better spatial resolution of momentum transfer
  - Accounts for the spatial effects of solids packing
- More accurate heat and mass transfer models
  - Effect of inter-particle contacts
  - Particle size distribution
  - Particle shape and mechanical properties
  - Surface properties, e.g. cohesion and liquid films
- Effect of particle – wall interaction
  - Complex geometry
  - Adhesion
  - Heat transfer

To approach a CCDDM-based simulation you can either use a CFD-DEM through UDF or a CFD-DEM coupling, the characteristics for these are:

### **CFD-DEM UDF [5]**

This approach uses a three dimensional CCDM model which can be used to simulate the gas-solid flow in pneumatic conveying bends. This is done by extending the CCDM code with FLUENT<sup>5</sup> as a platform, achieved by incorporating a DEM code into FLUENT through its user defined functions (UDF). According to Cho and Yu the modeling of solid flow by DEM is at the individual particle level, while the fluid flow by CFD is at the computational cell level. Their coupling is numerically achieved as follows. At each time step, DEM will give information, such as the positions and velocities of individual particles, for the evaluation of porosity and volumetric fluid-particles interaction force in a computational cell. CFD will then use these data to determine the gas flow field, which then yields the fluid forces acting on individual particles. Incorporation of the resulting forces into DEM will produce information about the motion of individual particles for the next time step.

Using UDF has been well established. Very reliable results can be obtained if the code is well developed and properly designed, but to develop the code for this solution could be very time consuming.

### **CFD-DEM Coupling [7]**

This approach is similar to CFD-DEM UDF, but instead of using the UDF to incorporate the DEM-code into FLUENT, the coupling uses EDEM<sup>6</sup> software as an additional plug-in to incorporate the DEM-code into FLUENT.

When taking fluid flow into consideration there are two relevant models in FLUENT, which are described below:

- Lagrangian – This model allows only momentum exchange between the fluid and the solid phases. Lagrangian coupling may be considered the equivalent of the discrete particle method (DPM) model.
- Eulerian – This model both allows momentum exchange between the fluid and solid phases, plus considers the effect of the particle solid fraction on the fluid phase. Eulerian coupling allows momentum exchange between the fluid and solid phases but additionally considers the effect of the particle solid fraction on the fluid phase.

Lagrangian coupling is considerably less compute-intensive than the Eulerian coupling, it should be used in cases where the local solid volume fraction (the solid fraction within a localized area of the simulation domain) remains below 10%.

---

<sup>5</sup> FLUENT is one of the world's leading engineering simulation software for computational fluid dynamics (CFD), Canonsburg, PA, USA

<sup>6</sup> EDEM is a Discrete element method program, developed by DEM Solutions, Edinburgh, UK

The flow of continuum gas is determined by computational fluid dynamics (CFD) calculated from the continuity and the Navier-Stokes equations based on the local mean variables over a computational cell scale with extended fluid density.

$$\frac{\delta \varepsilon \rho}{\delta t} + \nabla \cdot \rho \varepsilon \mathbf{u} = 0 \quad (3.5)$$

Where  $\varepsilon$ ,  $\mathbf{u}$ ,  $t$ ,  $\rho$  are, respectively porosity, fluid velocity, time and fluid density.

A similar equation exists for the conservation of momentum:

$$\frac{\delta \varepsilon \rho \mathbf{u}}{\delta t} + \nabla \cdot \rho \varepsilon \mathbf{u} \mathbf{u} = -\nabla p + \nabla \cdot (\eta \varepsilon \nabla \mathbf{u}) + \rho \varepsilon \mathbf{g} - \mathbf{M}_s \quad (3.6)$$

Where  $\varepsilon$ ,  $\mathbf{u}$ ,  $p$ ,  $t$ ,  $\mathbf{g}$ ,  $\eta$ ,  $\rho$ ,  $\mathbf{M}_s$  are, respectively porosity, fluid velocity, pressure, time, gravity force vector, viscosity, density and the momentum sink (momentum loss due to particles).

By the calculations of the momentum sink of the drag force, the coupling between the two phases is achieved. This force arises due to the relatively velocity between the phases. Therefore, the momentum sink  $\mathbf{M}_s$  is calculated by:

$$\mathbf{M}_s = \frac{\sum_{i=1}^n \mathbf{F}_D}{V} \quad (3.7)$$

Where  $\mathbf{F}_D$  is a summation of the drag force, exerting on the fluid in that mesh cell and  $V$  is the volume of the CFD mesh cell as the sink is volumetric.

To calculate the volume fraction of the CFD mesh cell occupied by the solid. Sample points are placed all over the cell, and if a sample point is within or on the boundary of the particle it is kept. As shown in Figure 3.1 below the red sample points outside the boundaries will be removed.

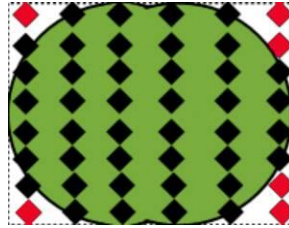


**Figure 3.1** – Sample point within a particle

To calculate the solid volume fraction within a particular mesh cell the percentage of the number sample points that lie within that mesh cell as given by:

$$\varepsilon_s = 1 - \varepsilon = \sum_{\text{particles}} \frac{n_c}{n_t} V_p \quad (3.8)$$

Where  $n_c$ ,  $n_t$ ,  $V_p$  are the number of sample points contained within the mesh cell of particle  $p$ , the total number of sample points of the particle and the volume of the particle  $p$ .

When calculating the force on the particles a modified spherical, free stream drag is used but when calculating the drag force on a non spherical particle, a bounding sphere is used. This bounding sphere is then used when calculating the drag force. All fluid parameters are taken from the CFD mesh element that contains the center of the DEM particle. Due to this only particles of the same size as, or smaller than the fluid mesh cell are calculable.

The drag coefficient,  $C_D$ , depends on the Reynolds number,  $Re$

$$Re = \frac{\xi \rho L |\mathbf{v}|}{\eta} \quad (3.9)$$

$$C_D = \begin{cases} \frac{24}{Re} & Re \leq 0.5 \\ \frac{24(1.0 + 0.15 Re^{0.687})}{Re} & 0.5 < Re \leq 1000 \\ 0.44 & Re > 1000 \end{cases} \quad (3.10)$$

Where  $\xi$ ,  $\rho$ ,  $L$ ,  $\mathbf{v}$ ,  $\eta$  are the free volume of the CFD mesh, fluid density, diameter of the particles bounding sphere, relative velocity and the fluid viscosity.

In addition to the drag force, the particles have natural buoyancy that is the upward force caused by fluid pressure that keeps things afloat. The net upward buoyancy force is equal to the magnitude of the weight of fluid displaced by the body. This force must also be taken into account.

$$F_B = \rho g V \quad (3.11)$$

Where  $\rho$ ,  $g$ ,  $V$  are the density, gravity and the volume.

### How the Coupling Works [7]

- DEM obtains the fluid velocity flow field from CFD
- DEM calculates drag on each particle using drag law modified for the presence of neighboring particles
- DEM calculates the solid-fluid exchange terms in the fluid mass, momentum and energy conservation equations

Computational considerations:

- Choosing the ratio of time-steps in DEM and CFD
$$\Delta t_{CFD} \approx 10^2 \times \Delta t_{DEM}$$
- Generation and removal of particles at the right stage in the simulation process
- Handling the ratio of particle size to mesh<sup>7</sup> size (eq. 3.8)

---

<sup>7</sup> Mesh defines the domain and then create elements within this defined boundary, the mesh splits the domain into elements, the finer mesh more accurate simulations results

Process flow for DEM – CFD:

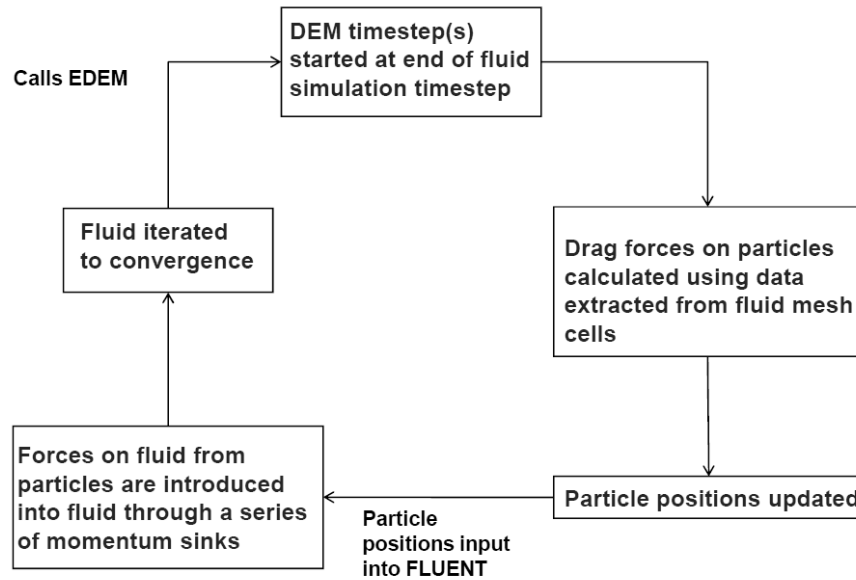


**Figure 3.2** Coupling process flow

Work flow for CFD-DEM coupling:

1. Start FLUENT
2. Read Mesh File (e.g. from Gambit)
3. Request coupled simulation
4. Set-up CFD part of simulation within FLUENT
5. Set-up DEM part of simulation within plug-in (EDEM)
6. Set-up coupling within FLUENT interface
7. Start simulation
8. Analyze results in FLUENT and EDEM
9. Further simulations, restart from step 4.



### **3.2 Comments – Conveying Simulations**

In the case of Tetra Pak's conveying systems, where many and large particles is flowing in the system, it is important to take into account how the particles interact with each other and pipe walls. For this type of simulation a CCDM is needed.

To achieve this you can either use a CFD-DEM coupling, where FLUENT is used as a platform with an extended plug-in from EDEM or by extending the CCDM by incorporating a DEM code into FLUENT through its UDF.

The same results can be obtained from both, but some factors may need to be considered:

If using the UDF, the DEM code needs to be developed and properly design for the solution which could be very time consuming. This also requires an extended understanding of the physics involved and how to incorporate this to the software. On the other hand, an extra license for EDEM and coupling plug-in is not needed.



## 4. Theory of Hopper Design

---

*This chapter explains the basic theory of hopper design, the material properties and process parameters that influences the flow in hoppers.*

### 4.1 Background [15]

The design of hoppers and bins for storage of bulk solids involves bulk material, bin geometry as well as structural considerations. Bulk material considerations are of big importance. The frictional and cohesive properties of the material can vary a lot from one solid to another, and have a big impact on the material behavior in the bin.

Potential problems due to bin geometry include arching across the bin outlet, rat holing through the material and flow pattern during discharge (Figure 4.1). Arching and rat holing problems are primarily related to the materials cohesive strength, while the flow pattern during discharge depends on the materials internal friction and the friction between the material and the hopper wall.

### 4.2 Hopper Flow Patterns [12]

Solids generally follow one of two basic flow patterns when moving through a hopper: funnel-flow or mass-flow (Figure 4.1). Funnel-flow is a result of either a too shallow wall angle, or a wall surface that is too rough. As a result, material will become stagnant along the lower parts of the hopper walls leading to a funnel-shaped channel above the outlet. The resulting first-in last-out flow has a greater likelihood of operational problems such as particle segregation, rat holing, flooding and reduced useable capacity.

However, there are some bulk materials that are well suited for funnel-flow pattern and they generally have the following characteristics:

- Coarse particles – usually a quarter of an inch and larger
- Free flowing materials – materials which do not stick to each other
- Non-degrading particles – materials which do not cake, spoil or oxidize when sitting without movement for a long period of time
- Segregation is not a problem – either the material is non-segregating or segregation does not affect downstream processes.

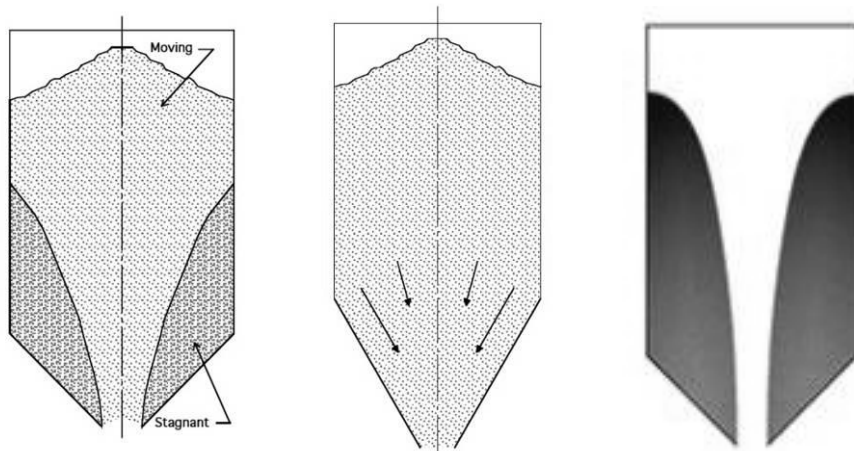


**Figure 4.1** – Funnel-flow (left), mass-flow (middle) and rat holing (right)

Provided that the material meets all four of these characteristics, a funnel-flow bin is the most economical storage device. One reason for this is that a shallower slope saves headroom within the facilities. Another is that by not having material sliding along the hopper walls, abrasive wear of the hopper walls is minimized.<sup>8</sup>

With mass-flow, all the powder is in motion as material is withdrawn at the outlet. Material from both the bin center and periphery moves toward the outlet. This first-in first-out flow eliminates rat holing and the associated problems of flooding of fine powders as well as reduced useable bin capacity. Problems like particle segregation, caking and oxidation are also minimized due to this type of flow pattern.

### 4.3 Designing a Hopper

The standard methodology for hopper design, for both funnel-flow and mass flow, is the one developed by Andrew W. Jenike. Jenike's design methodology is based on two parameters: flow factor and flow function.

#### 4.3.1 Flow Function [17,18]

The flow function depends purely on the shear strength of the bulk material and is a strength/pressure relationship. The cohesive strength of the bulk material is determined by measuring inter-particle shear stresses while the consolidation pressure is being applied. This relationship is usually measured using a direct shear tester (Figure 4.2).

<sup>8</sup> Abrasive wear is not an issue at Tetra Pak

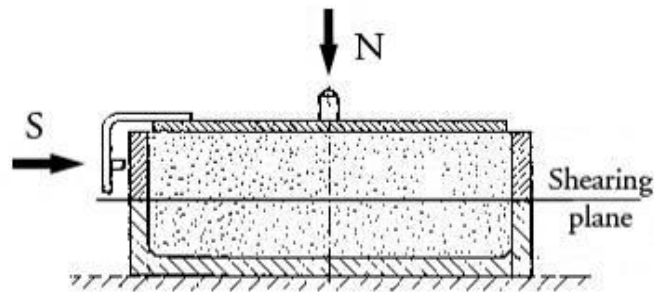


**Figure 4.2** – Direct shear tester

Consolidation of the sample is completed by a shearing operation which causes the material to flow under the consolidating stresses until a steady state is reached. This is performed by applying a normal load  $N$  incrementally to the cover and then applying the shearing force  $S$ . As shearing proceeds, a condition is reached when a layer of the material across the whole sample is caused to flow plastically and the recorded shear force reaches a steady value  $S$ . Consolidation determines point  $(N, S)$ .

The second stage of the test is the actual shearing of the sample under a load  $\bar{N}$  smaller than  $N$ . With  $\bar{N}$  in place, the shearing process is repeated and the shearing force  $\bar{S}$  is recorded.

The foregoing procedure enables one point  $(\bar{N}, \bar{S})_1$  to be plotted on the yield locus (Y.L.); the determination of a complete Y.L. requires the measurement of more points,  $(\bar{N}, \bar{S})_2$ ,  $(\bar{N}, \bar{S})_3$  etc. (Figure 4.4).

The various points  $(\bar{N}, \bar{S})$  are plotted and the smooth curve representing the yield locus is drawn through them. The point  $(N, S)$  representing the consolidation load condition is also plotted.

If the shear stress reduces proportional to the normal stress, the response is purely frictional and no effective cohesion develops: such is the case of free-flowing solids. However, in cohesive solids, a reduction in the normal stress does not lead to a proportional drop in the shear strength, and the internal friction effectively increases (Figure 4.3).

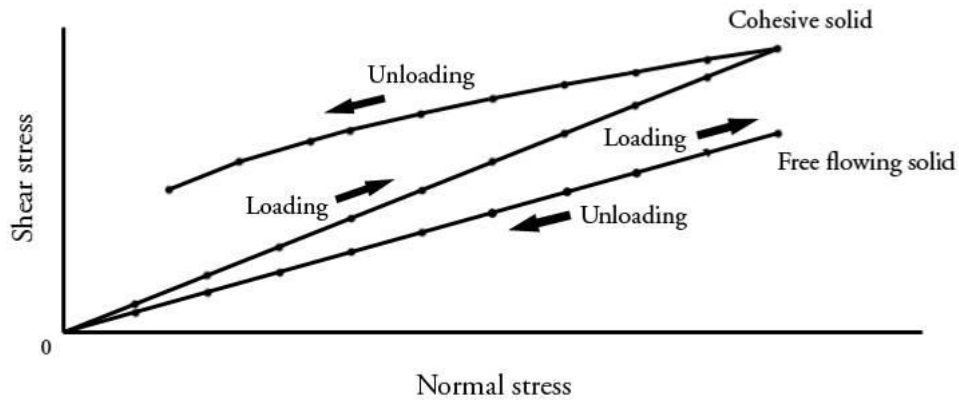


**Figure 4.3** – Frictional and cohesive solids in shear

Drawing a Mohr semi-circle tangential to the yield locus and passing through the point  $(N, S)$  defines the major principle force  $N_1$  and the major consolidating principal stress given from

$$\sigma_1 = \frac{N_1}{A} \quad (4.1)$$

Where  $A$  is the area of the shear cell.

Also of interest is the unconfined yield force  $F$ . This is obtained by drawing a Mohr semi-circle through the origin and tangential to the yield locus and the point  $F$  is defined. The unconfined yield stress  $\sigma_c$  is a measure of the material's strength at a free surface (i.e. the hopper opening) and is a function of the major consolidating stress (Figure 4.4).  $\sigma_c$  is given from

$$\sigma_c = \frac{F}{A} \quad (4.2)$$

Repeating the aforementioned test for other consolidating loads will enable a range of yield locus curves to be obtained. The flow function can then be plotted from the relations of the unconfined yield stresses and major consolidating stresses (Figure 4.5 & Figure 4.6). Figure 4.6 shows two different flow-functions. The upper one (b) illustrates what the flow-function could have been for the same bulk material as in (a) if being affected by higher moisture levels, temperature or longer time of consolidation.

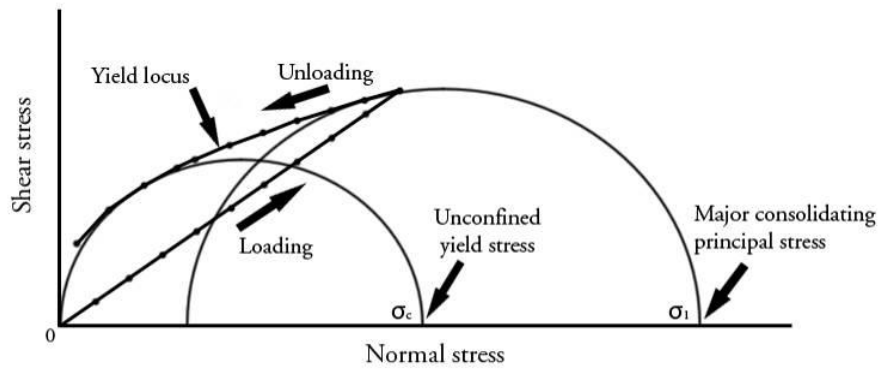


**Figure 4.4** – Unconfined yield stress and major consolidating principal stress

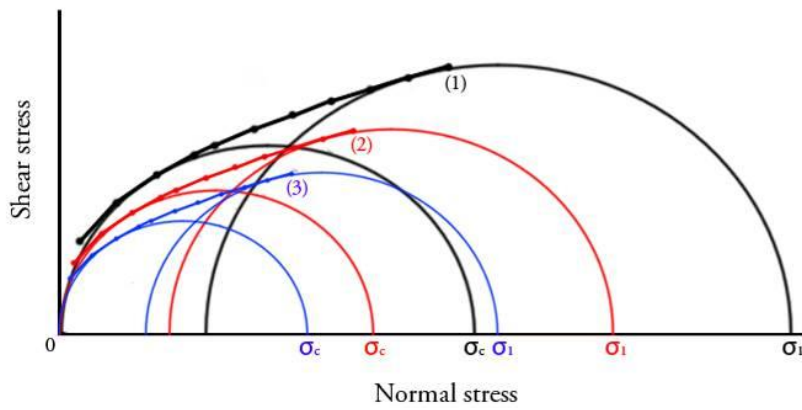


**Figure 4.5** – Range of yield locus curves

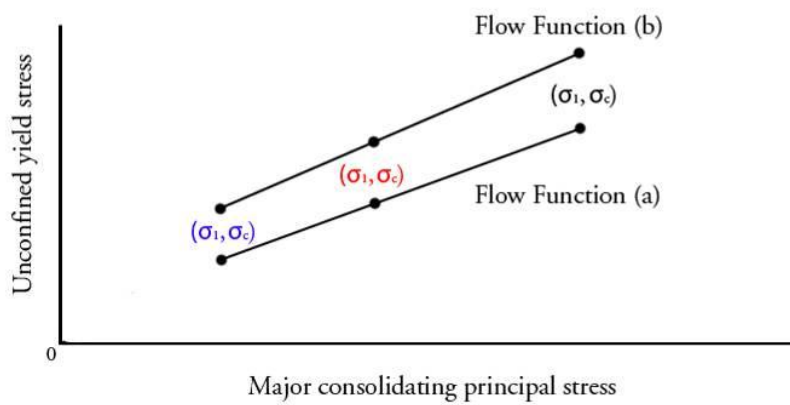


**Figure 4.6** – Flow function

### 4.3.2 Flow Factor

The Flow factor depends on the characteristics of the hopper such as the geometry of the hopper, material of construction as well as the properties of the bulk material. For any specific hopper configuration the flow factor is a function of the hopper wall angle  $\theta$ , the kinematic angle of friction between the flowing solid and the wall  $\phi_w$ , and the effective angle of internal friction  $\delta$ . Once these three angles have been derived the flow factor can be obtained using Jenike's design charts<sup>9</sup>. The determination of  $\theta$  and  $\phi_w$  will be explained in the next section – Deciding the Hopper Wall Angle.

The effective angle of internal friction  $\delta$  is derived from the line which is tangential to the Mohr circle defining the major consolidating principal stress from the tests explained in the previous section 4.3.1 (Figure 4.7). [16-18]

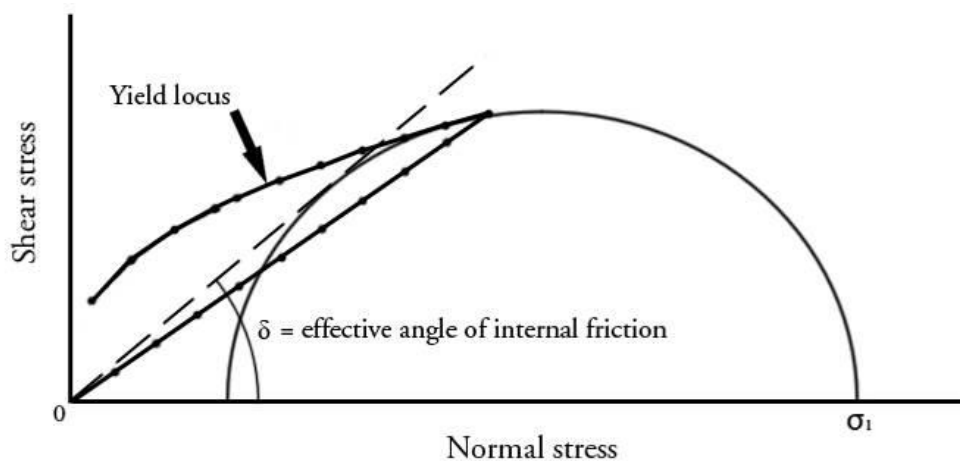


**Figure 4.7** Effective angle of internal friction

It is worth noting that a common misconception, according to Jenike, is using the angle of repose to determine flowability of solids. “Angle of repose. When an unconsolidated (loose) bulk solid is deposited on a horizontal surface so as to form a pile, and the velocity of the stream onto the top of the pile is negligible, the particles of the solid roll down the pile and the slope of the pile forms an angle of repose with the horizontal. The angle of repose assumes values between 30° and 40° and is not a measure of flowability of solid. In fact, it is only useful in the determination of the contour of a pile, and its popularity among engineers and investigators is due not to its usefulness but to the ease with which it is measured.”[16]

---

<sup>9</sup> Jenike's design charts can be found in Storage and Flow of Solids, bulletin 123 by A. W. Jenike



A wide range of particle sizes cause segregation. Finer particles collect along the trajectory while larger, coarser particles roll to the edges of the pile. Adding more solid from a height, the finer particles compact due to the impact of larger particles and gain strength, forming a slope angle steeper than the angle of repose. The opposite happens when a powder or flaky solid is added to the pile from a height—it aerates and spreads at an angle smaller than the angle of repose. [16]

#### 4.3.3 Deciding the Hopper Wall Angle

The difference between funnel-flow and mass-flow is determined by the angle of the hopper wall. Mass-flow is achieved when the hopper walls are steep and smooth enough for the bulk material to slide along them. To do this, the wall friction must be determined and overcome.

There are several factors that affect wall friction. For a given bulk material, wall friction can be affected by:

- Wall material – It is important that the friction test is performed with the actual bulk and wall material
- Temperature – both the temperature of the wall and the bulk material can affect the outcome of the friction test<sup>10</sup>
- Moisture – changes in moisture of the bulk material can affect the wall friction
- Corrosion – If a hopper is fabricated from carbon steel it may corrode creating a rougher surface
- Abrasive wear – As a surface wears it often becomes polished but can also become rougher
- Time at rest – Bulk materials can stick to the wall surface while remaining at rest under pressure. [12]

It is important to test the materials flow properties under the conditions that will be present in the bin. Tests should be run under the conditions that match the worst-case scenario the material is expected to be handled in to ensure the desired flow pattern even under these conditions. For instance, run the tests with materials at the maximum temperature and moisture and after the longest time at rest that is expected

---

<sup>10</sup> At Tetra Pak's facilities a hot extruder is located directly underneath the hopper which will heat up the lower parts of the hopper

in the process. If the bulk material is expected to degrade during conveying into the hopper, test a sample that has been conveyed under the same conditions. [14]

Wall friction tests are performed using a direct shear tester (Figure 4.8) by measuring the shear force as a function of applied normal force while sliding the bulk material along the stationary wall material. From the results the wall yield locus representing the normal and shear stresses along the wall can be plotted for the kinematic angle of wall friction  $\phi_w$  to be determined. Since the wall yield locus is usually represented by a curved line, the  $\phi_w$  varies as a function of the pressure at the wall.

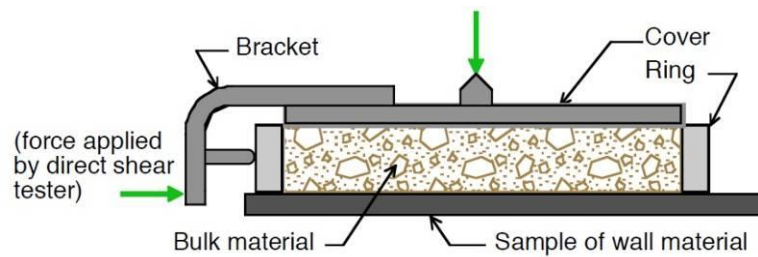


**Figure 4.8** – Direct Shear Tester

First the effective angle of friction  $\delta$  and the major consolidating principal stress  $\sigma_1$  at the wall of the outlet are determined. This permits the drawing of the effective yield locus and the tangential Mohr semi-circle through  $\sigma_1$ . The point  $(\sigma', \tau')$ , located on the wall yield locus, that describes the normal and shearing stresses at the wall of the outlet is then determined. The kinematic angle of wall friction  $\phi_w$  is found by drawing a straight line from the origin to the point  $(\sigma', \tau')$ . (Figure 4.9)

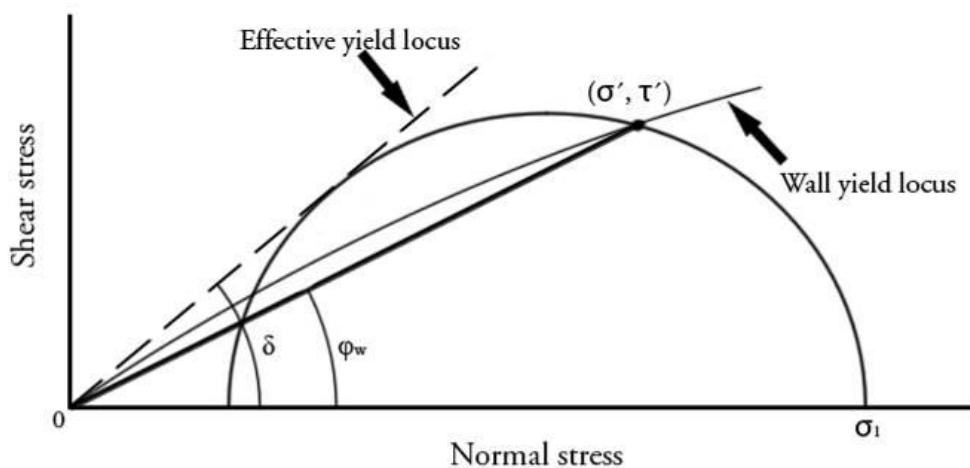


**Figure 4.9** – Kinematic angle of wall friction

Using the kinematic angle of wall friction in Jenike's design charts, the maximum hopper angle  $\theta$  needed for mass-flow can be determined for both conical and wedge hoppers. [16]

The wedge hopper design is the more forgiving of the two and capable of handling materials with a wider range of flowability than the conical geometry. Typically the hopper angle is  $12^\circ$  less steep on the wedge hopper than the required angle needed to achieve mass-flow in a conical hopper. Hence, mass-flow wedge-shaped configurations require significantly less headroom than conical hoppers. [12]

#### 4.3.4 Outlet Size Determination

After determining the hopper wall angle the next step in the design process is to determine the size of the outlet. Outlet size directly affects two types of flow obstructions related to arching that can occur with bulk materials in bins. The first is an interlocking arch that is formed above the outlet where particles lock together mechanically (Figure 4.10). The minimum outlet size required to prevent this type of arch to be formed is directly related to the particle size provided that the particles are at least  $\frac{1}{4}$  inch (6.35 mm) or larger. As a rule of thumb, the circular outlet size must be at least six to eight times larger than the biggest particle. For wedge shaped hoppers the dimensions of the outlet should be such that the width is at least three to four times the biggest particle, and the length of the outlet must be three times larger than the width.

If most of the particles are less than  $\frac{1}{4}$  inch in size, the flow obstructions can occur by cohesive arching (Figure 4.10). This is due to particles bonding together electrically, physically or chemically. If using the Jenike methodology, this bonding tendency, the cohesiveness of a bulk material, can be characterized by determining its flow function by measuring the cohesive strength of the material as mentioned in section 4.3.1. This strength is directly related to the ability of the bulk material to form arches and rat holes in bins and hoppers.

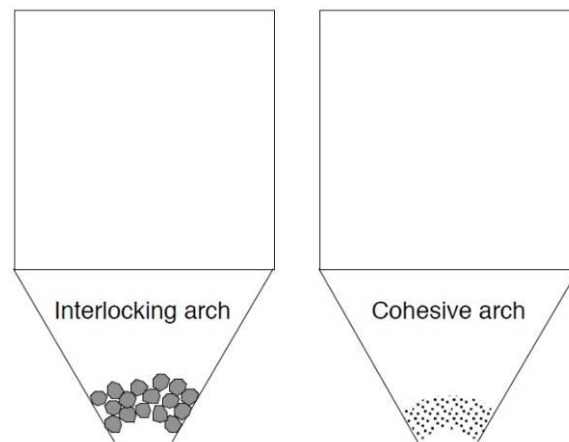


**Figure 4.10 – Arching**

Several parameters affect the cohesive strength of the bulk solid including:

- Particle size and shape – Generally finer particles have greater cohesive strength and a larger outlet size is required to prevent arching. Particle shape is of less importance but should be considered since more irregular shape generally means more difficulties to flow.
- Temperature – It is essential to consider temperature when performing tests of the material. The temperature can have a substantial impact on its cohesive strength whether it is constant or changing.<sup>11</sup>
- Moisture – Typically as moisture increases, the cohesive strength of the bulk solid also increases. Only when saturation moisture is approached, does a solid's strength decrease.<sup>12</sup>
- Time at rest – When bulk material is left at rest for a period of time, typically overnight or longer, the flow is not always restored because of an increase in cohesiveness.
- Relative humidity – hygroscopic bulk materials exposed to humidity experience an increase in moisture and gain in strength.

---

<sup>11</sup> At Tetra Pak's facilities a hot extruder is located directly underneath the hopper which will heat up the lower parts of the hopper

<sup>12</sup> Using plastic polymer the moisture can act as a lubricant (WBL)

Again, it is important to investigate the material properties under the circumstances that will be present in the bin. [12]

Once the flow function has been determined, the minimum outlet size to prevent arching can be calculated using the hopper's flow factor. By comparing the flow factor and flow function, the critical point, where the major principal stress  $\bar{\sigma}_1$  acting in the hypothetical arch and the strength of the material  $\sigma_c$  are equal, can be determined (Figure 4.11).

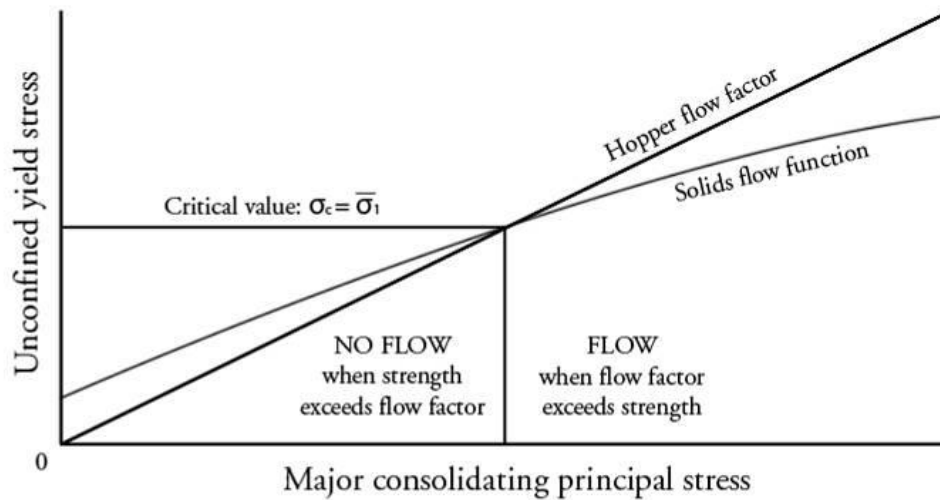


**Figure 4.11** – Intersection of the flow function and the flow factor

Imagine now a flow-function of the same bulk solid but under different conditions, e.g. flow-function (b) instead of (a) in Figure 4.6, the intersection between the two curves would occur at higher stress levels. Hence, it would require a larger  $\bar{\sigma}_1$  to prevent arching, leading to a larger required outlet. A change in the flow-factor due to e.g. a different material of construction of the hopper or a different wall angle would also result in a different intersection point.

After the determination of the critical point, the minimum outlet size required to prevent cohesive arching can be calculated by

$$B = \frac{\bar{\sigma}_1 H(\alpha)}{\rho g} \quad (4.3)$$

Where  $B$  is the outlet width/diameter,  $\bar{\sigma}_1$  is the major principal stress acting in the arch at the outlet,  $H(\alpha)$  is a function that takes account of variation in the arch

thickness, hopper angle and hopper geometric configuration and is given graphically in Jenike's design charts,  $\rho$  is the bulk density when consolidated and  $g$  is the acceleration due to gravity.

Selecting the proper feeder is also very important. The feeder must be able to withdraw the material from the entire outlet if mass-flow is to occur. A lip, ledge, partially open gate or a mismatched flange at the outlet that can prevent the feeder from withdrawing from the entire outlet can be fatal to mass-flow. [14]

#### 4.3.5 Flow Rate Considerations [12]

A third factor that must be considered when designing a bin is the discharge rate needed in the process. Bulk materials have a maximum rate at which they can be discharged out of the bin outlet at a given size. Usually this rate is well beyond the required for coarser particles but for finer powders, which have a considerably lower maximum discharge rate, this rate might not meet the requirement. This is due to the interaction between the particles and air as reflected in the permeability of the material. Flow rate is affected by the following factors:

- Particle size and shape – Finer particles or a great range of particle sizes generally means lower permeability, leading to lower flow rate.
- Level of material in bin – As the level of materials increase in the bin more air within the spaces between the particles is pushed upwards in the bin, creating a vacuum condition in the lower part of the hopper. Generally the maximum flow rate decreases due to this occurrence.
- Outlet size – For fine powders the outlet size of the hopper is in direct proportion to the maximum flow rate. Thus, flow rate limitations can sometimes be overcome by increasing the outlet size. However, the size of the feeder device that controls the discharge rate must also be considered.
- Outlet shape – Generally materials can flow with a higher rate through rectangular slots than through circular outlets since they usually have a greater cross-sectional area.
- Residence time – A short time of residence can be helpful to provide some deaeration so that the material does not flood through the outlet. On the other hand, too long time of residence can provide too much deaeration leading to a significant decrease in maximum rate of discharge.

## 4.4 Segregation Problems

Although segregation can have a negative effect on the flow in a bin, the main problems with segregation come when there is a mixture of products in the bin that needs to be withdrawn in a homogenous mix. If the bin is to store one material only, a uniform storage and discharge still may need to be concerned. Coarse and fine particles of the same material can perform quite differently. If the downstream process is designed to handle a wide range of particle size, the bin should be designed to prevent the discharge of only all fines or all coarse particles.

However, as mentioned before, the segregation problem can be minimized by ensuring mass-flow in the bin. Ensuring that the height-to-diameter ratio of the cylinder section, the top section of the bin with vertical walls, of a mass-flow bin is above 1.0 usually results in a uniform velocity pattern across the top surface and helps minimizing segregation.

Another way to diminish segregation is to use a patented BINSERT<sup>®</sup>, which consists of a hopper within a hopper. With this it is possible to design a system that provides a completely uniform velocity profile and thereby an absolute minimum level of segregation. [15,17]

### 4.4.1 Segregation Mechanisms [17]

The following are, according to the literature, the five major mechanisms responsible for most segregation problems:

**Sifting** – The most common mechanism of the five. Sifting occurs when the smaller particles are moving through the mixture of the larger particles usually leading to higher concentrations of fines in the center of the bin with striations out towards the periphery of the bin. In order for sifting to take place, it is essential for the following four conditions to be present:

- A difference in particle size, the larger the variation in size between the particles, the greater the tendency for particle segregation by sifting.
- Large mean particle diameter. For mixtures with a mean particle diameter below 500  $\mu\text{m}$  the tendency to segregate by sifting decreases significantly.
- Free-flowing material, no agglomerates can be formed. This usually requires low moisture content and little or no fine particles.
- If particles are moving with a uniform velocity, they are essentially locked together and segregation becomes almost nonexistent.

**Particle velocity on a surface** – Typically if there are variations in particle size or shape, the smaller particles and those who are of irregular shape have a higher frictional drag along a wall surface. This can cause a mass-flow bin to develop a funnel-flow pattern as the higher drag particles can become stagnant along the hopper walls.

**Air entrainment** – Fine particles tend to retain air longer in their void spaces than coarse particles due to their lower permeability. Thus, when the coarse particles are driven into the bed after being charged into the bin, the fine particles remain fluidized near the top surface developing a vertical segregation pattern.

**Entrainment of particles in an air stream** – When filling the bin fine particles can remain suspended in an air stream longer than the coarse particles. This effect becomes more important with particles around 50  $\mu\text{m}$  and is very common with particles around 10  $\mu\text{m}$ . Fine particles are also generally more affected by air resistance as they fall, resulting in a lower free-fall velocity when entering the bin.

**Dynamic effects** – Differences in dynamic characteristics like resilience and inertia can also cause the particles to segregate. An example of this resulted in a segregation pattern where the fine particles, who were the most resilient, ended up at the periphery of the bin, unlike with sifting where the fines are usually concentrated along the center.



#### **4.5 Comments – Theory of Hopper Design**

The Jenike methodology has been generally accepted as a standard method for hopper design. Jenike & Johanson Inc. provides services including analyzing material properties, deriving flow function and flow factor as well as determining required hopper angle and outlet size to achieve a desired flow pattern.

According to many sources, this method is very reliable and generates a satisfying result in most cases. However, Tetra Pak is not just looking for a solution to the flow problems they experience in some hoppers. They want to gain an understanding of what causes these problems in order to prevent them in the future. Consulting Jenike & Johanson Inc. to perform these analyses will provide a solution to the problem but not the desired understanding.

Jenike's theory illustrates the critical importance of the flow function and the flow factor in hopper design. Any change in the flow function or flow factor will affect the critical dimensions of the hopper outlet. If, let's say, a hopper is to be replaced by another, any difference in material of construction, geometry or wall angle will alter the flow factor and a different outlet size will be required to achieve flow for the same bulk solid. If, instead, a hopper is to be used for a different bulk solid from the one it was originally designed for, this will alter both the flow function and the flow factor. This could mean that neither the wall angle or outlet size will be adequate to achieve flow.

Also to be considered is that a specific bulk solid being handled in a specific hopper configuration might work in one plant, but not in another where temperature levels and humidity are different.

Even though this methodology is not being used in this project, studying it has helped to gain an understanding of what parameters and factors that have a great impact on a bulk solid's flowability in a hopper.



## 5. Theory of Computer Based Hopper Simulations

---

*This chapter introduces the software and explains briefly how it works.*

### 5.1 Computer Software

For the computer based simulations in this thesis it was initially planned to use the ANSYS FLUENT software. This CFD (Computational Fluid Dynamics) software is available at Tetra Pak and successfully used for many applications. However, after some research and consulting with persons<sup>13</sup> experienced in the area, it was realized that CFD software is not the most appropriate for this specific application. CFD software is not designed to handle solids in this range and does not have default contact models for the interactions between particles. When conducting computer based simulations of this kind, the interactions between the particles and the boundaries are crucial. This is not a fluid dynamics problem since the particles are not transported in a fluid, but rather a pack of particles loaded into a hopper, flowing through it due to the gravitational forces only.

Further research was conducted and showed that these types of simulations were most often performed using a DEM (Discrete Element Method) software [19,23-26]. Discrete element modeling of granular materials involves tracking the movement of all the particles in a system and the detection of their collisions with other particles and the boundaries. In order to calculate the motion of each particle, all the forces acting on a particle are summed and the resulting equations of motion are numerically integrated with a fixed time-step. The EDEM software developed by DEM Solutions was chosen for this project. This software has default contact models in place to describe the contacts between particles as well as interactions with the hopper walls.

### 5.2 Contact Models [20-23,27]

DEM software provides a range of contact models, including the classical Hertz-Mindlin and linear spring contact. These involve the calculation of normal and shear contact stiffness of two adjacent bodies (Figure 5.1). The Hertz-Mindlin relates, in addition to the contact stiffness, also to the confining pressure via the radii and elastic moduli of the bodies.

---

<sup>13</sup> Michael Olsson, Flow Group at Tetra Pak, meeting October 2<sup>nd</sup> 2009

Robert Bjärnemo, Professor at Machine Design, Lunds Tekniska Högskola, meeting September 24<sup>th</sup> 2009

Robert Hansson, Technical support at Medeso, telephone conversation October 1<sup>st</sup> 2009

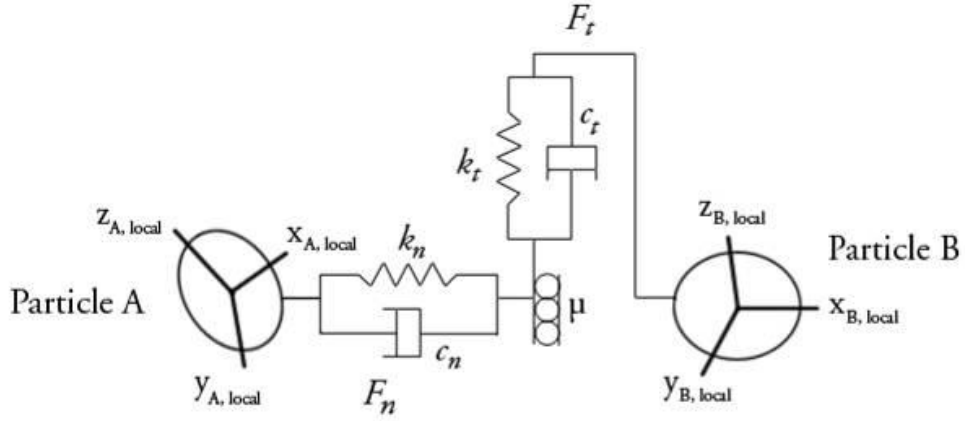


**Figure 5.1** – Particle contact force model [22]

The normal force  $F_n$  and the tangential force  $F_t$  acting on the particle are described by

$$F_n = k_n \delta_n + c_n v_n \quad (5.1)$$

$$F_t = \min(\mu F_n, k_t \delta_t + c_t v_t) \quad (5.2)$$

Where  $\delta$  is the overlap between the particles, which represents the deformation that occurs when two bodies collide;  $k$  is the stiffness,  $c$  is the coefficient of restitution or damping coefficient,  $\mu$  is the friction coefficient between the bodies and  $v$  is the velocity.

The Hertz-Mindlin model yields the particle stiffness

$$k_n = \frac{4aG}{1-\nu} \quad (5.3)$$

$$k_t = \frac{8aG}{2-\nu} \quad (5.4)$$

Where  $a$  is the radius of the contact area between two particles (Figure 5.2),  $G$  and  $\nu$  are the particle shear modulus and the poisson's ratio respectively. The radius  $a$  is related to the confining force  $F_n$  and the contact curvature radius  $R_C$

$$a = \left[ \frac{3F_n R_C (1-\nu)}{8G} \right]^{\frac{1}{3}} \quad (5.5)$$

Where  $R_C$  is related to the radii of the two bodies in contact,  $R_A$  and  $R_B$

$$\frac{1}{R_C} = \frac{1}{2} \left( \frac{1}{R_A} + \frac{1}{R_B} \right) \quad (5.6)$$

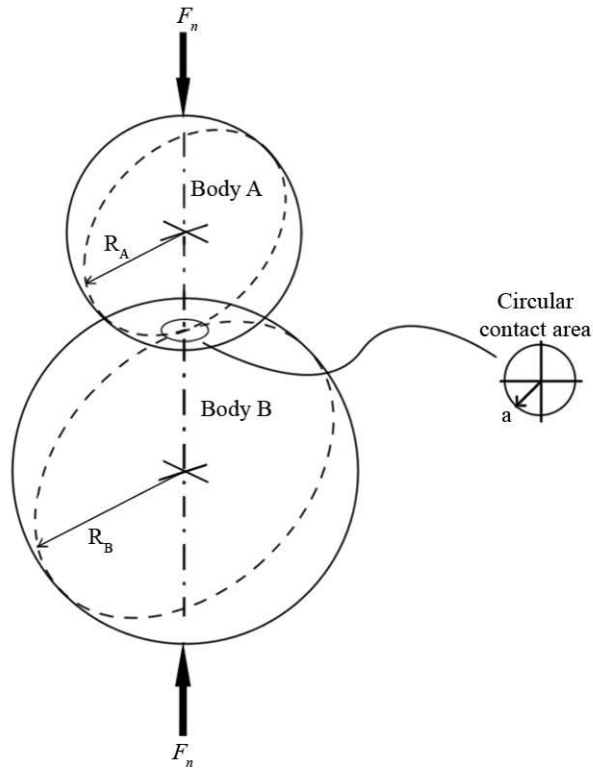


**Figure 5.2** – Contact between two bodies

The shear modulus  $G$  is defined as the ratio of the shear stress  $\tau$  to the shear strain  $\gamma$

$$G = \frac{\tau}{\gamma} \quad (5.7)$$

Where

$\tau = \frac{F_t}{A}$ ;  $F_t$  is the tangential force acting on the body;  $A$  is the area on which  $F_t$  is

acting;  $\gamma = \frac{\Delta x}{y} = \tan(\theta)$ ;  $\Delta x$  is the transverse displacement;  $y$  is the initial height

(Figure 5.3)

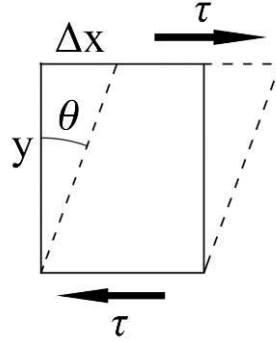


**Figure 5.3** – Shear strain

When all forces acting on a particle  $i$ , either from other particles or from boundaries, are known, the problem is reduced to the integration of Newton's equations of motion for the translational and the rotational degrees of freedom. The motion of each particle  $i$  in time  $t$  is described by

$$m_i \frac{d^2}{dt^2} \mathbf{x}_i(t) = \mathbf{F}_i(t) \quad (5.8)$$

$$I_i \frac{d^2}{dt^2} \Phi_i(t) = \mathbf{M}_i(t) \quad (5.9)$$

Where  $m$  is the mass of the particle,  $I$  is the moment of inertia given by  $I_i = q_i m_i (d_i / 2)^2$  where  $q_i$  is a dimensionless shape factor. The vectors  $\mathbf{x}_i$  and  $\Phi_i$  give the position and the orientation in space of particle  $i$ , respectively.

The vectors  $\mathbf{F}_i$  and  $\mathbf{M}_i$  present the sum of gravity and inter-particle contact forces and torques, which act on the particle  $i$ , respectively

$$\mathbf{F}_i = \sum_{j=1, j \neq i}^N \mathbf{F}_{ij} + m_i \mathbf{g} \quad (5.10)$$

$$\mathbf{M}_i = \sum_{j=1, j \neq i}^N \mathbf{M}_{ij} = \sum_{j=1, j \neq i}^N \mathbf{d}_{cij} \times \mathbf{F}_{ij} \quad (5.11)$$

Where  $\mathbf{d}_{cij}$  is the geometric vector pointing from the particle center to the contact point while  $\mathbf{g}$  is the vector of gravity.

### 5.3 Frictions [19]

In difference from the macroscopic friction angles measured when using the Jenike approach, for computer based simulations the microscopic friction coefficients are desired instead.

The macroscopic friction, usually measured using a direct shear tester, describes the frictional characteristics of a bulk assembly of particles. In contrast to the macroscopic friction, the microscopic friction is a measurement of inter-particle friction coefficients and describes the Coulombic frictional characteristics between two bodies engaged in a binary contact.

Both methods measure the Coulomb friction between two bodies. In addition the macroscopic friction is affected by other characteristics such as particle shape and the cohesiveness of the particles within the assembly. Rounded particles have a tendency to move past each other more easily while blocky particles have greater strength and a higher macroscopic friction. This tendency is due to the availability of rolling as a stress release mechanism. In a similar way, cohesive materials also have a greater internal strength and macroscopic friction due to the attractive forces between particles.

### 5.4 DEM Computational Cycle [22]

During the simulation process the EDEM software is using the computational cycle as shown in Figure 5.4 below.

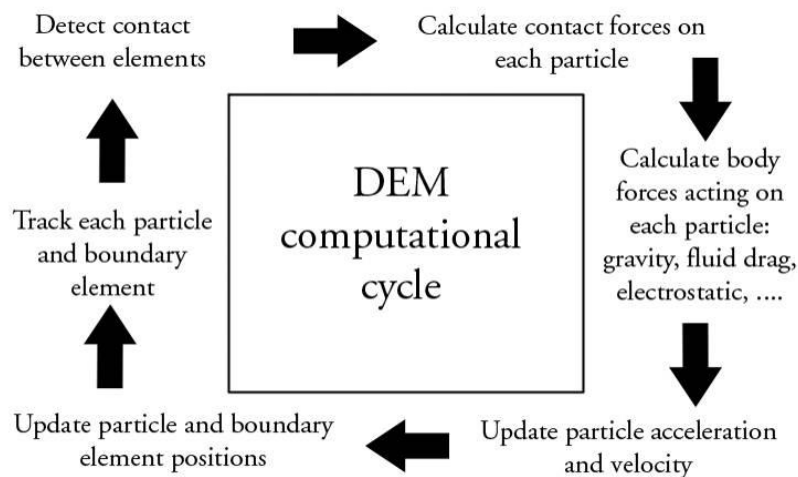


Figure 5.4 – DEM computational cycle





## 6. Material Properties Tests

---

*This chapter explains the methods used for testing the material properties and the results from these.*

### 6.1 Laboratory Analysis

#### 6.1.1 Coefficient of Restitution

##### **Theory**

One way to measure the coefficient of restitution is to let a sample bounce against a flat stationary surface. By measuring the height from where the sample was dropped and the height to which it rebounds, the coefficient of restitution  $c$  can be calculated by

$$c = \sqrt{\frac{h_2}{h_1}} \quad (6.1)$$

Where  $h_1$  is the height from where it was dropped and  $h_2$  is the height to which it rebounds.

##### **Sample Preparation**

To prepare the samples used in the test, polymer pellets were taken from octabins and placed in a Teflon covered mold. The pellets were then melted and shaped, using an instrument with a pre-programmed temperature and pressure cycle, into approximately 50 mm squares with a thickness of 4 mm (Figure 6.1 & Figure 6.2). To minimize changes of the material properties the pellets were heated as gentle as possible (Table 6.1).

**Table 6.1** – Set temperatures and programs

Sample	Program	Temperature
mPE <sup>14</sup>	LDPE	130°C
LDPE <sup>15</sup>	LDPE	130°C
mLLDPE <sup>16</sup>	LDPE	130°C
PP <sup>17</sup>	PP	175°C



**Figure 6.1** – Polymer pellets in mold before melting

---

<sup>14</sup> Metallocene Polyethylene

<sup>15</sup> Low density Polyethylene

<sup>16</sup> Metallocene low density Polyethylene

<sup>17</sup> Polypropylene

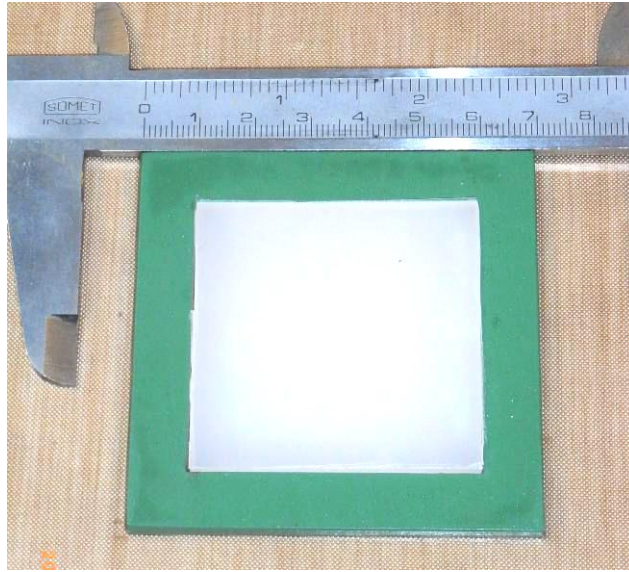


**Figure 6.2** – Polymer sample in mold after melting

The instrument used to melt the polymers comprises two heating blocks—upper and lower—that apart from heating also apply pressure to the sample, and two cooling plates to cool and solidify the sample after the melting procedure (Figure 6.3 & Figure 6.4).

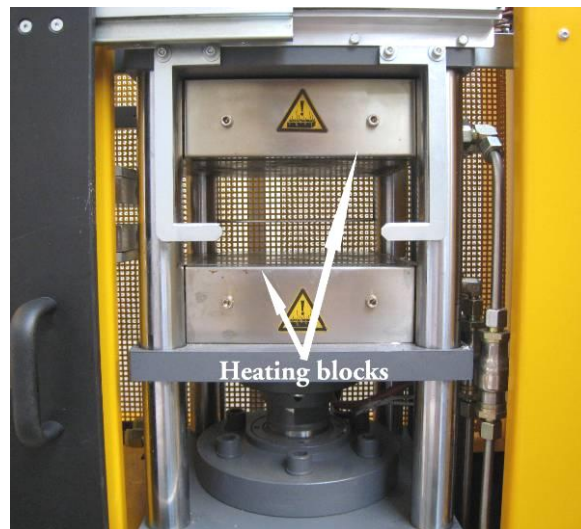


**Figure 6.3** – Instrument with heating blocks

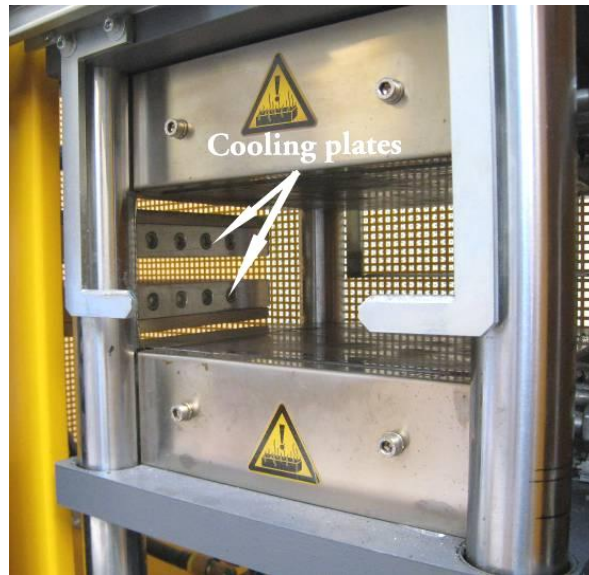


**Figure 6.4** – Cooling plates of the instrument

### **Procedure**

- A suitable program, for the polymer to be melted, with a pre-set pressure and time cycle was selected to process the polymer. The appropriate temperature was set manually.
- The sample was placed inside the instrument between the two heating blocks and the blocks were heated to the pre-set temperature.
- The blocks were then activated to apply heat to the sample with low pressure,  $2 \text{ N/cm}^2$ .
- Once the sample reached the correct temperature, the pressure was increased to the pre-set limit and was constantly applied for the pre-set period of time.
- The heating blocks were then disengaged and the cooling plates were activated and applied.

### **Purpose**

The coefficient of restitution, or the damping coefficient, is needed for the computer based simulations where it is used as a shock absorber in the contact models for the particles.

## Instrument and Method

Testing equipment<sup>18</sup> available in Tetra Pak's lab facilities was used to measure the coefficient of restitution (Figure 6.5). This instrument is equipped with an arm that is initially set to a horizontal position and then dropped to a vertical position where it hits the test sample. The instrument then measures the ratio of the height to which the arm rebounds ( $h_2$ ) to the height from where it was initially dropped ( $h_1$ ). This procedure is repeated three times per sample and the coefficient of restitution is calculated.

To evaluate the method Gage R&R<sup>19</sup> was used in which three persons participated in the testing procedure. Each person tested three samples of each polymer, and to ensure the reliability of the method, four different polymer types were tested (Appendix A).

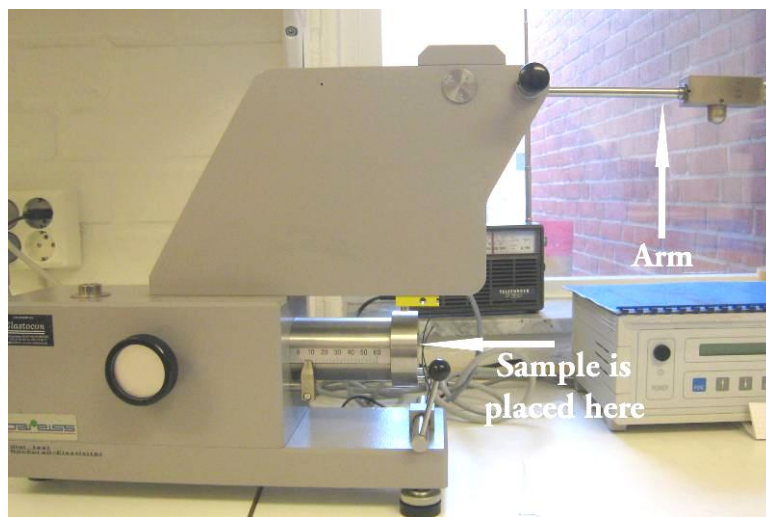


**Figure 6.5** – Coefficient of restitution tester

---

<sup>18</sup> Heinrich Bareiss Prüfgerätebau GmbH, Oberdischingen, Germany

<sup>19</sup> Gage R&R is a statistical tool that measures the amount of variation in the measurement system arising from the measurement device and the people taking the measurement.

## 6.1.2 Coefficient of Static Friction

### Theory

A relatively simple way to measure the coefficient of static friction is to place a sample on a flat surface, or a ramp, and then tilt the ramp up until the point where the sample begins to slide. By measuring the height to which the ramp is lifted the tilting angle can be determined. The coefficient of static friction,  $\mu$ , can then be calculated using the equations below. (Figure 6.6)

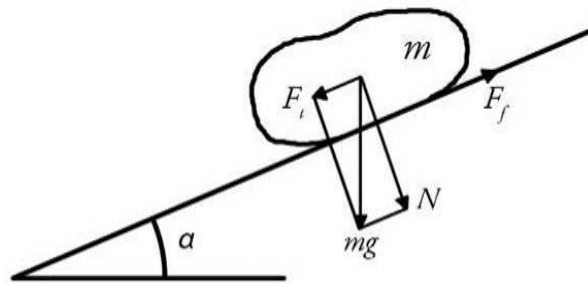


Figure 6.6 – Pellet on a tilted ramp

$$F_f = \mu N \quad (6.2)$$

$$\tan(\alpha) = \frac{F_t}{N} \quad (6.3)$$

Where  $N$  is the normal force;  $F_f$  is the friction force;  $F_t$  is the tangential force parallel to the ramp and  $\alpha$  is the tilting angle.

Sliding initiates precisely when  $F_t$  exceeds  $F_f$ . The coefficient of static friction can then be calculated by

$$\mu = \frac{F_t}{N} = \tan(\alpha) \quad (6.4)$$

### Sample Preparation

To prepare the samples used in the test of the static friction between pellets, the same method as in the coefficient of restitution section was used. For this test, squares of

approximately 110 mm and a thickness of 0.4 mm was prepared. Again, to minimize changes of the material properties the pellets were heated as gentle as possible. (Figure 6.7 & Figure 6.8)



**Figure 6.7** – Polymer pellets in mold before melting

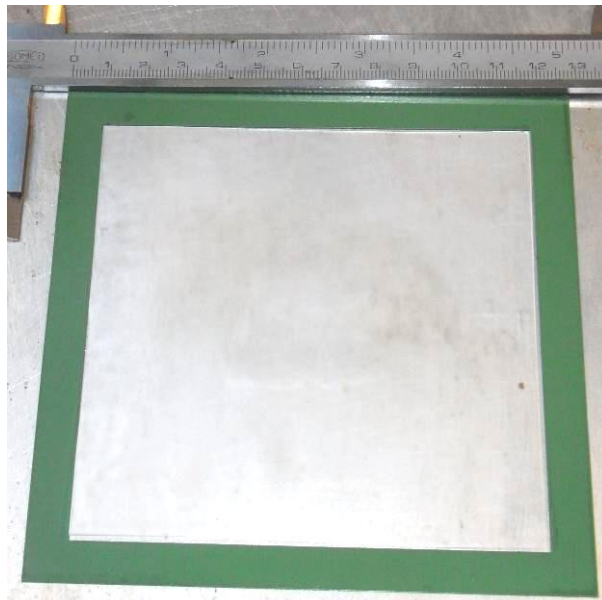


**Figure 6.8** – Polymer sample in mold after melting



## Purpose

The coefficient of static friction is used in the contact models that describe the interaction between particles in the computer software used for the simulations.

## Instrument and Method

For the test of the static friction between pellets, the test samples were glued onto a ramp for the test. The pellets were then placed on top of the sample and a small hydraulic lift was used to tilt the ramp by lifting one end. The ramp was tilted up until the point, where the pellets began to slide down, was reached (Figure 6.9). The height to which the ramp was lifted was measured and the tilting angle  $\alpha$  was then calculated by

$$\alpha = \arcsin\left(\frac{h_2 - h_1}{L}\right) \quad (6.5)$$

Nine pellets were placed on the sample for each test, and the minimum, mean and maximum values of the friction coefficient were determined. Four tests were performed on each test sample to account for possible variations.

The same method was used to measure the friction coefficient between the pellets and the hopper wall. Instead of the test sample made from melted polymer, a sample made of the same material as the hopper was used.

To evaluate the method two persons performed tests on four test samples each made of a different type of polymer. The results were then evaluated using Gage R&R.

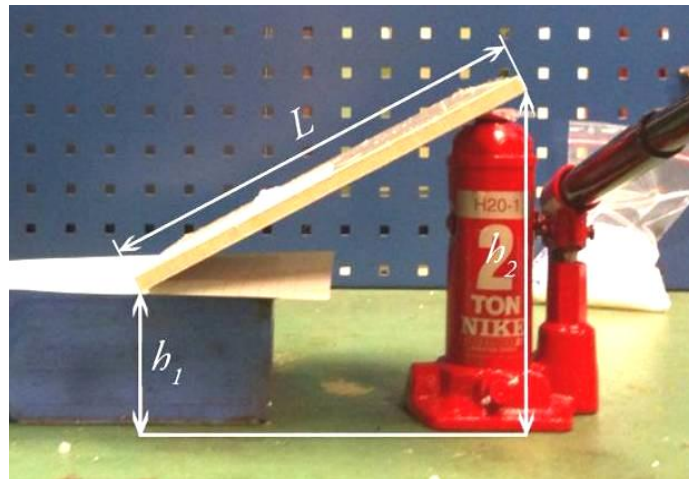


Figure 6.9 – Friction test



### 6.1.3 Pellet Size and Shape Distribution – PSSD

#### **Theory [28]**

The PSSD is a modular inspection system that rapidly analyses size and shape of polymer pellets. The pellets to be inspected are loaded into a hopper and transported and separated by the vibrating channels towards a free fall (Figure 6.11). In the free fall the pellets are measured individually between the high resolution CCD (charge coupled device) camera and the light source. After free falling, the pellets are collected in a bin.

The system is able to analyze up to 50 kg pellets per hour, depending on size and bulk density, minimum size 80  $\mu\text{m}$ .

#### **Sample Preparation**

Approximately 500 grams of pellets was collected from each polymer type for the test.

#### **Purpose**

The purpose of the PSSD measurement was to see how the particle size and shape distribution varied. This variation will be accounted for in the computer based simulation.

#### **Instrument and Method**

The instrument was set to collect and record particle sizes in ranges from 1600-5100  $\mu\text{m}$ . Particles smaller than 1600  $\mu\text{m}$  were registered in the lowest range and particles larger than 5100  $\mu\text{m}$  in the largest. The PSSD instrument<sup>20</sup> used is displayed in Figure 6.10.

---

<sup>20</sup> Optical Control Systems GmbH, Witten, Germany



**Figure 6.10** – PSSD instrument

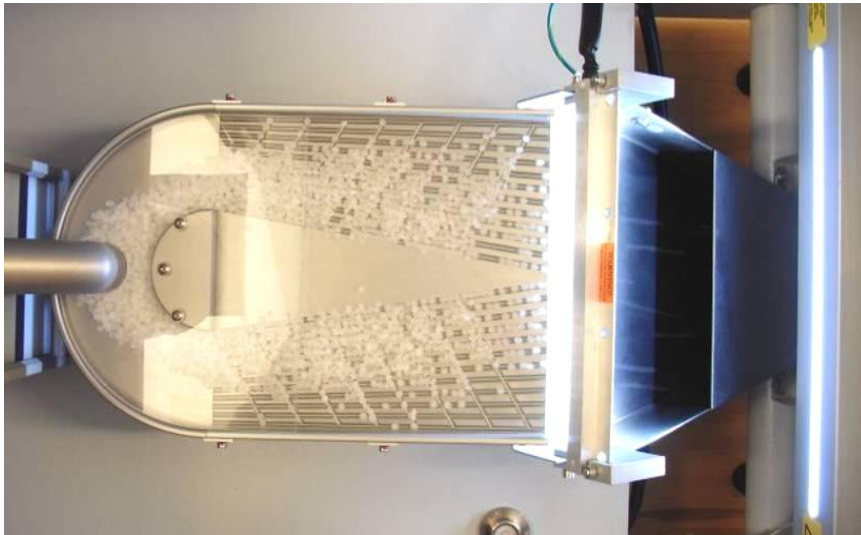


**Figure 6.11** – Transporting vibrating channels

## 6.2 Results Laboratory Analysis

### 6.2.1 Coefficient of Restitution

The method used to determine the coefficient of restitution was proved to be very reliable according to Gage R&R. The results for the coefficient of restitution for the two polymers to be further investigated in this work are shown in Table 6.2 below. All the test results and Gage R&R results are listed in Appendix A.

**Table 6.2** – Coefficient of restitution

Polymer	Average $\frac{h_2}{h_1}$ for the tests	Average Coefficient of Restitution $\sqrt{\frac{h_2}{h_1}}$ for the tests
mPE	0.234	0.484
PP	0.203	0.451

### 6.2.2 Coefficient of Static Friction

This method was also proven to be reliable according to Gage R&R. The results were similar both for the different samples and operators. However, using this method for measuring the static friction between polymers, leads to changes in the surface roughness when preparing the test samples which might have an impact on the results.

The results for the static friction between pellets are shown in Table 6.3 below and the static friction between the pellets and the wall are shown in Table 6.4. All the test results and Gage R&R results are listed in Appendix A.

**Table 6.3** – Coefficient of static friction between polymers

<b>Polymer</b>	<b>Average minimum for the tests</b>	<b>Average mean for the tests</b>	<b>Average maximum for the tests</b>
mPE	0.60	0.72	0.85
PP	0.49	0.62	0.84

**Table 6.4** – Coefficient of static friction between polymer and glass wall

<b>Polymer</b>	<b>Average minimum for the tests</b>	<b>Average mean for the tests</b>
mPE	0.47	0.60
PP	0.38	0.48

### 6.2.3 Pellet Size and Shape Distribution – PSSD

Table 6.5 and Table 6.6 below shows the size distribution results from the PSSD analysis.

**Table 6.5 – mPE**

	<b>Ø – Particle size</b>	<b>4.08 mm</b>
	<b>Particle standard deviation</b>	0.36 mm
<b>Size (µm)</b>	<b>Total</b>	<b>Total (%)</b>
0 – 1600	128	0.38
1600 – 2400	2	0.01
2400 – 2800	6	0.02
2800 – 3500	562	1.67
3500 – 3900	8083	24.09
3900 – 4300	16147	48.12
4300 – 4700	8460	25.21
4700 – 5100	149	0.44
>5100	20	0.06
<b>Total</b>	<b>33557</b>	<b>100</b>

**Table 6.6 – PP**

	<b>Ø – Particle size</b>	<b>3.76 mm</b>
	<b>Particle standard deviation</b>	0.52 mm
<b>Size (µm)</b>	<b>Total</b>	<b>Total (%)</b>
0 – 1600	51	0.14
1600 – 2400	424	1.14
2400 – 2800	1286	3.45
2800 – 3500	8184	21.93
3500 – 3900	11197	30
3900 – 4300	11651	31.22
4300 – 4700	4241	11.36
4700 – 5100	123	0.33
>5100	165	0.44
<b>Total</b>	<b>37322</b>	<b>100</b>

## 7. Practical Tests

---

*This chapter explains how the practical tests were set up and how they were reviewed.*

To verify the computer based simulations, practical tests were conducted. For these tests two different 1000 ml glass flasks<sup>21</sup>, Hopper 1 and Hopper 2, with the bottom cut out were used to mimic a hopper (Figure 7.1). The two glass hoppers had distinct variations in geometry such as wall angle and outlet size (Appendix E). Models of these glass hoppers were then created in Pro/ENGINEER<sup>22</sup> to be used for the computer based simulations.



**Figure 7.1** – Glass hopper used for practical tests

There are a number of reasons why these glass hoppers were used instead of a full-size hopper. The main reason was to reduce the simulation time. Due to its size, a full-size hopper contains millions of particles and it may take several months to complete a simulation; whereas the glass hoppers hold approximately 15,000, significantly reducing simulation times. Another advantage to using glass hoppers is its transparency, which allows for direct observation of particle movement in the

---

<sup>21</sup> Schott AG, Jena Glass, Duran 50, Mainz, Germany

<sup>22</sup> Pro/ENGINEER is a parametric, integrated CAD/CAM/CAE software, developed by Parametric Technology Corporation (PTC), Needham, Massachusetts, USA

flask. Furthermore, because the glass hopper and the full-size hopper share similar physical geometry, adjustments can be made to the simulation parameters to achieve the same effect as in a real hopper.

## 7.1 Setup

To perform the tests a test rig was set up. The glass hopper was placed in a stand and a camcorder was setup to record the process. A container was placed below the hopper to collect the pellets after being emptied to ensure that the same number of pellets was used for the following tests (Figure 7.2). During the filling of the hopper a steel ruler was used to block the outlet to prevent the pellets from exiting. The ruler was then quickly removed to start the emptying process.

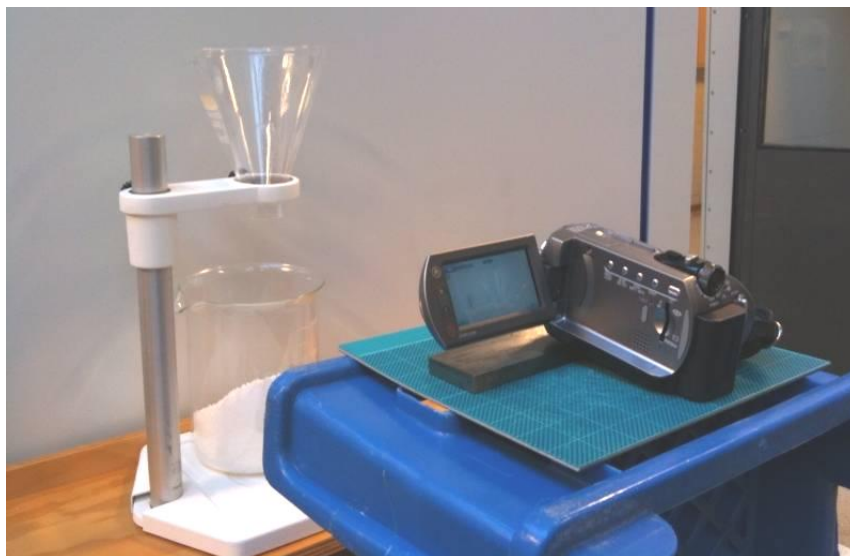


Figure 7.2 – Test setup

## 7.2 Methods

### 7.2.1 Time to Empty

Three tests were conducted on each hopper and polymer type to determine the time to empty them. This was done by filling the hoppers with pellets and then removing the ruler from the outlet to empty them (Figure 7.3). The process was recorded on video and analyzed to determine the exact time for emptying.





**Figure 7.3** – Filled hopper

### 7.2.2 Flow Pattern – Top View

To distinguish the flow pattern, the pellets were color coded and divided into sections at the top of the hoppers (Figure 7.4). The emptying process was video recorded from the top of the hoppers to capture the flow pattern.

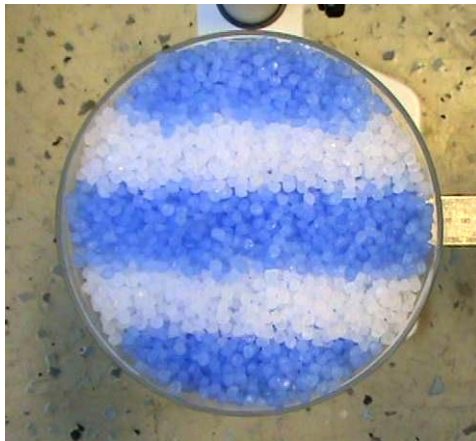


**Figure 7.4** – Color coded – Top view

### 7.2.3 Flow Pattern – Side View

This test involved color coding where the pellets are positioned in horizontal layers, the emptying process was recorded from the side (Figure 7.5).

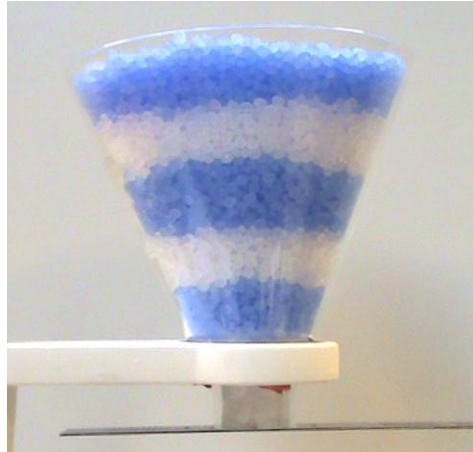


**Figure 7.5** – Color coded – Side view

## 7.3 Test Listing

Practical tests were completed using two different polymer types, mPE and PP, in both hopper geometries.

**Table 7.1** – Practical tests conducted

	Geometry	Polymer	Time to Empty	Flow Pattern Top	Flow Pattern Side
<b>Practical test 1</b>	Hopper 1	mPE	X	X	X
<b>Practical test 2</b>	Hopper 2	mPE	X	X	
<b>Practical test 3</b>	Hopper 1	PP	X	X	
<b>Practical test 4</b>	Hopper 2	PP	X	X	

## 8. Computer Based Simulations

---

*This chapter explains how the computer based simulations are set up and declares all the parameters and simulation settings used.*

### 8.1 EDEM User Interface [29]

EDEM consists of three main components; Creator, Simulator and Analyst. First the simulation model is setup in the Creator, then the Simulator runs the simulation and the Analyst is where the results are reviewed.

#### 8.1.1 EDEM Creator

##### **Step 1: Set the Global Model Parameters**

The first step in creating a model is to set the units used throughout EDEM.

The second step is to set the contact models to describe the interaction between particle-particle and particle-geometry.

Next, the gravity and the materials are defined. Every particle or section of geometry used in a model is made of a particular material. All materials and the interactions between them must be defined in the materials section. The gravity is set in x, y or z direction, positive or negative. Materials can be created directly or imported from the EDEM material database. EDEM's material database contains material data for the most common materials. If the material of interest is not specified in the database it can easily be created and material properties are set manually. The material data needed are; Poisson's ratio, Shear Modulus and Density.

After defining the materials the interactions between them are defined. Three parameters are used in EDEM to describe how materials interact; coefficient of restitution, coefficient of static friction and coefficient of rolling friction. These three parameters have to be set for all the materials that will interact during the simulation.

##### **Step 2: Define the Base Particles**

The next step is to define the base particle. All the particles used in a model are defined in the particles pane. These are the base or the prototype particles on which the rest of the particles are based upon when created. Particles are made up of one or more spherical surfaces. The radii of these spherical surfaces are set and the particle properties such as; mass, volume and the moment of inertia for the x, y and z direction are calculated based on the particle material, size and shape.

### **Step 3: Define the Geometry and Domain**

The geometry is the physical body the particles interact with. Geometries are defined as sections and can either be imported from a CAD package or defined in EDEM. In EDEM simple sections can be defined as a box, cylinder or as an n-sided polygon. Sections of geometry can be static or dynamic. Static sections stay in a fixed position throughout the simulation whereas dynamic sections move. Dynamic sections can move under translation or rotation by linear or sinusoidal motion.

The domain is the area in which the simulation occurs. In EDEM the domain is represented by a red box and its size and position can be set either manually or automatically to fit the geometry. Periodic boundaries in the x, y or z direction can also be set in this section. This determines what happens to a particle once it leaves the domain. If enabled, any particle leaving the domain in that direction will instantly reenter it on the opposite side.

### **Step 4: Create the Particle Factories**

A particle factory defines where, when, and how particles appear in the simulation. Particles are created within one of the defined geometries, either in a geometry included in the simulation, or one that is created specifically for producing particles.

The particle factories can be dynamic or static. Dynamic factories will make a specified number of attempts to create the amount of particles set while a static will only make one attempt to create the set number of particles. If there is not enough room at that point to create all the particles, the static will not retry to create those particles while the dynamic will.

The total number of particles to create in the factory is specified, as well as the creation rate (particles/s). A start time for the creation and the maximum attempts (dynamic only) to create particles are also set.

Last the parameters of the particles are specified such as size distribution, velocity, angular velocity, orientation etc.

#### **8.1.2 EDEM Simulator**

Once the model is set-up in EDEM Creator, the simulation is run in EDEM Simulator.

### **Step 1: Set the Time-step and Simulation Time**

The first step in the simulator is to set the time-step and simulation time. The time-step is the amount of time between iterations. EDEM suggests an idealized DEM time-step, a Rayleigh time-step, defined as the time taken for a shear wave to

propagate through a solid particle. A time-step is then chosen as a percentage of the Rayleigh time-step, between 5% and 40% should ensure a stable simulation. For simulations with densely packed particles, such as the ones in this work, a time-step of 20% or less is recommended.

If the time-step is too large, particles can behave erratically. For example, if two particles are moving towards each other at time-step 1 with some distance apart, if the time-step is too long, when the position is recalculated at time-step 2 they may be overlapping a lot. The particle forces and energies are recalculated at this point, and will due to the large overlap be very large. This in turn will result in large and incorrect velocities of the particles in time-step 3.

After setting the time-step the total simulation time is set. The simulation time is the amount of real time the simulation represents.

### **Step 2: Define the Grid Size**

To detect contacts between particles EDEM divides the domain into grid cells. The size of these grid cells needs to be specified.

The detection of contacts is the main computational challenge in DEM. By dividing the domain into grid cells, the simulator can check each cell and analyze only those that contain two or more particles, and therefore can contain a possible contact, thus reducing process time. The results from the simulation are not affected by the grid size, only the time taken to reach them.

The fewer particles per grid cell, the more efficient the simulator is. The idealized grid size is  $2R_{\min}$  where  $R_{\min}$  is the minimum base particle radius in the simulation.

### **Step 3: Start the Simulation**

The simulation can be stopped and restarted at any point without losing calculated data.

#### **8.1.3 Analyzing the Simulation**

The EDEM Analyst is the post-processor used to review the results of the simulation. Here the simulation can be played back as an animation, the results can be graphed, videos created or data exported for examination elsewhere.

There is endless information to be gathered in the Analyst section. The information of interest in this work is explained in the Results section of this report.

## 8.2 Simulation Setup

The following simulation settings and material properties have been kept constant throughout all the simulations conducted in this work.

### 8.2.1 Contact Model

The most common contact models used in DEM are the Hertz-Mindlin together with a Linear Spring model. The contact model used for all the simulations in this work is the Hertz-Mindlin model.

The Linear Spring is generally a quicker model to run because of the reduction in number of calculations required, however whilst the qualitative particle behavior is comparable to the Hertz-Mindlin model, the actual values for the forces, velocities etc. can vary due to the simplifications in the model. If a quantitative evaluation of a simulation is required, using the Hertz-Mindlin model is preferable<sup>23</sup>.

### 8.2.2 Material Properties and Particle Size

**Table 8.1** – Material Properties

	<b>Glass hopper</b>	<b>mPE</b>	<b>PP</b>
Poisson's ratio	0.19	0.30	0.30
Density (kg/m <sup>3</sup> )	2180	911	910

**Table 8.2** – Particle size

	<b>Base particle radius (mm)</b>	<b>Normalized mean value</b>	<b>Normalized standard deviation</b>
mPE	2.04	1	0.088235
PP	1.88	1	0.138298

---

<sup>23</sup> DEM-solutions' technical support

### 8.2.3 Simulation Settings

For all the simulations the fixed time step was set to 20% and the grid size was set to  $2R_{\min}$ . According to DEM Solutions these are appropriate values for these types of simulations.

Each simulation starts with a filling procedure where the hopper is filled with a number of particles. For this the hopper outlet is closed by modeling a temporary lid to keep the particles from exiting. The lid is then removed first when the particles have settled under gravity. The time for the particles to settle is dependent on the number of particles in the simulation and where the particle factory is positioned. Hence, the time when the lid is removed varies and is specified for each simulation. The lid is removed by assigning it a translational velocity with a time to start and a time to end the motion.

### 8.3 Simulation 1 – Hopper 1, mPE

The first hopper simulation was conducted with the parameter values from the laboratory analysis, estimated values and values based on literature research. When filling the hopper the particles were created by dynamic factories. This was done in four steps to let the particles have a chance to settle under gravity between each filling. The particles created by the first factories have a greater distance to travel, hence a greater initial velocity was applied to them. The lid was then removed after two seconds allowing all the particles to settle. This simulation was then compared to practical test 1, where the time to empty and the flow pattern was compared.

**Table 8.3 – Particle factory**

Particle factory	Amount	Velocity (m/s)	Creation rate (particles/s)	Start time (s)	Type
1	9000	0.5	100000	0	Dynamic
2	2000	0.5	100000	0.2	Dynamic
3	2000	0.1	100000	0.4	Dynamic
4	500	0.1	100000	0.7	Dynamic

**Table 8.4 – Remove lid**

Start (s)	End (s)	Velocity (m/s)
2	2.01	4



**Table 8.5 – Material properties**

	<b>Glass</b>	<b>Polymer</b>
Shear modulus (GPa)	28.0 <sup>24</sup>	0.117 <sup>25</sup>
Moment of inertia (kgm <sup>2</sup> )	-	5.393E-11 <sup>26</sup>

**Table 8.6 – Coefficients**

	<b>Particle – Wall</b>	<b>Particle – Particle</b>
Coefficient of restitution	0.48 <sup>27</sup>	0.5 <sup>28</sup>
Coefficient of static friction	0.3 <sup>28</sup>	0.72 <sup>27</sup>
Coefficient of rolling friction	0.01 <sup>28</sup>	0.01 <sup>28</sup>

---

<sup>24</sup> MatWeb, [www.matweb.com](http://www.matweb.com)

<sup>25</sup> Cambridge Encyclopedia, <http://encyclopedia.stateuniversity.com>

<sup>26</sup> Calculated by EDEM (based on the spherical shape used in the model)

<sup>27</sup> Measured (see chapter 6)

<sup>28</sup> Estimated

## 8.4 Sensitivity Analysis – Design of Experiments

### 8.4.1 Theory [30]

Design of Experiments (DoE) is a way of ensuring that the selected experiments produce the maximum amount of relevant information. The traditional method of performing tests is called the Cost approach and changes only one factor at a time, which in most cases leads to more tests run to gain the same amount of information as DoE. DoE approach is to change several relevant factors simultaneously. It has been proven that this way of performing tests makes it easier to reach optimum conditions. This allows you to widely understand how your factors behave and interact with each other.

Input information is factors, response and objective. Once the data has been collected it is analyzed and a DoE model is constructed.

### 8.4.2 Sensitivity Analysis [30]

MODDE<sup>29</sup> was used to generate the DoE model for the sensitivity analysis. A fractional factorial design with resolution IV, supporting a linear model, was used in the screening of the input parameters. The objective was to determine the magnitude and range by which the input parameters affect the responses and to see how the input parameters are correlated.

Input parameters:

- Particle – Particle {
  - Coefficient of static friction (SFI)
  - Coefficient of rolling friction (RFI)
  - Coefficient of restitution (REI)
  
- Particle – Wall {
  - Coefficient of static friction (SFW)
  - Coefficient of rolling friction (RFW)
  - Coefficient of restitution (REW)
  
- Shear Modulus (SM)
- Moment of inertia (I)

---

<sup>29</sup> MODDE is a program for Design of Experiments and Optimization developed by UMETRICS, Umeå, Sweden

To determine the min and max values for some coefficients, previous investigations of the material properties (chapter 6) were taken into account. For these simulations spherical particles were used even though the particles have a different shape in reality. To account for these differences and the effects from them, moment of inertia and coefficient of rolling friction were investigated in the sensitivity analysis. Adjusting them could compensate for the use of spherical particles.

According to John Favier<sup>30</sup> the shear modulus of the particle has a great impact on the simulation time. Therefore this parameter was investigated to see if it affected the simulation result.

The responses chosen to be investigated are:

- Time to empty (s)
- Simulation time (h)
- Discharge rate (m/s)
- Average velocity along wall (m/s)
- Average velocity center (m/s)

After selecting the input parameters and response, MODDE gives you a list of experiments you have to run to complete the DoE model. The DoE list contains different combinations of min, mid and max values of the input parameters.

---

<sup>30</sup> John Favier, CEO of DEM Solutions

### 8.4.3 Simulation Setup - DoE

17 different simulations were conducted to complete the model. To reduce the simulation time the hopper was filled with 5000 particles for these 17 simulations. A dynamic factory with a specified creation rate was used to create the particles (Table 8.7). The particle size was set to the normal distribution received from the PSSD test, with a normalized mean radius and a standard deviation.

**Table 8.7** – Factory

<b>Particle factory</b>	<b>Amount</b>	<b>Velocity (m/s)</b>	<b>Creation rate (particles/s)</b>	<b>Start time (s)</b>	<b>Type</b>
1	5000	0.5	100000	0	Dynamic

**Table 8.8** – Remove lid

<b>Start time (s)</b>	<b>End time (s)</b>	<b>Velocity (m/s)</b>
0.3	0.31	4

### 8.4.4 Simulations

17 different simulations were conducted on the model representing Hopper 1, with the settings presented in Appendix B. All the other settings were kept constant.

## 8.5 Sensitivity Analysis – Simulation Time

To determine how the amount of particles affects the simulation time, a number of simulations with various amounts of particles were conducted. To save time, simulation 1 was included in this sensitivity analysis where the hopper was filled to its limit. All the settings from simulation 1 were applied to the other four simulations conducted in this sensitivity analysis and only the number of particles was changed.

**Table 8.9** – Simulations to run

<b>Nr</b>	<b>Particles</b>	<b>Remove Lid (s)</b>
1	1000	0.3
2	2000	0.3
3	4000	0.3
4	8000	0.3
5	13500	2.0

## 8.6 Simulation 2 – Hopper 1, mPE

In the second hopper simulation the parameters were adjusted from simulation 1 to match the results from practical test 1. The sensitivity analysis showed that the coefficients of restitution and the rolling frictions had little or no influence on the responses. The shear modulus was shown to have a major impact on the simulation time, but no significant influence on the simulation results. Due to this, the shear modulus was kept to a minimum to save simulation time, the rolling frictions and the coefficients of restitution, which did not affect the results, was set to the mid values retrieved from the sensitivity analysis.

The coefficients of static friction (wall and internal), which were shown to have a significant influence on the results, were set to the measured values from the laboratory analysis. The last parameter, the moment of inertia, was predicted in MODDE to  $1.1E-9 \text{ kgm}^2$  by setting the desired discharge rate needed for the time to empty to match the practical test. Based on the simulation result with this predicted value another three simulations were conducted before a representable value of the moment of inertia was found.

Due to the larger moment of inertia used in this simulation the consolidation of the particles is lower. This in turn means that fewer particles fit in the hopper. The number of particles created by factory 3 was therefore reduced from 2000 to 1500.

**Table 8.10** – Particle factory

Particle factory	Amount	Velocity (m/s)	Creation rate (particles/s)	Start time (s)	Type
1	9000	0.5	100000	0	Dynamic
2	2000	0.5	100000	0.2	Dynamic
3	1500	0.1	100000	0.4	Dynamic
4	500	0.1	100000	0.7	Dynamic

**Table 8.11** – Remove lid

Start (s)	End (s)	Velocity (m/s)
2	2.01	4

**Table 8.12** – Material properties

	<b>Glass</b>	<b>Polymer</b>
Shear modulus (GPa)	28.0	0.001 <sup>31</sup>
Moment of inertia (kgm <sup>2</sup> )		
- Simulation 2.1	-	1.1E-09
- Simulation 2.2	-	5.0E-10
- Simulation 2.3	-	3.0E-10
- Simulation 2.4	-	2.0E-10

**Table 8.13** – Coefficients

	<b>Particle – Wall</b>	<b>Particle – Particle</b>
Coefficient of restitution	0.45	0.45
Coefficient of static friction	0.6	0.72
Coefficient of rolling friction	0.0275	0.0275

---

<sup>31</sup> Minimum shear modulus allowed in EDEM

### **8.7 Simulation 3 – Hopper 2, mPE**

Once all the parameters were adjusted so that the results from Simulation 2 corresponded with the results from the practical test, these exact parameters were used in a simulation involving the second hopper geometry, with steeper walls and a larger outlet. If the parameters are representable, they should provide good results for Hopper 2 as well and match the results from the practical tests made on this hopper geometry. All the simulation settings are identical with the ones in simulation 2, only the hopper geometry is different.



### 8.8 Simulation 4 – Hopper 1, PP

Another polymer type different from mPE was tested to further evaluate the simulation model. The coefficients of static friction were compiled from practical tests and the parameters that did not affect the DoE responses were set to the mid values. To find a representable moment of inertia for this polymer, simulations were conducted until the result corresponded with the practical tests. The final moment of inertia of  $2.0E-10 \text{ kgm}^2$  from the simulations representing the mPE pellets was used in this simulation as a starting point.

**Table 8.14** – Particle factory

Particle factory	Amount	Velocity (m/s)	Creation rate (particles/s)	Start time (s)	Type
1	9000	0.5	100000	0	Dynamic
2	3000	0.5	100000	0.2	Dynamic
3	3000	0.1	100000	0.4	Dynamic
4	3000	0.1	100000	0.7	Dynamic
5	1000	0.1	100000	1.0	Dynamic

**Table 8.15** – Remove lid

Start (s)	End (s)	Velocity (m/s)
2	2.01	4

**Table 8.16** – Material properties

	<b>Glass</b>	<b>Polymer</b>
Shear modulus (GPa)	28.0	0.001
Moment of inertia (kgm <sup>2</sup> )		
- Simulation 4.1	-	2.0E-10
- Simulation 4.2	-	1.0E-11

**Table 8.17** – Coefficients

	<b>Particle – Wall</b>	<b>Particle – Particle</b>
Coefficient of restitution	0.45	0.45
Coefficient of static friction	0.48	0.62
Coefficient of rolling friction	0.0275	0.0275

### **8.9 Simulation 5 – Hopper 2, PP**

All the simulation settings are identical with the ones in simulation 4, only the hopper geometry is different. If the parameters are representable, they should also provide good results for hopper 2 and match the results from the practical tests made on this hopper geometry.



## 9. Results

---

*In this chapter all the results from the practical tests and the computer based simulations are presented and evaluated.*

### 9.1 Practical Test 1 and Simulation 1

#### 9.1.1 Time to Empty

After analyzing the videos recorded from the first practical test the time to empty hopper 1 with the mPE polymer was determined (Table 9.1).

**Table 9.1** – Time to empty hopper 1 with mPE

Test	Time to empty (s)
1	6.21
2	6.25
3	6.25

The result from the first simulation was shown not to be accurate when it comes to time to empty. In this simulation that time was 4.54 s which is approximately a 27% deviation from the mean value 6.25 s from the practical test.

#### Comments

For the first simulation the measured values from the laboratory analysis were used for the coefficient of static friction and the coefficient of restitution while the rolling friction was estimated. One reason why the results do not correlate could be that this estimation is incorrect. Another reason could be that whilst experimental measured parameter values provide a good starting point, directly applying the measured parameters can produce disappointing results in DEM.

The reason for this is that DEM is an approximation of real-life. Some factors may not be considered in the contact model such as permanent deformation or surface roughness. Another factor that is not implemented in the model is the exact shape of

the particles<sup>32</sup>. Only spherical particles are modeled in DEM because of the complexity in the mathematical models for non-spherical particles that would be very time consuming to solve.

Due to this inaccuracy in the first simulation it was decided to investigate what parameters that influence the time to empty the hopper in a sensitivity analysis.

#### 9.1.2 Flow Pattern – Center Plane

During the emptying of the hopper a pit emerges in the center of the hopper where the particles have a higher downward velocity than those along the wall. However, the pit emerging in the practical test seemed deeper than that in the simulation (Figure 9.1). The particles tend to roll faster towards the center in the simulation refilling the pit created there. The reason for this is most likely because the mathematical model used in EDEM is based on spherical particles and the particles therefore roll easier towards the center than the non-spherical particles in reality. (The particles in the figures are just a visual representation of the particle geometry; all calculations are based on spheres).

---

<sup>32</sup> Calibration of DEM Parameters, David Curry, Senior Consulting Engineer, DEM Solutions

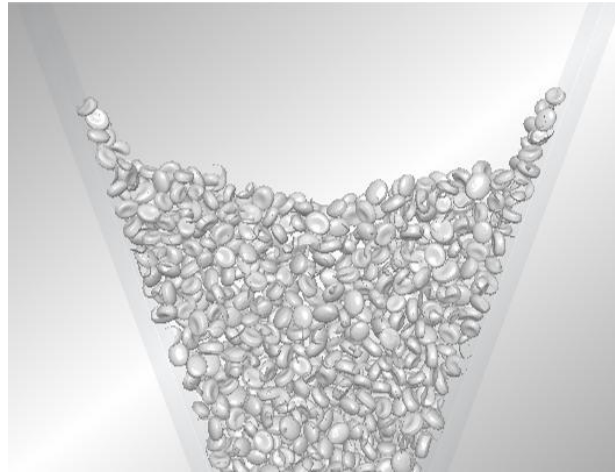


**Figure 9.1** – Flow pattern - center plane



**Figure 9.2** – Pit emerging in center

## 9.2 Sensitivity Analysis – Design of Experiments

### 9.2.1 Reviewing the DoE Simulation Results

When reviewing the simulation results for average velocity along wall and center geometry bins were used. One bin was placed in the center of the hopper and two bins along the wall (Figure 9.3). The center bin had a depth and width of two particle diameters and the wall bins had the same depth but only the width of one particle diameter. By this the wall bins have the same volume together as the center bin alone. The bins were strategically placed in the glass hopper where the velocities are at a steady state. To determine the average velocities in these bins, the velocities at ten time steps were measured. These ten time steps were evenly distributed from the first time step shortly after the flow initiated and the last when the particle level reached the bottom of the bins. All the velocities were measured in downward direction, and for the wall bins the velocities were recalculated to the wall direction. The raw data from the measurements are presented in Appendix C. The other responses time to empty, simulation time and discharge rate were given directly from the program.

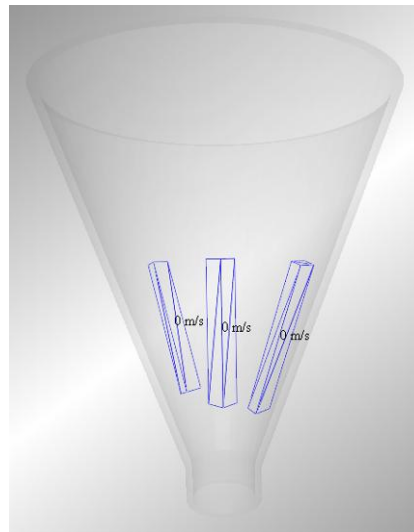


**Figure 9.3** – Geometry bins to measure velocities

The response results from the sensitivity analysis were imported to MODDE as additional information to analyze the model. MODDE creates diagrams of each response showing how the input parameters affect this. These diagrams are presented in Appendix B.



### 9.2.2 Analyzing the DoE Model

The diagrams showed that the moment of inertia and the coefficients of static friction (wall and internal) had a significant influence on the responses; time to empty, discharge rate and average velocity along wall and center. Meanwhile the other parameters had little or no influence at all. These parameters were removed from the model one at a time to investigate if this changed the influence of the remaining parameters. The summary of fit after the removal is presented in Figure 9.4.

**Summary of fit**

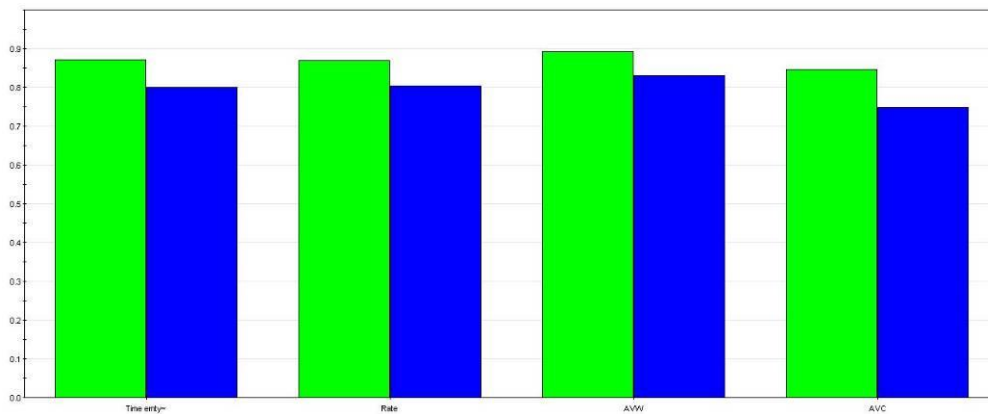


**Figure 9.4** – From left: Time to empty, Discharge rate, Average velocity along wall and center

Where the left bar R2, illustrates the goodness of fit describing the reliability of the model and the right bar Q2 is the goodness of prediction, the ability of the model to predict.

The figures below show the parameters effect on respective response, after the removal of the non affecting parameters. Figures before the removal are presented in Appendix B.

### Time to empty

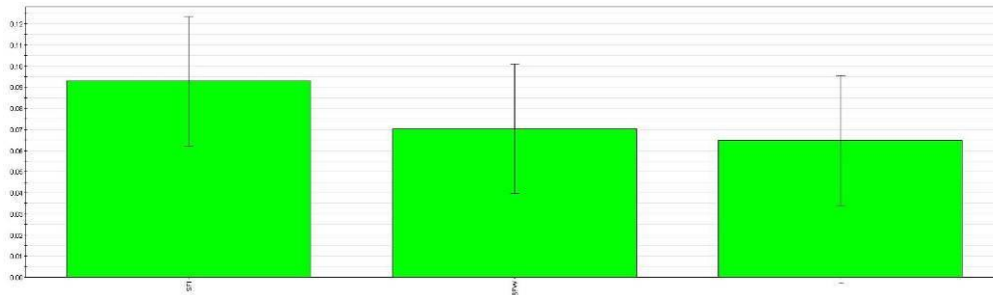


**Figure 9.5** – Left: SFI, middle: SFW and right: I

### Average velocity along center

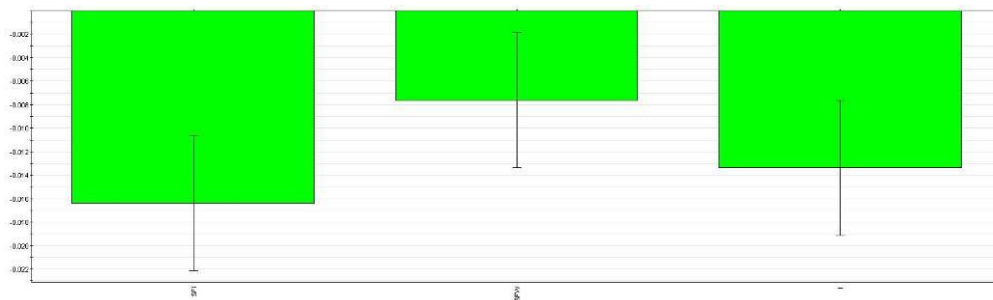


**Figure 9.6** – Left: SFI, middle: SFW and right: I

### Average velocity along wall

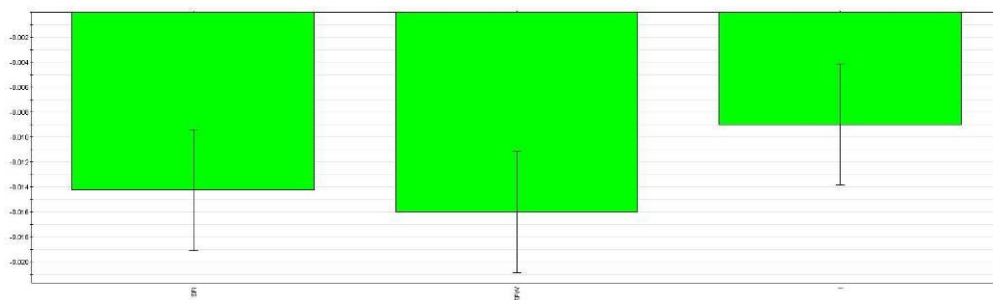


**Figure 9.7** – Left: SFI, middle: SFW and right: I

The results also showed that only the shear modulus had a significant influence on the simulation time.

### **Comments**

Since the shear modulus only affected the simulation time and none of the other responses, to save time, it will be kept to a minimum value in further simulations. For the coefficients of static friction (wall and internal) the measured values from the laboratory analyses will be used and the parameters that did not influence the simulation results will be set to the mid values from this sensitivity analysis. Furthermore, the moment of inertia will be adjusted to compensate for the inaccuracies in the simulation model.

### 9.3 Sensitivity Analysis – Simulation Time

The simulation time is highly dependent on the number of particles in the simulation. Table 9.2 and Figure 9.8 below show how the simulation time increases exponentially with the number of particles.

**Table 9.2** – Simulation time

Nr	Particles	Simulation time (h)
1	1000	0,16
2	2000	0,4
3	4000	1,26
4	8000	4,36
5	13500	20,3

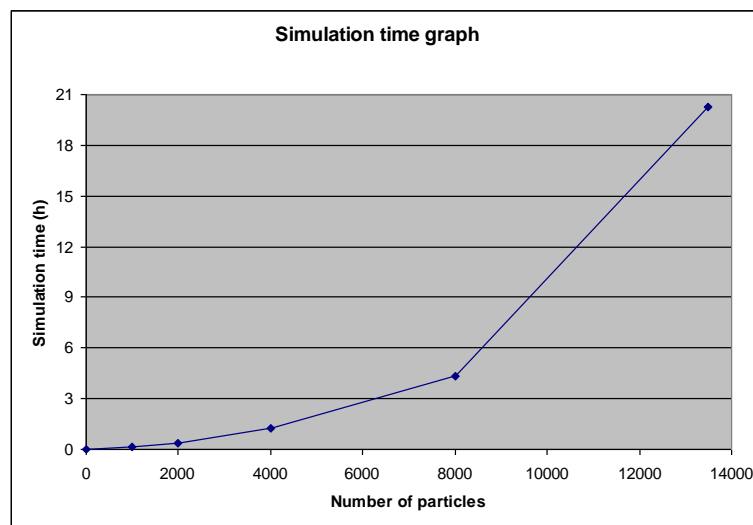


**Figure 9.8** – Simulation time graph

## **Comments**

It is clear that completing simulations on a full-size hopper that contains millions of particles would be very time consuming. Instead a slice or a small section could be simulated to represent a full-size hopper. For this it would first have to be investigated what size this slice or section should be to be representative for the hopper.

## 9.4 Practical Test 1 and Simulation 2

### 9.4.1 Time to Empty

Four simulations were conducted before an acceptable deviation from the practical test was reached (Table 9.3). The predicted value for the moment of inertia generated by MODDE did not give a result matching the practical test. Another three simulations were conducted, based on this result, before the target of 6.25 s to empty the hopper was within an acceptable range.

**Table 9.3** – Results from simulations

<b>Simulation</b>	<b>Moment of inertia (kgm<sup>2</sup>)</b>	<b>Time to empty (s)</b>	<b>Deviation (%)</b>
2.1	1.1E-09	7.46	19.4
2.2	5.0E-10	6.90	10.4
2.3	3.0E-10	6.36	1.76
2.4	2.0E-10	6.18	1.12

Table 9.3 above shows that a moment of inertia of 2.0E-10 kgm<sup>2</sup> results in a time to empty of 6.18 s which is only a 1.12 % deviation from the mean value 6.25 s from the practical test. This is well within the limits for an acceptable simulation result.

### Comments

By keeping the parameters that was shown to have no impact on the result fixed and fixing the coefficients of static friction to the measured values, the moment of inertia could be adjusted so that the result from the simulation corresponded with the result from the practical test. By increasing the moment of inertia, compensation is made for the inaccuracies in the simulation such as the shape of the particles, possible variations in surface roughness of both particles and geometry, and other approximations in the model. The moment of inertia is directly related to the density, size and shape of the particles.

#### 9.4.2 Flow Pattern – Top View

The flow pattern with color coded pellets viewed from top presented in Figure 9.9 below was also corresponding well with the practical test.

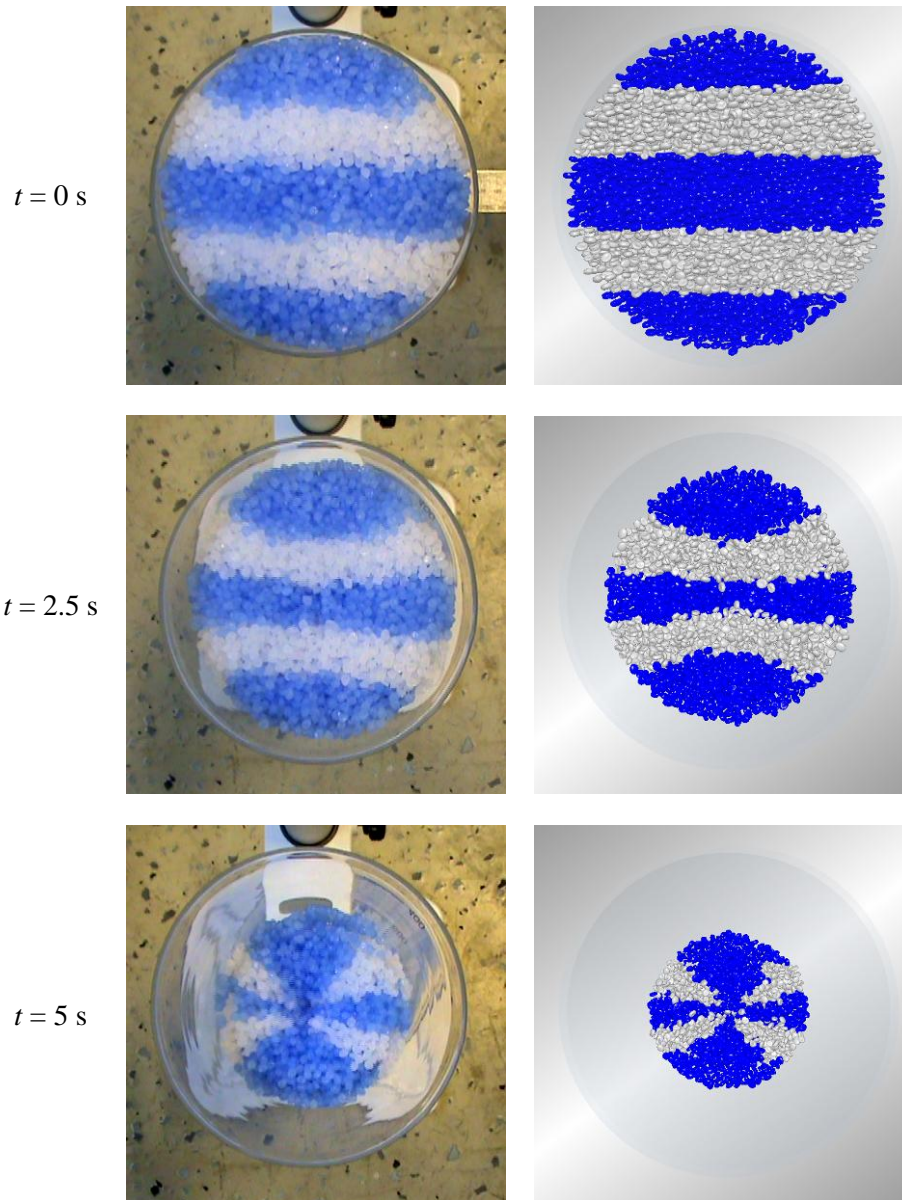


**Figure 9.9** – Flow pattern - top view

### **Comments**

The pattern that occurs is caused by the velocity differences of the particles in the center and those along the wall. This creates a pit in the center where the particles have a higher downward velocity, causing the particles on top move towards the center.



### 9.4.3 Flow Pattern – Side View



**Figure 9.10** – Flow pattern - side view

## **Comments**

Even though these results are similar, differences can be seen between the two. During the practical tests variations between tests were noticed. The flow pattern was not exactly the same for every test run. One reason for this is that all the particles do not have the exact same properties. Variations in shape and surface roughness do occur between particles in real-life causing differences between the tests, while in the simulation all the particles are exactly the same when it comes to these properties. Another reason could be variations in the surface roughness of the glass hopper which affects the friction between the particles and the wall leading to inconsistent velocities along the wall.

Due to these reasons this method of verifying the simulations was discarded.

### **9.4.4 Flow Pattern – Center Plane**

The pit emerging in the center during emptying also corresponds better with the practical tests for this simulation. The pattern was very similar to the practical tests with some particles piled up against the wall and a noticeably deep pit in the center (Figure 9.11 & Figure 9.12).

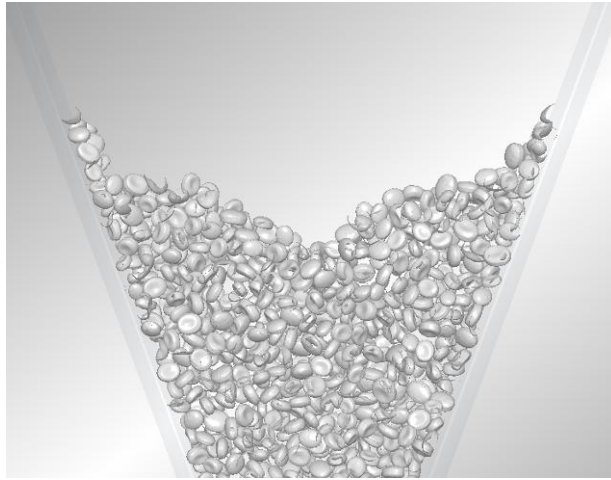


**Figure 9.11** – Flow pattern - center plane



**Figure 9.12** – Pit emerging in center

The flow pattern along the center plane of the hopper with color coded pellets is presented in Figure 9.13. No comparison is made between simulations and practical tests because of the difficulties to investigate this practically. It is however clear that the particles are moving faster along the center than along the walls.

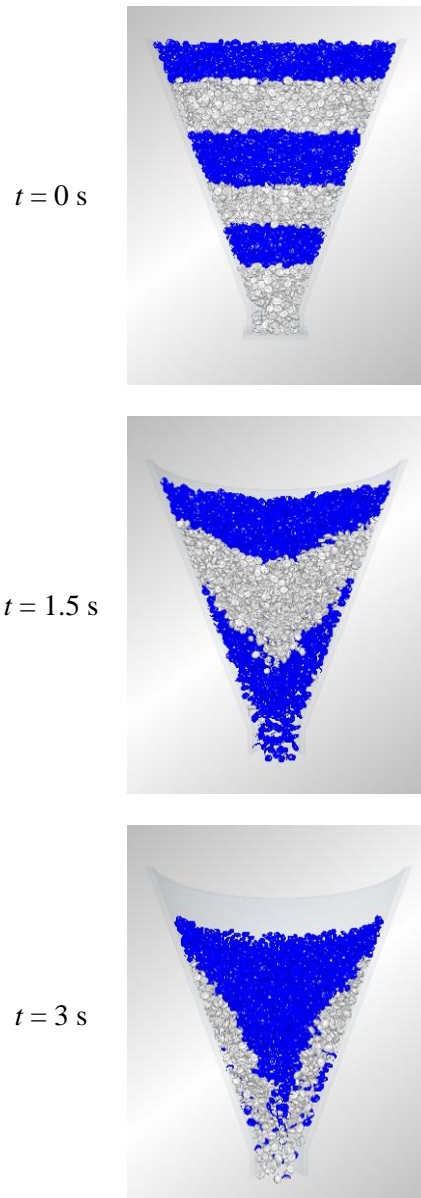


**Figure 9.13** – Flow pattern - center plane

## 9.5 Practical Test 2 and Simulation 3

### 9.5.1 Time to Empty

After analyzing the videos recorded from the practical tests the time to empty hopper 2 with the mPE polymer was determined (Table 9.4).

**Table 9.4** – Time to empty hopper 2 with mPE

<b>Test</b>	<b>Time to empty (s)</b>
1	1.88
2	1.88
3	1.96

The moment of inertia of  $2.0E-10$  proved to give good results in this geometry as well. In the simulation the time to empty was 1.95 s which is a 3.72 % deviation from the mean value 1.88 s from the practical test.

### 9.5.2 Flow Pattern – Top View

The flow pattern with color coded pellets viewed from top presented in Figure 9.14 below, was just like in the previous simulation corresponding well with the practical test.

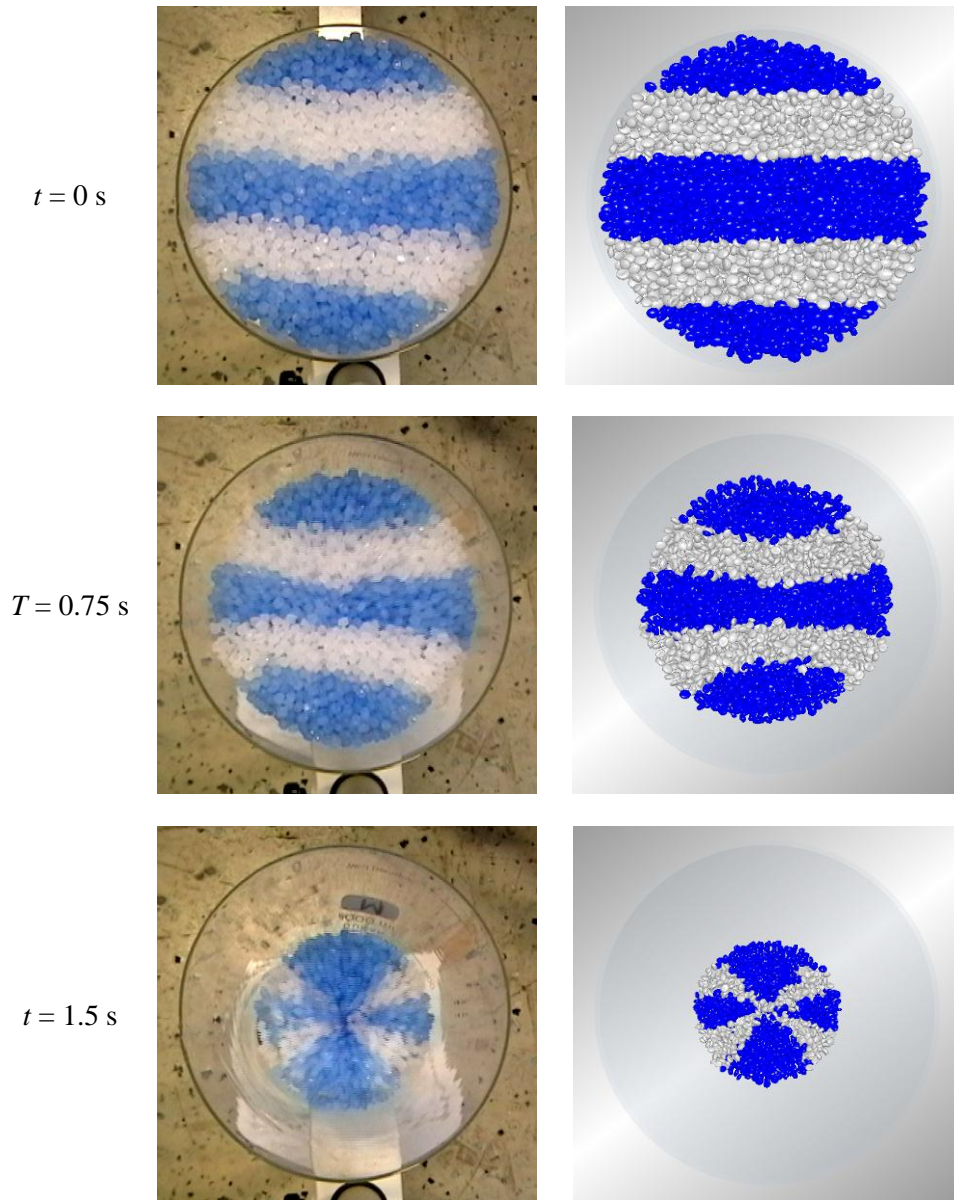


**Figure 9.14** – Flow pattern - top view

## **Comments**

This flow pattern seems to occur in every simulation and was not be used as a way of verifying the results in any further simulations. It has however shown that the simulations are accurate in terms of this flow pattern.

### 9.5.3 Flow Pattern – Center Plane

Also the flow pattern when it comes to the depth of the pit in the center is corresponding well in this simulation. The pit was slightly shallower than the one emerging in hopper 1, which matches the observations made during the practical test.

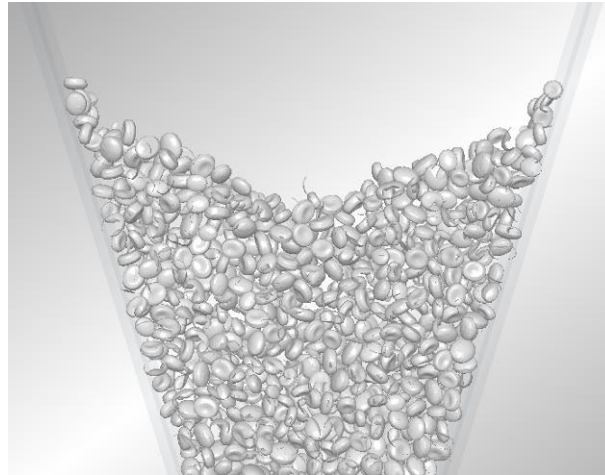


**Figure 9.15** – Flow Pattern - center plane



**Figure 9.16** – Pit emerging in center



## 9.6 Practical Test 3 and Simulation 4

### 9.6.1 Time to Empty

After analyzing the video recordings from the practical tests, the time to empty hopper 1 with the PP polymer was determined (Table 9.5). The PP emptied approximately 1.5 s faster than the mPE.

**Table 9.5** – Time to empty hopper 1 with PP

Test	Time to empty (s)
1	4.71
2	4.71
3	4.71

Two simulations were conducted before a result corresponding to the practical tests was reached.

**Table 9.6** – Results from simulations

Simulation	Moment of inertia (kgm <sup>2</sup> )	Time to empty (s)	Deviation (%)
4.1	2.0E-10	5.61	16.0
4.2	1.0E-11	4.76	1.05

Table 9.6 shows that a moment of inertia of 1.0E-11 kgm<sup>2</sup> results in a time to empty of 4.76 s which is a 1.05 % deviation from the mean value 4.71 s from the practical tests.

### Comments

The representable moment of inertia for the PP was considerably lower than that of the mPE. This makes sense since the PP is smaller, has a slightly rounder shape and has approximately the same density as the mPE.

### 9.6.2 Flow Pattern – Center Plane

The pit emerging in the center was noticeably shallower in the practical tests for the PP polymer than with the mPE polymer, most likely because of its smaller size and lower friction coefficients. The simulation shows a similar result with a pit a lot shallower than the previous simulations representing the mPE, which had a much higher moment of inertia.

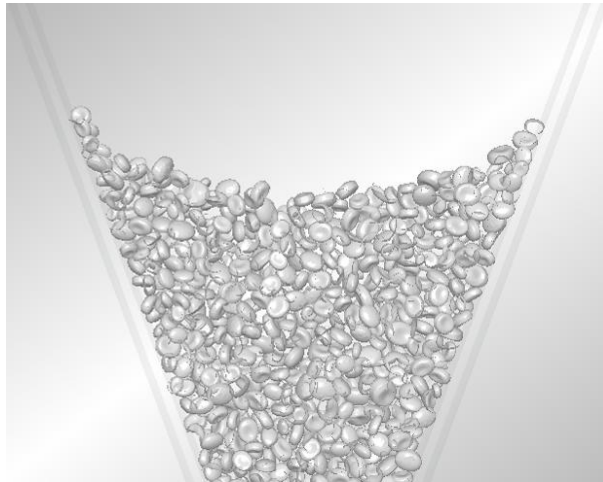


**Figure 9.17** – Flow pattern - center plane



**Figure 9.18** – Pit emerging in center

## 9.7 Practical Test 4 and Simulation 5

### 9.7.1 Time to Empty

The results from the practical tests involving hopper 2 and PP are presented in Table 9.7.

**Table 9.7** – Time to empty hopper 2 with PP

<b>Test</b>	<b>Time to empty (s)</b>
1	1.54
2	1.50
3	1.58

The result from this simulation was proven to be accurate as well. In the simulation the time to empty was 1.60 s which is a 3.90 % deviation from the mean value 1.54 s from the practical test.

### 9.7.2 Flow Pattern – Center Plane

The flow pattern in the simulation corresponded well with that from the practical tests. Again, the pit emerging in the center was somewhat shallower than for the mPE matching the observations made during the practical tests.

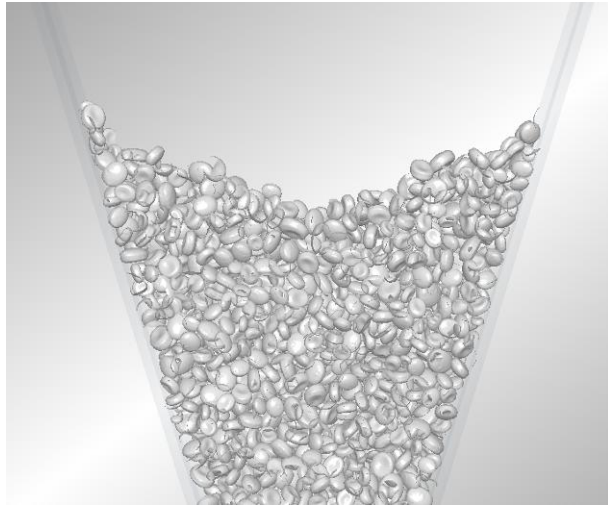


**Figure 9.19** – Flow pattern - center plane



**Figure 9.20** – Pit emerging in center

## **9.8 Comments – Results**

By using the coefficients of static, inter-particle and wall frictions—obtained from the laboratory analysis—and finding a representative moment of inertia, the computer based simulations proved to be very accurate. The simulation models, both mPE and PP, were verified by applying the exact same material properties and simulation settings on a second hopper geometry, to ensure the credibility.

The time to empty the hoppers in the simulations was within a 3.9 % deviation from the practical tests, and the flow patterns corresponded well with the observations made during the practical tests.

It is worth noting, however, that hopper 2 with its steep walls and large outlet was not optimal for these tests. It emptied so fast (1.88 s with mPE and 1.54 s with PP) that erroneous measurements, off by only hundredths of a second, result in a significant percentage difference. It is very difficult to determine the exact time using a regular camcorder and the error margin is somewhere around  $\pm 0.05$  s.



## 10. Conclusions

---

One of the objectives of this thesis was to investigate how to conduct computer based simulations of polymer pellets flow in hoppers and conveying systems.

The information gathered during the literature research showed that a DEM software such as EDEM is needed to simulate the flow of particles in hoppers. To simulate the flow of particles in conveying systems, a CFD software, such as FLUENT, combined with a DEM software is necessary. The CFD software then simulates the flow of the fluid/gas while the DEM software accounts for the particle interactions.

DEM simulations are very time consuming and conducting full-size hopper simulations could take several months because the simulation time depends upon the amount of particles involved. As an alternative, downscaled models can be used to perform sensitivity analyses where EDEM serves as a powerful tool. After conducting four different practical tests with two different hopper geometries and two polymer types, the corresponding simulations performed in EDEM showed comparable results.

In this thesis a sensitivity analysis was performed by DoE to investigate the influence a number of material properties had on the flow pattern. This analysis showed that the frictions between particle-particle and particle-wall both have a significant impact on the flow pattern, which corresponds well with the learnings from the literature study. Furthermore, it showed that the moment of inertia also affects the flow and can be adjusted to compensate for inaccuracies, such as shape, in the simulation models.

Additionally, the test methods used to measure the essential friction coefficients was proven reliable when evaluated in Gage R&R.





## 11. Discussion and Further Work

---

Attempting to duplicate a complex process such as the flow in hoppers in a computer based simulation is not easy and is very time consuming. While simulations may provide reliable data that are consistent with real-world conditions, it is worth keeping in mind that simulations are just an approximation. Some factors may not be considered in the contact model, such as permanent deformation, variations in surface roughness and the exact shape of the particles. However, it is possible to come very close to reality and once the model is validated, EDEM is a very powerful tool for investigating how different material properties and hopper geometries affect the flow.

Further investigation is recommended in the following areas: The effects of variations in particle size distribution; differences between wedge- and conical-shaped hoppers; and the effect of the particle shape. Concerning the latter, particle shape can be studied by combining multiple spheres into one particle in EDEM to replicate the real particle shape.

In future studies, we recommend using slightly larger models than the ones used in this thesis. Although the simulations will be more time consuming, the overall accuracy of the tests will be enhanced, and the ability to detect slight, but important, variations between practical tests will increase. For example, hopper 2 used in this work emptied so fast that erroneous measurements, off by only hundredths of a second, result in a significant percentage difference. This fast emptying time will also make it hard to distinguish between two similar tests, e.g. two tests with the same polymer but different size distribution.



## Notation

---

$v_p$	Particle velocity [m/s]
$w_p$	Particle rotational velocity [m/s]
$p$	Pressure [N/m <sup>2</sup> ]
$D$	Pipe diameter [m]
$R_B$	Radius of curvature [m]
$R$	Pipe radius [m]
$r_i$	Inner pipe radius [m]
$r_o$	Outer pipe radius [m]
$r^*$	Non-dimensional wall distance [-]
$\varepsilon$	Gas porosity [-]
$u$	Fluid velocity [m/s]
$t$	Time [s]
$g$	Gravity [m/s <sup>2</sup> ]
$\eta$	Viscosity [Pa s]
$\rho_f$	Fluid density [kg/m <sup>3</sup> ]
$M_s$	Momentum sink [N/m <sup>3</sup> ]
$F_D$	Drag force [N]
$V$	Volume [m <sup>3</sup> ]
$n$	Number of sample points [-]
$n_t$	Total number of sample points [-]
$Re$	Reynolds number [-]
$C_D$	Drag coefficient [-]
$\zeta$	Free volume of the CFD mesh
$L$	Diameter of the particles bounding sphere [m]
$F_B$	Natural buoyancy [kgm/s <sup>2</sup> ]
$N$	Normal force [N]
$S$	Shear force [N]
$N_I$	Major principal force [N]
$\sigma_I$	Major consolidating principal stress [N/m <sup>2</sup> ]
$\sigma'$	Normal stress at the wall of the outlet [N/m <sup>2</sup> ]
$\tau'$	Shear stress at the wall of the outlet [N/m <sup>2</sup> ]
$\sigma_c$	Unconfined yield stress [N/m <sup>2</sup> ]
$A$	Area of shear cell [m <sup>2</sup> ]
$F$	Unconfined yield force [N]
$\theta$	Hopper wall angle [°]
$\varphi_w$	Kinematic angle of friction between solid and wall [°]
$\delta$	Effective angle of internal friction [°]

$B$	Outlet width/diameter [m]
$\rho_b$	Bulk density when consolidated [ $\text{kg/m}^3$ ]
$F_t$	Tangential force acting on particle [N]
$F_n$	Normal force acting on particle [N]
$\delta_t$	Tangential overlap between particles [m]
$\delta_n$	Normal overlap between particles [m]
$c$	Coefficient of restitution [-]
$\mu$	Coefficient of static friction [-]
$a$	Radius of contact area between two particles [m]
$G$	Shear modulus [Pa]
$\nu$	Poisson's ratio [-]
$R_c$	Contact curvature radius [m]
$R$	Particle radius [m]
$\tau$	Shear stress [ $\text{N/m}^2$ ]
$\gamma$	Shear strain [-]
$I$	Moment of inertia [ $\text{kg m}^2$ ]
$m$	Particle mass [kg]
$M$	Torque [N m]
$F_f$	Friction force [N]
$\alpha$	Angle of tilted ramp [ $^\circ$ ]

## References

---

- [1] Dr MSA Bradley. (2002). *Understanding and Controlling Attrition and Wear In Pneumatic Conveying*, Wolfson Center for Bulk Solids Handling Technology, University of Greenwich, London, UK
- [2] Hans Schneider, Harald Wilms. (2008). *Wear Testing of Polymers In Pneumatic Conveying Systems*, Zeppelin Silos & Systems GmbH, Friedrichshafen, Germany
- [3] Shrikant Dhodapkar, Paul Solt, George Klinzing. (2009). *Understanding Bends In Pneumatic Conveying Systems*
- [4] K.W. Chu, A.B. Yu. (2007). *Numerical simulation of complex particle-fluid flows*, University of New South Wales, Sydney, Australia
- [5] K.W. Chu, A.B. Yu. (2007). *Numerical simulation of the Gas-Solid Flow in Three-Dimensional Pneumatic Conveying Bends*, University of New South Wales, Sydney, Australia
- [6] Pelletron Corporation, *Pneumatic Conveying Systems – Conveying Modes*, [www.pelletroncorp.com](http://www.pelletroncorp.com)
- [7] DEM Solutions. (2009). *EDEM-CFD Coupling Module for FLUENT User Guide*, EDEM 2.2, Revision 2B, Edinburgh, UK
- [8] K-E Rydberg, O Olsson. (1995). *Compendium in Hydraulics*, Institute of Technology, Dept. of Mechanical Engineering, Linköping, Sweden
- [9] K-E Rydberg. (1997) *Basic Theory for Pneumatic System Design*, Institute of Technology, Dept. of Mechanical Engineering, Linköping, Sweden
- [10] Z.F. Tian, K. Inthavong, J.Y. Tu, G.H. Yeoh. (2007). *Numerical investigation into the effects of wall roughness on a gas-particle flow in a 90° bend*, Royal Melbourne Institute of Technology, Bundoora, Australia, University of New South Wales, Menai, Australia
- [11] Pierre Chapelle, Nicholas Christakis, Hadi Abou-Chakra, Ian Bridle, MSA Bradeley, Mayur Patel and Mark Cross. (2003). *Computational model for prediction of particle degradation during dilute-phase pneumatic conveying: modeling of dilute-phase pneumatic conveying*, University of Greenwich, University of Surrey, London, UK

- [12] Carson, J. W., & Marinelli, J. (2001). *Solve Solids Flow Problems in Bins, Hoppers, and Feeders*. Chemical Engineering Progress, Jenike & Johanson Inc, Toronto, Canada
- [13] Freeman, T. (2009). *Optimizing the Lifetime Cost of Hoppers*, Powder Bulk Solids, Vol. 27, No. 6, 22-25, Los Angeles, CA, USA
- [14] Purutyan, H., Pittenger, B. H., & Carson, J. W. (1999). *Six Steps to Designing a Storage Vessel That Really Works*, Jenike & Johanson Inc, Toronto, Canada
- [15] Carson, J. W., & Jenkyn, R. T. (1993). *Load Development and Structural Considerations in Silo Design*, Jenike & Johanson Inc, Toronto, Canada
- [16] Jenike, A. W. (1964). *Storage and Flow of Solids*, Bulletin 123 of the Utah Engineering Experiment Station, University of Utah, Salt Lake City, USA
- [17] Rotter, J. M. (2001). *Guide for the economic design of circular metal silos*, London: Spon Press.
- [18] Arnold, P. C., McLean, A. G., & Roberts, A. W. (1978). *Bulk solids: Storage, flow and handling*. Newcastle: TUNRA Bulk Solids Handling Research Associates.
- [19] William R. Ketterhagen, Jennifer S. Curtis, Carl R. Wassgren, Bruno C. Hancock. (2009). *Predicting the flow mode from hoppers using the discrete element method*. Powder Technology 195
- [20] Ran Bachrach, Jack Dvorkin and Amos M. Nur. (2000). *Seismic velocities and Poisson's ratio of shallow unconsolidated sands*. Geophysics, vol.65, no.2.
- [21] H.G. Matuttis, S. Luding and H.J. Herrmann. *Discrete Element Simulations of Dense Packings and Heaps of Spherical and Non-Spherical Particles*. (1999). Institute of Computer Applications 1, Stuttgart, Germany.
- [22] DEM-Solutions. (2005). *Experts in particle mechanics simulation*. [www.dem-solutions.com](http://www.dem-solutions.com)
- [23] R. Balevicius, R. Kacianauskas, Z. Mroz, I. Sielamowicz. (2006). *Discrete element method applied to multiobjective optimization of discharge flow parameters in hoppers*, Struct Multidisc Optim 31
- [24] Tibor J. Goda, Fritz Ebert. (2005). *Three-dimensional discrete element simulations in hoppers and silos*. Chair of Particle Technology and Fluid Mechanics, University of Kaiserslautern, Kaiserslautern, Germany

- [25] William R. Ketterhagen, Jennifer S. Curtis, Carl R. Wassgren, Angela Kong, Padma J. Narayan, Bruno C. Hancock. (2007). *Granular segregation in discharging cylindrical hoppers: A discrete element and experimental study*, Chemical Engineering Science 62
- [26] William R. Ketterhagen, Jennifer S. Curtis, Carl R. Wassgren, Bruno C. Hancock. (2007). *Modeling granular segregation in flow quasi-three-dimensional, wedge-shaped hoppers*, Powder Technology 179
- [27] Gwindon W. Stachowiak, Andrew W. Batchelor. (2001). *Engineering Tribology, Second Edition*, Butterworth-Heinemann, Woburn, MA, USA
- [28] Optical Control Systems GmbH. *Pellet Size & Shape Distribution PSSD*, Witten, Germany
- [29] DEM Solutions. (2009). *EDEM User guide*, Edinburgh, UK
- [30] L.Eriksson, E.Johansson, N.Kettaneh-Wold, C.Wikström & S.Wold. (2008). *Design of Experiments – Principles and Applications*, Umetrics AB, Umeå, Sweden





## Appendix A – Gage R&R

---

### Polymer coefficients of restitution and static friction

The aim of the work was to find a method that could analyze the differences between polymers dependent on the chemical properties. The influence of the shape was to be eliminated.

A Gage R&R (Repeatability & Reproducibility) was performed for the two methods established during this thesis work to be able to quantify the coefficients of restitution and static friction needed for the simulations.

The results were evaluated with Gage R&R using MiniTab software.

Gage R&R explains the total variation by dividing it into *Part-to-part variation* and *Variations caused by the measuring system* such as the gage and the operator. The repeatability and the reproducibility is calculated from the results and compared against the total variation to evaluate if the total measure system is able to distinguish the different parts/samples that have been measured.

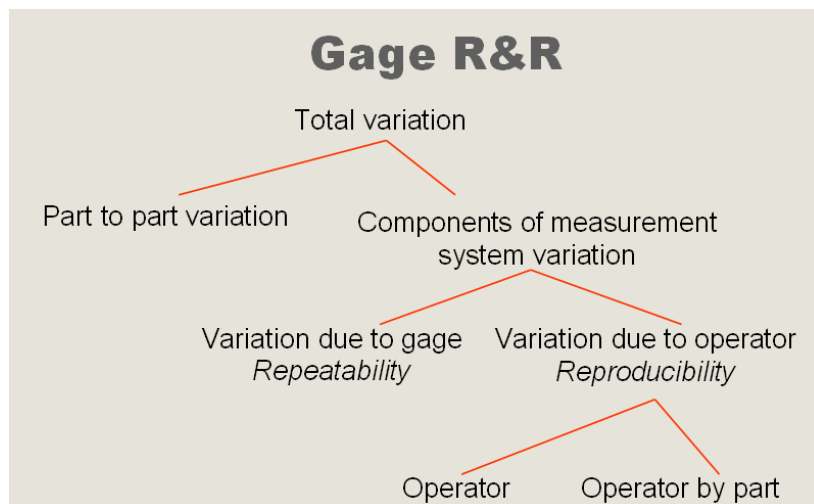


Figure A.1 – Schematic picture over variation explained in a Gage R&R<sup>33</sup>

---

<sup>33</sup> Sven Keiter, Tetra Pak, Lamination group, Lund

The studies can be performed in several different ways and in this case the restitution was made with three operators as there is no high level of training needed to perform the tests.

For the static friction the method is more dependent on the operator and two persons are needed for the experiment to be able to give a good judgment. If qualifying the static friction method as a standard e.g. an automatic detector (camera or likewise) might be needed combined with an easier way to apply the granules (See chapter 6.1.2 for more information).

Looking at the values on contribution of variation in the studies a rule of thumb is that the part-to-part variation should be  $>70\%$ . Divided into more level values between 70% and 80% are on the border line to be able to separate the samples and in the range 80% to 90% it is acceptable. Above 90% the gage R&R is good which means that the measurements in the coming studies can distinguish the different polymer grades.

Furthermore the study reveals if the variations not belonging to the desired part-to-part variation are caused by the equipment or the operator. Here there are no specific limits between the two categories but the ratio implies if improvements can be achieved by training operators, creating a better routine/procedure or if the problem is the equipment accuracy.

Another rule of thumb is that the amount of categories should ideally be five or more. This requires of course that there are five or more samples in the test set up.

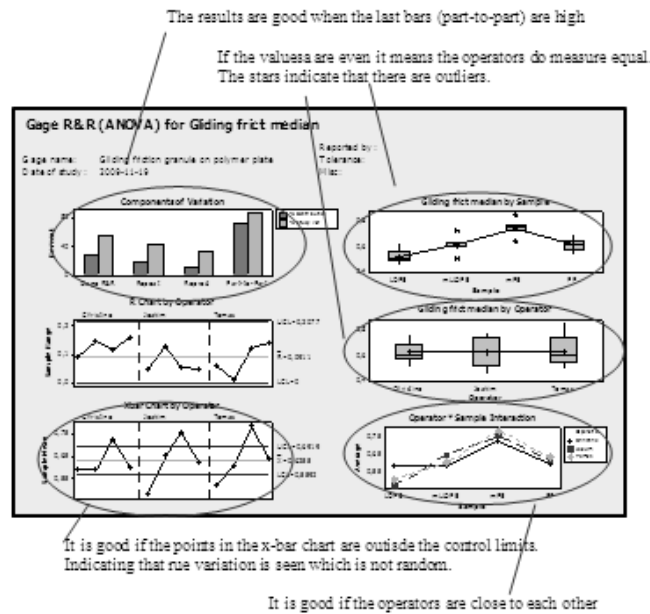


Figure A.2 – Graph Explanation

Static friction – Gage R&R

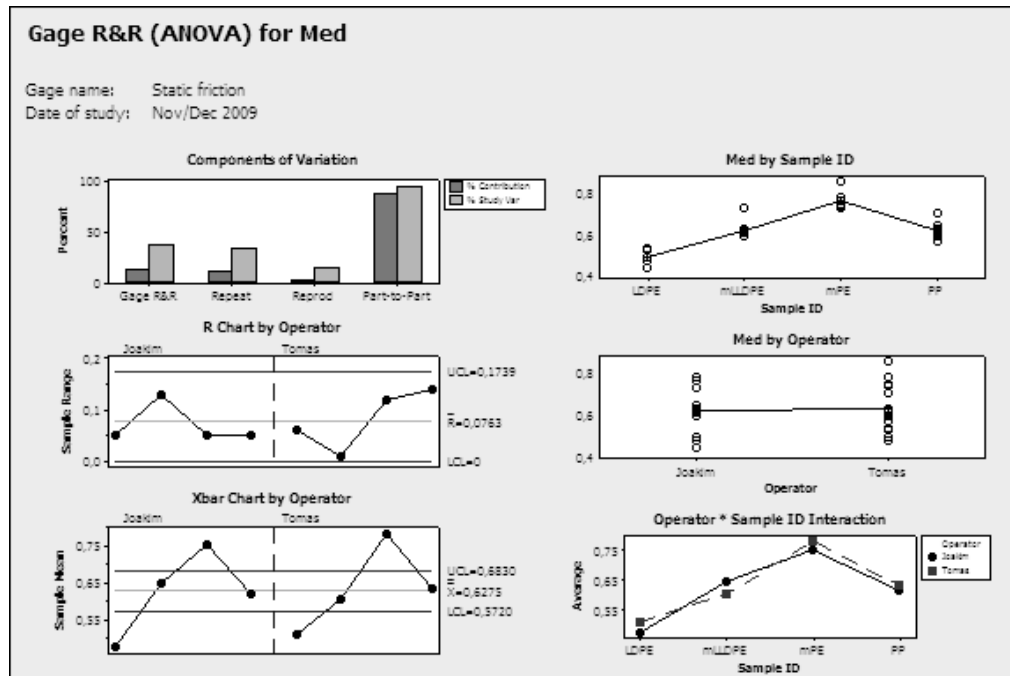


Figure A.3 – Static friction, Gage R&R with two operators and four polymer grades

**Table A.1 - Gage R&R for Static friction with two operators**

Source	VarComp	%Contribution (of VarComp)	
Total Gage R&R	0,0011823	11,96	
Repeatability	0,0004977	5,04	
Reproducibility	0,0006846	6,93	
Operator	0,0000000	0,00	
Operator*Sample	0,0006846	6,93	
Part-To-Part	0,0087017	88,04	
Total Variation	0,0098840	100,00	

Source	StdDev (SD)	Study Var (6 * SD)	%Study Var (%SV)
Total Gage R&R	0,0343845	0,206307	34,59
Repeatability	0,0223090	0,133854	22,44
Reproducibility	0,0261649	0,156989	26,32
Operator	0,0000000	0,000000	0,00
Operator*Sample	0,0261649	0,156989	26,32
Part-To-Part	0,0932830	0,559698	93,83
Total Variation	0,0994183	0,596510	100,00

Number of Distinct Categories = 3

The results of the study are that the method is approved with part-to-part contributing with close to 90%, which is considered good. Number of distinct categories is 3 and in this case the method can not separate mLLDPE and PP.

### Comments

The Gage R&R for static friction between a polymer plate and granules (see chapter 6.1.2 for information about the method) was initially made with three operators. The third operator was less trained and did some of tests alone. It was noticed that it was hard to make an accurate judgment on when the granules started to slide and at the same time tilt the ramp. In the evaluation it became obvious that the “single” operator deviated from the other two, both in average results and in stability.

Knowing this and the reason behind the “odd operator” it was decided to use only the first two operators’ results.

Another source for variation is the plates that are prepared. They do vary slightly as seen below in figure A.3. Here is also room for improvements.

## Notes

In the test, different plates have been prepared so the variations in the parts are included in the approved study.

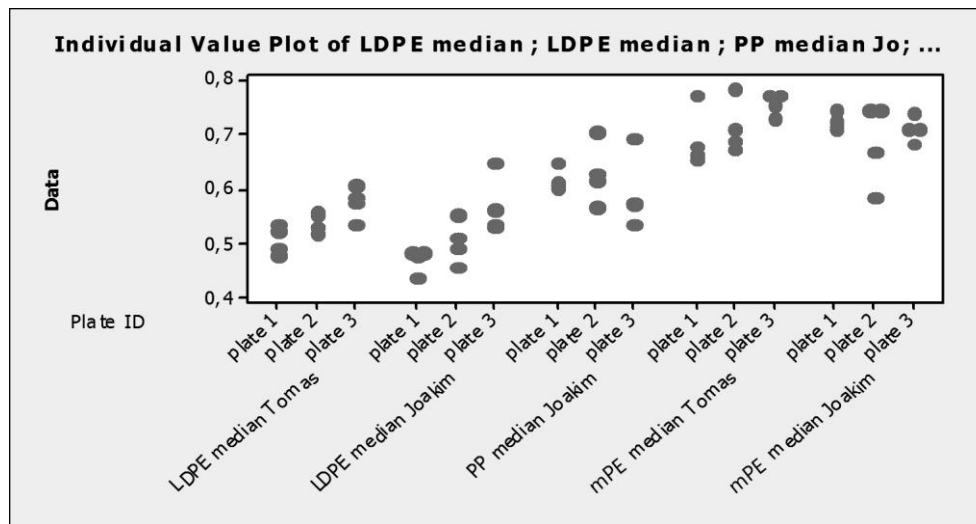


**Figure A.4** – Example of variations between different plates from three polymer grades and the static friction plotted vs. operator and plate ID

**Table A.2** – LDPE raw data for static friction with two operators, mean values used in study

<b>Operator</b>	<b>Sample</b>	<b>Static friction mean</b>	<b>Static friction min</b>	<b>Static friction max</b>
Tomas	LDPE	0,48	0,43	0,53
Tomas	LDPE	0,54	0,47	0,60
Tomas	LDPE	0,53	0,42	0,61
Tomas	LDPE	0,49	0,42	0,64
Joakim	LDPE	0,44	0,40	0,58
Joakim	LDPE	0,48	0,40	0,58
Joakim	LDPE	0,49	0,42	0,61
Joakim	LDPE	0,49	0,42	0,59

**Table A.3** – PP raw data for static friction with two operators, mean values used in study

<b>Operator</b>	<b>Sample</b>	<b>Static friction mean</b>	<b>Static friction min</b>	<b>Static friction max</b>
Joakim	PP	0,65	0,48	0,88
Joakim	PP	0,60	0,51	0,71
Joakim	PP	0,61	0,48	0,95
Joakim	PP	0,61	0,47	0,78
Tomas	PP	0,71	0,50	0,96
Tomas	PP	0,57	0,53	0,70
Tomas	PP	0,63	0,47	0,83
Tomas	PP	0,62	0,47	0,91

**Table A.4** – mPE raw data for static friction with two operators, mean values used in study

<b>Operator</b>	<b>Sample</b>	<b>Static friction mean</b>	<b>Static friction min</b>	<b>Static friction max</b>
Joakim	mPE	0,73	0,65	0,91
Joakim	mPE	0,77	0,72	0,89
Joakim	mPE	0,73	0,63	0,90
Joakim	mPE	0,78	0,62	1,08
Tomas	mPE	0,74	0,65	0,92
Tomas	mPE	0,78	0,68	0,91
Tomas	mPE	0,75	0,61	0,85
Tomas	mPE	0,86	0,61	1,01

**Table A.5** – mLLDPE raw data for static friction with two operators, mean values used in study

<b>Operator</b>	<b>Sample</b>	<b>Static friction mean</b>	<b>Static friction min</b>	<b>Static friction max</b>
Joakim	mLLDPE	0,60	0,52	0,72
Joakim	mLLDPE	0,63	0,52	0,69
Joakim	mLLDPE	0,73	0,63	0,76
Joakim	mLLDPE	0,63	0,50	0,81
Tomas	mLLDPE	0,61	0,56	0,81
Tomas	mLLDPE	0,60	0,53	0,89
Tomas	mLLDPE	0,60	0,51	0,66
Tomas	mLLDPE	0,60	0,49	0,69

# Restitution – Gage R&R

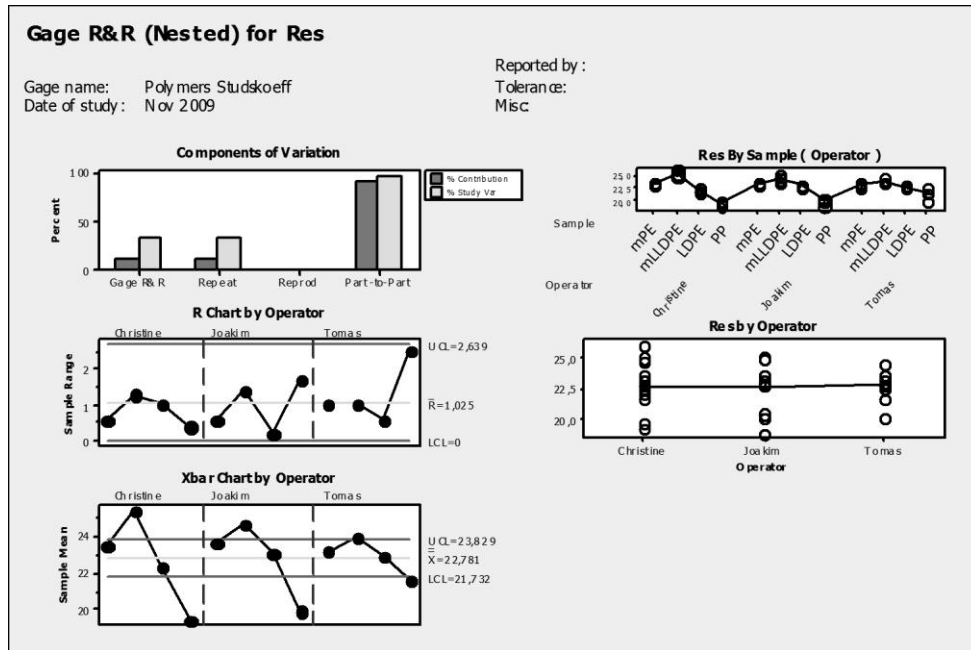


Figure A.5 – Graph’s from Gage R&R study on restitution between polymer grade and wall



**Table A.6** – Gage R&R for coefficient of restitution

Gage R&R			
Source	%Contribution		
	VarComp	(of VarComp)	
Total Gage R&R	0,38694	9,59	
Repeatability	0,38694	9,59	
Reproducibility	0	0	
Part-To-Part	3,64827	90,41	
Total Variation	4,03522	100	
Source	Study Var		%Study Var
	StdDev (E (6 * SD)		(%SV)
Total Gage R&R	0,62205	3,7323	30,97
Repeatability	0,62205	3,7323	30,97
Reproducibility	0	0	0
Part-To-Part	1,91004	11,4603	95,08
Total Variation	2,00878	12,0527	100
Number of Distinct Categories = 4			
Gage R&R (Nested) for Res			

In this study a "Nested" Gage R&R was chosen as the samples are destroyed during testing. Total Gage R&R is good with a part-to-part variation of slightly above 90% and four categories.

**Table A.7** – Raw data, coefficient of restitution

Operator	Sample	Res	(% median from three measures)	Operator	Sample	Res
Tomas	mPE	22,8		Tomas	mLLDPE	23,6
Tomas	mPE	22,8		Tomas	mLLDPE	24,6
Tomas	mPE	23,8		Tomas	mLLDPE	23,8
Joakim	mPE	23,2		Joakim	mLLDPE	23,8
Joakim	mPE	23,8		Joakim	mLLDPE	25,2
Joakim	mPE	23,8		Joakim	mLLDPE	25
Christine	mPE	23,2		Christine	mLLDPE	24,8
Christine	mPE	23,4		Christine	mLLDPE	25,2
Christine	mPE	23,8		Christine	mLLDPE	26,1
Tomas	LDPE	22,6		Tomas	PP	20,3
Tomas	LDPE	23,2		Tomas	PP	21,6
Tomas	LDPE	22,8		Tomas	PP	22,8
Joakim	LDPE	23		Joakim	PP	20,3
Joakim	LDPE	23,2		Joakim	PP	18,9
Joakim	LDPE	23		Joakim	PP	20,6
Christine	LDPE	22,2		Christine	PP	19,7
Christine	LDPE	21,8		Christine	PP	19,3
Christine	LDPE	22,8		Christine	PP	19,3

## Appendix B – DoE

---

Table B.1 – Input values

Nr	RFI	RFW	SFI	SFW	REI	REW	SM (kg/m <sup>2</sup> )	I (kgm <sup>2</sup> )
1	0,005	0,005	0,1	0,1	0,1	0,1	1,00E+07	5,39E-11
2	0,05	0,005	0,1	0,1	0,1	0,8	1,00E+09	1,00E-09
3	0,005	0,05	0,1	0,1	0,8	0,1	1,00E+09	1,00E-09
4	0,05	0,05	0,1	0,1	0,8	0,8	1,00E+07	5,39E-11
5	0,005	0,005	1	0,1	0,8	0,8	1,00E+09	5,39E-11
6	0,05	0,005	1	0,1	0,8	0,1	1,00E+07	1,00E-09
7	0,005	0,05	1	0,1	0,1	0,8	1,00E+07	1,00E-09
8	0,05	0,05	1	0,1	0,1	0,1	1,00E+09	5,39E-11
9	0,005	0,005	0,1	1	0,8	0,8	1,00E+07	1,00E-09
10	0,05	0,005	0,1	1	0,8	0,1	1,00E+09	5,39E-11
11	0,005	0,05	0,1	1	0,1	0,8	1,00E+09	5,39E-11
12	0,05	0,05	0,1	1	0,1	0,1	1,00E+07	1,00E-09
13	0,005	0,005	1	1	0,1	0,1	1,00E+09	1,00E-09
14	0,05	0,005	1	1	0,1	0,8	1,00E+07	5,39E-11
15	0,005	0,05	1	1	0,8	0,1	1,00E+07	5,39E-11
16	0,05	0,05	1	1	0,8	0,8	1,00E+09	1,00E-09
17	0,028	0,028	0,6	0,55	0,5	0,45	5,05E+08	5,27E-10

RFI = Rolling friction particle-particle

RFW = Rolling friction particle-wall

SFI = Static friction particle-particle

SFW = Static friction particle-wall

REI = Restitution particle-particle

REW = Restitution particle-wall

SM = Shear modulus

I = Moment of inertia

**Table B.2** – Output values

<b>Nr</b>	<b>Time to empty (s)</b>	<b>Simulation time (h)</b>	<b>Discharge rate (kg/s)</b>	<b>Average velocity wall (m/s)</b>	<b>Average velocity center (m/s)</b>	<b>Total mass (kg)</b>
1	1,02	0,637	0,1294402	0,107	0,142	0,132029
2	1,14	4,660	0,1207342	0,093	0,121	0,137637
3	1,16	4,550	0,1191483	0,103	0,128	0,138212
4	1,19	0,543	0,1174807	0,098	0,115	0,139802
5	1,29	4,150	0,1056481	0,087	0,111	0,136286
6	2,07	0,686	0,0678812	0,054	0,072	0,140514
7	1,98	0,674	0,0708884	0,057	0,08	0,140359
8	1,48	5,050	0,0931797	0,077	0,107	0,137906
9	1,68	0,695	0,0821494	0,061	0,091	0,138011
10	1,36	4,800	0,1014632	0,072	0,127	0,13799
11	1,21	4,590	0,1136645	0,083	0,129	0,137534
12	1,87	0,713	0,0747064	0,045	0,093	0,139701
13	2,89	7,410	0,0474785	0,035	0,065	0,137213
14	2,02	0,671	0,0691099	0,047	0,098	0,139602
15	1,81	0,602	0,0773619	0,049	0,093	0,140025
16	3,07	7,580	0,0444163	0,028	0,058	0,136358
17	2,17	4,510	0,0634576	0,049	0,084	0,137703

### Simulation time

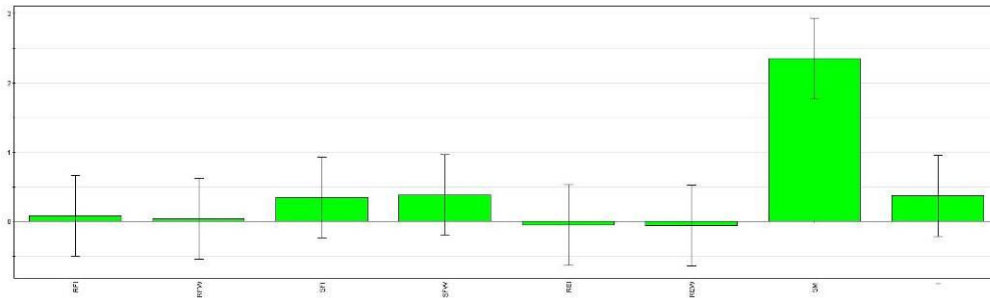


**Figure B.1** - From left: RFI, RFW, SFI, SFW, REI, REW, SM and I

### Discharge rate

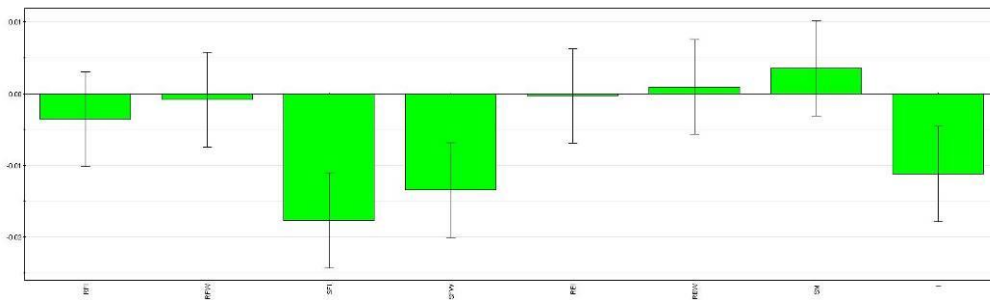


**Figure B.2** - From left: RFI, RFW, SFI, SFW, REI, REW, SM and I

### Time to empty

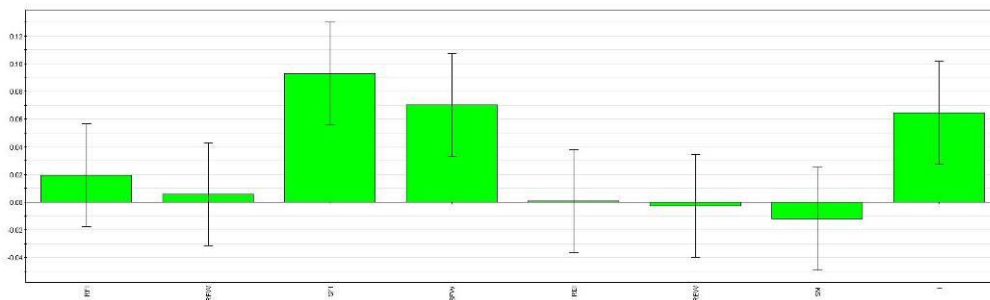


**Figure B.3** - From left: RFI, RFW, SFI, SFW, REI, REW, SM and I

### Average velocity along center

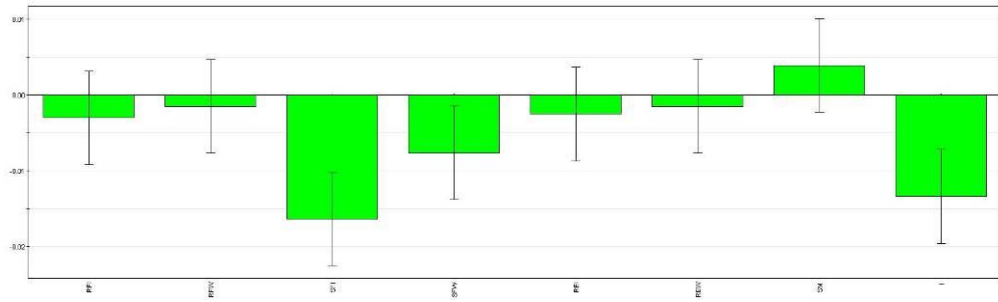


Figure B.4 - From left: RFI, RFW, SFI, SFW, REI, REW, SM and I

### Average velocity along wall

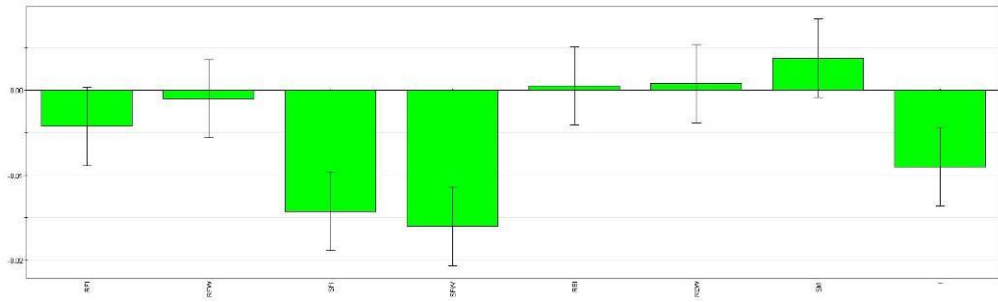


Figure B.5 - From left: RFI, RFW, SFI, SFW, REI, REW, SM and I

## Appendix C – Bin velocities

---

Table C.1 - DoE 1

Time Step	Side A	Center	Side B	Average Side	Side A (Y)	Side B (Y)
1	0,080	0,110	0,086	0,083	0,075	0,081
2	0,086	0,124	0,102	0,094	0,081	0,096
3	0,067	0,099	0,082	0,075	0,063	0,077
4	0,095	0,119	0,079	0,087	0,089	0,074
5	0,114	0,141	0,097	0,105	0,107	0,091
6	0,094	0,127	0,090	0,092	0,088	0,084
7	0,108	0,130	0,105	0,107	0,101	0,099
8	0,113	0,172	0,131	0,122	0,106	0,123
9	0,136	0,169	0,139	0,137	0,128	0,130
10	0,176	0,231	0,153	0,165	0,165	0,144
<b>Average</b>		<b>0,142</b>		<b>0,107</b>		

**Table C.2 - DoE 2**

<b>Time Step</b>	<b>Side A</b>	<b>Center</b>	<b>Side B</b>	<b>Average Side</b>	<b>Side A (Y)</b>	<b>Side B (Y)</b>
1	0,064	0,076	0,063	0,063	0,060	0,059
2	0,077	0,102	0,087	0,082	0,072	0,082
3	0,076	0,112	0,083	0,079	0,071	0,078
4	0,072	0,099	0,059	0,066	0,068	0,055
5	0,099	0,116	0,071	0,085	0,093	0,067
6	0,097	0,122	0,096	0,096	0,091	0,090
7	0,101	0,136	0,092	0,096	0,095	0,086
8	0,113	0,138	0,118	0,116	0,106	0,111
9	0,108	0,146	0,128	0,118	0,101	0,120
10	0,158	0,167	0,091	0,124	0,148	0,085
<b>Average</b>		<b>0,121</b>		<b>0,093</b>		

**Table C.3 - DoE 3**

<b>Time Step</b>	<b>Side A</b>	<b>Center</b>	<b>Side B</b>	<b>Average Side</b>	<b>Side A (Y)</b>	<b>Side B (Y)</b>
1	0,075	0,096	0,067	0,071	0,070	0,063
2	0,069	0,099	0,072	0,071	0,065	0,068
3	0,078	0,113	0,085	0,082	0,073	0,080
4	0,056	0,098	0,077	0,067	0,053	0,072
5	0,076	0,118	0,088	0,082	0,071	0,083
6	0,096	0,123	0,090	0,093	0,090	0,084
7	0,097	0,146	0,121	0,109	0,091	0,114
8	0,126	0,160	0,110	0,118	0,118	0,103
9	0,152	0,141	0,107	0,129	0,143	0,100
10	0,213	0,181	0,205	0,209	0,200	0,192
<b>Average</b>		<b>0,128</b>		<b>0,103</b>		



**Table C.4 - DoE 4**

<b>Time Step</b>	<b>Side A</b>	<b>Center</b>	<b>Side B</b>	<b>Average Side</b>	<b>Side A (Y)</b>	<b>Side B (Y)</b>
1	0,068	0,092	0,062	0,065	0,064	0,058
2	0,077	0,104	0,078	0,077	0,072	0,073
3	0,086	0,118	0,071	0,079	0,081	0,067
4	0,095	0,121	0,092	0,093	0,089	0,086
5	0,101	0,107	0,095	0,098	0,095	0,089
6	0,092	0,111	0,085	0,088	0,086	0,080
7	0,088	0,115	0,097	0,093	0,083	0,091
8	0,108	0,124	0,110	0,109	0,101	0,103
9	0,110	0,123	0,139	0,124	0,103	0,130
10	0,157	0,139	0,155	0,156	0,147	0,145
<b>Average</b>		<b>0,115</b>		<b>0,098</b>		

**Table C. 5 - DoE 5**

<b>Time Step</b>	<b>Side A</b>	<b>Center</b>	<b>Side B</b>	<b>Average Side</b>	<b>Side A (Y)</b>	<b>Side B (Y)</b>
1	0,063	0,089	0,067	0,065	0,059	0,063
2	0,055	0,080	0,068	0,062	0,052	0,064
3	0,070	0,095	0,067	0,069	0,066	0,063
4	0,076	0,120	0,083	0,079	0,071	0,078
5	0,068	0,093	0,079	0,074	0,064	0,074
6	0,076	0,101	0,065	0,070	0,071	0,061
7	0,079	0,122	0,099	0,089	0,074	0,093
8	0,115	0,135	0,109	0,112	0,108	0,102
9	0,125	0,146	0,091	0,108	0,117	0,085
10	0,156	0,128	0,136	0,146	0,146	0,128
<b>Average</b>		<b>0,111</b>		<b>0,087</b>		

**Table C.6 - DoE 6**

<b>Time Step</b>	<b>Side A</b>	<b>Center</b>	<b>Side B</b>	<b>Average Side</b>	<b>Side A (Y)</b>	<b>Side B (Y)</b>
1	0,033	0,043	0,036	0,035	0,031	0,034
2	0,037	0,047	0,040	0,039	0,035	0,038
3	0,027	0,044	0,029	0,028	0,025	0,027
4	0,040	0,068	0,050	0,045	0,038	0,047
5	0,033	0,049	0,034	0,034	0,031	0,032
6	0,055	0,079	0,053	0,054	0,052	0,050
7	0,080	0,086	0,070	0,075	0,075	0,066
8	0,047	0,079	0,063	0,055	0,044	0,059
9	0,050	0,069	0,071	0,061	0,047	0,067
10	0,111	0,156	0,115	0,113	0,104	0,108
<b>Average</b>		<b>0,072</b>		<b>0,054</b>		

**Table C.7 - DoE 7**

<b>Time Step</b>	<b>Side A</b>	<b>Center</b>	<b>Side B</b>	<b>Average Side</b>	<b>Side A (Y)</b>	<b>Side B (Y)</b>
1	0,040	0,053	0,031	0,036	0,038	0,029
2	0,055	0,059	0,045	0,050	0,052	0,042
3	0,045	0,058	0,045	0,045	0,042	0,042
4	0,055	0,077	0,061	0,058	0,052	0,057
5	0,060	0,077	0,058	0,059	0,056	0,054
6	0,053	0,082	0,054	0,054	0,050	0,051
7	0,064	0,082	0,054	0,059	0,060	0,051
8	0,071	0,096	0,055	0,063	0,067	0,052
9	0,052	0,102	0,064	0,058	0,049	0,060
10	0,090	0,109	0,082	0,086	0,084	0,077
<b>Average</b>		<b>0,080</b>		<b>0,057</b>		

**Table C.8 - DoE 8**

<b>Time Step</b>	<b>Side A</b>	<b>Center</b>	<b>Side B</b>	<b>Average Side</b>	<b>Side A (Y)</b>	<b>Side B (Y)</b>
1	0,052	0,063	0,043	0,047	0,049	0,040
2	0,052	0,070	0,055	0,054	0,049	0,052
3	0,042	0,057	0,047	0,044	0,039	0,044
4	0,070	0,110	0,087	0,079	0,066	0,082
5	0,078	0,105	0,077	0,077	0,073	0,072
6	0,081	0,125	0,076	0,078	0,076	0,071
7	0,083	0,111	0,071	0,077	0,078	0,067
8	0,086	0,109	0,091	0,088	0,081	0,085
9	0,086	0,160	0,117	0,102	0,081	0,110
10	0,134	0,159	0,117	0,126	0,126	0,110
<b>Average</b>		<b>0,107</b>		<b>0,077</b>		

**Table C.9 - DoE 9**

<b>Time Step</b>	<b>Side A</b>	<b>Center</b>	<b>Side B</b>	<b>Average Side</b>	<b>Side A (Y)</b>	<b>Side B (Y)</b>
1	0,035	0,062	0,045	0,040	0,033	0,042
2	0,046	0,071	0,046	0,046	0,043	0,043
3	0,048	0,079	0,047	0,047	0,045	0,044
4	0,062	0,080	0,037	0,050	0,058	0,035
5	0,053	0,083	0,040	0,047	0,050	0,038
6	0,054	0,092	0,060	0,057	0,051	0,056
7	0,054	0,083	0,060	0,057	0,051	0,056
8	0,068	0,104	0,058	0,063	0,064	0,054
9	0,099	0,114	0,079	0,089	0,093	0,074
10	0,110	0,139	0,115	0,112	0,103	0,108
<b>Average</b>		<b>0,091</b>		<b>0,061</b>		

**Table C.10 - DoE 10**

<b>Time Step</b>	<b>Side A</b>	<b>Center</b>	<b>Side B</b>	<b>Average Side</b>	<b>Side A (Y)</b>	<b>Side B (Y)</b>
1	0,043	0,105	0,054	0,048	0,040	0,051
2	0,044	0,088	0,047	0,045	0,041	0,044
3	0,066	0,111	0,062	0,064	0,062	0,058
4	0,060	0,105	0,067	0,063	0,056	0,063
5	0,059	0,115	0,064	0,061	0,055	0,060
6	0,059	0,127	0,080	0,069	0,055	0,075
7	0,071	0,129	0,056	0,064	0,067	0,053
8	0,094	0,156	0,090	0,092	0,088	0,084
9	0,104	0,158	0,102	0,103	0,098	0,096
10	0,090	0,180	0,128	0,109	0,084	0,120
<b>Average</b>		<b>0,127</b>		<b>0,072</b>		

**Table C.11 - DoE 11**

<b>Time Step</b>	<b>Side A</b>	<b>Center</b>	<b>Side B</b>	<b>Average Side</b>	<b>Side A (Y)</b>	<b>Side B (Y)</b>
1	0,063	0,098	0,079	0,071	0,059	0,074
2	0,064	0,107	0,061	0,062	0,060	0,057
3	0,060	0,109	0,064	0,062	0,056	0,060
4	0,070	0,130	0,075	0,072	0,066	0,070
5	0,066	0,110	0,075	0,070	0,062	0,070
6	0,083	0,135	0,076	0,079	0,078	0,071
7	0,078	0,117	0,090	0,084	0,073	0,084
8	0,097	0,149	0,081	0,089	0,091	0,076
9	0,123	0,161	0,130	0,126	0,115	0,122
10	0,114	0,175	0,116	0,115	0,107	0,109
<b>Average</b>		<b>0,129</b>		<b>0,083</b>		

**Table C.12 - DoE 12**

<b>Time Step</b>	<b>Side A</b>	<b>Center</b>	<b>Side B</b>	<b>Average Side</b>	<b>Side A (Y)</b>	<b>Side B (Y)</b>
1	0,022	0,052	0,031	0,027	0,021	0,029
2	0,040	0,068	0,031	0,036	0,038	0,029
3	0,033	0,074	0,039	0,036	0,031	0,037
4	0,037	0,094	0,032	0,035	0,035	0,030
5	0,043	0,073	0,033	0,038	0,040	0,031
6	0,037	0,103	0,037	0,037	0,035	0,035
7	0,035	0,095	0,040	0,038	0,033	0,038
8	0,059	0,116	0,070	0,064	0,055	0,066
9	0,065	0,126	0,064	0,064	0,061	0,060
10	0,069	0,129	0,083	0,076	0,065	0,078
<b>Average</b>		<b>0,093</b>		<b>0,045</b>		

**Table C.13 - DoE 13**

<b>Time Step</b>	<b>Side A</b>	<b>Center</b>	<b>Side B</b>	<b>Average Side</b>	<b>Side A (Y)</b>	<b>Side B (Y)</b>
1	0,023	0,039	0,021	0,022	0,022	0,020
2	0,031	0,048	0,028	0,029	0,029	0,026
3	0,035	0,060	0,030	0,032	0,033	0,028
4	0,026	0,049	0,031	0,028	0,024	0,029
5	0,025	0,054	0,030	0,027	0,023	0,028
6	0,030	0,056	0,027	0,028	0,028	0,025
7	0,033	0,065	0,026	0,029	0,031	0,024
8	0,034	0,073	0,044	0,039	0,032	0,041
9	0,034	0,104	0,040	0,037	0,032	0,038
10	0,080	0,097	0,068	0,074	0,075	0,064
<b>Average</b>		<b>0,065</b>		<b>0,035</b>		

**Table C.14 - DoE 14**

<b>Time Step</b>	<b>Side A</b>	<b>Center</b>	<b>Side B</b>	<b>Average Side</b>	<b>Side A (Y)</b>	<b>Side B (Y)</b>
1	0,026	0,052	0,031	0,028	0,024	0,029
2	0,028	0,069	0,037	0,032	0,026	0,035
3	0,018	0,088	0,049	0,034	0,017	0,046
4	0,061	0,107	0,042	0,051	0,057	0,039
5	0,017	0,087	0,038	0,028	0,016	0,036
6	0,055	0,114	0,063	0,059	0,052	0,059
7	0,048	0,070	0,042	0,045	0,045	0,039
8	0,030	0,077	0,051	0,040	0,028	0,048
9	0,069	0,136	0,080	0,075	0,065	0,075
10	0,077	0,178	0,079	0,078	0,072	0,074
<b>Average</b>		<b>0,098</b>		<b>0,047</b>		

**Table C.15 - DoE 15**

<b>Time Step</b>	<b>Side A</b>	<b>Center</b>	<b>Side B</b>	<b>Average Side</b>	<b>Side A (Y)</b>	<b>Side B (Y)</b>
1	0,029	0,053	0,029	0,029	0,027	0,027
2	0,037	0,075	0,043	0,040	0,035	0,040
3	0,046	0,081	0,036	0,041	0,043	0,034
4	0,037	0,068	0,045	0,041	0,035	0,042
5	0,037	0,075	0,037	0,037	0,035	0,035
6	0,044	0,111	0,043	0,043	0,041	0,040
7	0,055	0,127	0,039	0,047	0,052	0,037
8	0,075	0,110	0,055	0,065	0,070	0,052
9	0,056	0,092	0,061	0,059	0,053	0,057
10	0,069	0,140	0,100	0,085	0,065	0,094
<b>Average</b>		<b>0,093</b>		<b>0,049</b>		

**Table C.16 - DoE 16**

<b>Time Step</b>	<b>Side A</b>	<b>Center</b>	<b>Side B</b>	<b>Average Side</b>	<b>Side A (Y)</b>	<b>Side B (Y)</b>
1	0,013	0,031	0,016	0,014	0,012	0,015
2	0,017	0,047	0,018	0,018	0,016	0,017
3	0,030	0,039	0,016	0,023	0,028	0,015
4	0,019	0,034	0,019	0,019	0,018	0,018
5	0,022	0,046	0,037	0,030	0,021	0,035
6	0,025	0,050	0,022	0,023	0,023	0,021
7	0,028	0,051	0,021	0,025	0,026	0,020
8	0,029	0,054	0,026	0,027	0,027	0,024
9	0,044	0,094	0,049	0,046	0,041	0,046
10	0,043	0,136	0,070	0,056	0,040	0,066
<b>Average</b>		<b>0,058</b>		<b>0,028</b>		

**Table C.17 - DoE 17**

<b>Time Step</b>	<b>Side A</b>	<b>Center</b>	<b>Side B</b>	<b>Average Side</b>	<b>Side A (Y)</b>	<b>Side B (Y)</b>
1	0,034	0,058	0,031	0,032	0,032	0,029
2	0,037	0,072	0,036	0,037	0,035	0,034
3	0,028	0,053	0,030	0,029	0,026	0,028
4	0,046	0,090	0,043	0,044	0,043	0,040
5	0,037	0,080	0,036	0,037	0,035	0,034
6	0,051	0,085	0,055	0,053	0,048	0,052
7	0,054	0,095	0,050	0,052	0,051	0,047
8	0,056	0,113	0,066	0,061	0,053	0,062
9	0,051	0,078	0,044	0,047	0,048	0,041
10	0,104	0,119	0,080	0,092	0,098	0,075
<b>Average</b>		<b>0,084</b>		<b>0,049</b>		

## Appendix D – EDEM Considerations

---

During this work some issues using the EDEM software were discovered. A major one was that since EDEM presents the results visually by playing back the simulation as a video, it requires a graphics card. Initially in this work, the software was run on a calculation server which was lacking graphics cards altogether. This server is optimal to run calculations due to its processor speed and memory capacity, but not as favorable when it comes to reviewing results in EDEM.

The result of this was that EDEM crashed during post-processing. When the program requested graphics memory from the server, which was not there, EDEM simply shut down.

EDEM is mainly developed to be run on a desktop computer and is not yet optimized for server configurations. All desktop computers have some kind of graphics engine and running the program on such would prevent it from crashing.

In this work, this issue was solved by installing EDEM both on the server and on a desktop computer. The simulations were then set up and run on the server, saved and transferred to the desktop for post-processing. Both installations used the same license file, which was installed on the desktop and directed to from the server.

Another issue noticed was regarding the use of periodic boundaries. When investigating the possibilities of running simulations on a section instead of on the whole geometry periodic boundaries were used in the slice. This causes problems when the geometry is rounded as in the case of a conical hopper, and the section is set by limiting the domain only.

Broadly speaking the periodic boundary method makes use of 'ghost particles' to recreate the correct behavior when particles interact across the boundary. Whilst the ghost particles share a level of symmetry with their 'real' counterparts across the boundary, the same is not true of the geometry elements i.e. triangles on one side of the boundary may not match those on the other. The results are slight variations in the contact forces with particles interacting with geometry elements near a periodic boundary, resulting in a series of small explosions in the particles<sup>34</sup>.

The workaround to this problem is to trim the geometry in a CAD package before it is imported to EDEM, so that only the elements that lie within the periodic boundary remain in the model.

---

<sup>34</sup> DEM-solutions' technical support



# Appendix E – Hopper Drawings

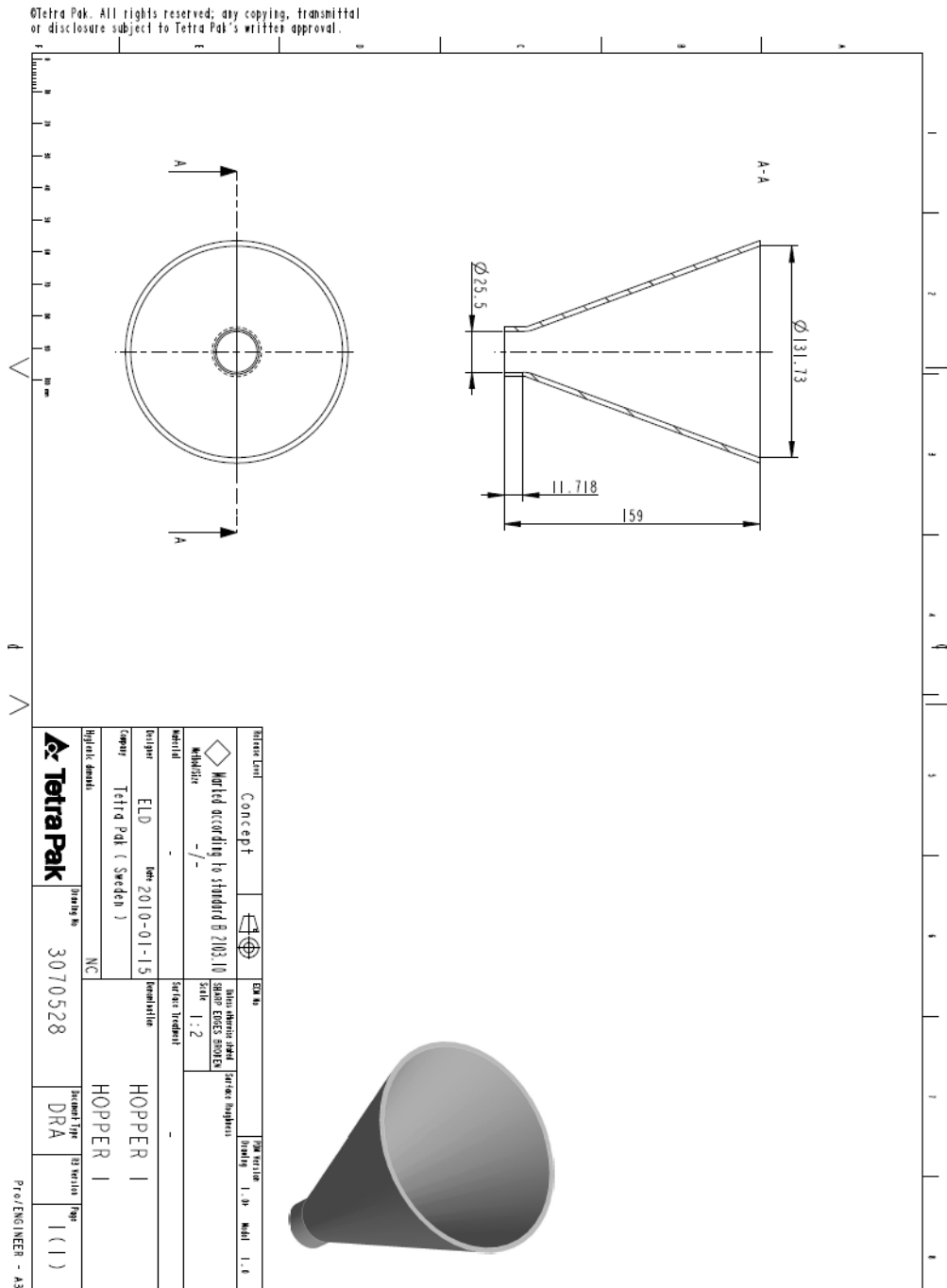


Figure E. 1 – Hopper 1 drawing

©Tetra Pak. All rights reserved; any copying, transmittal or disclosure subject to Tetra Pak's written approval.

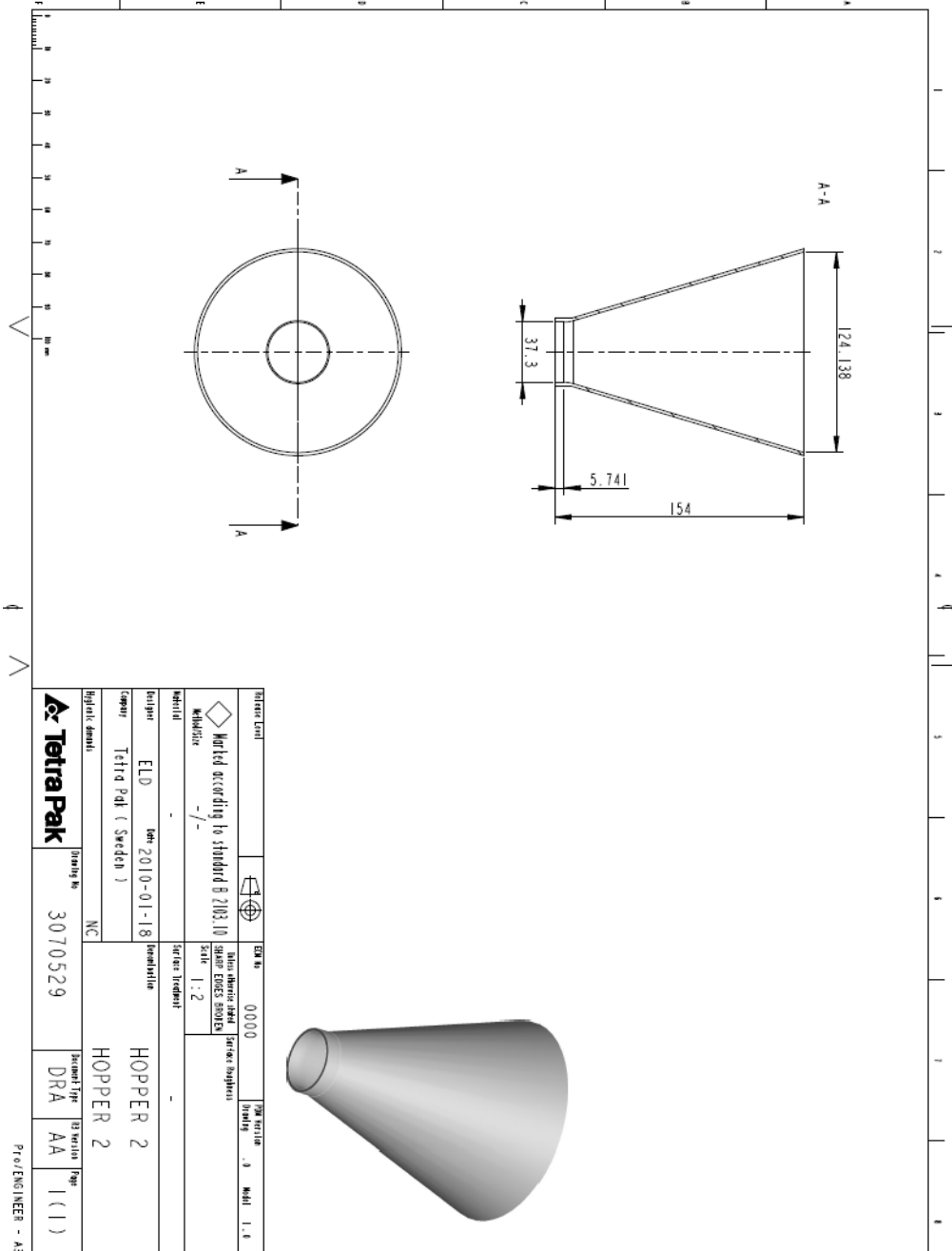


Figure E. 2 – Hopper 2 drawing